UNIVERSITY OF MISKOLC
FACULTY OF MECHANICAL ENGINEERING AND INFORMATICS

NUMERICAL INVESTIGATION OF HEAT TRANSFER ENHANCEMENT IN CORRUGATED CHANNELS USING VORTEX GENERATORS

PHD THESES

Prepared by

Aimen Tanougast
Mechanical Engineering Department (BSc),
Mechanical Engineering Department (MSc)

ISTVÁN SÁLYI DOCTORAL SCHOOL OF MECHANICAL ENGINEERING SCIENCES
TOPIC FIELD OF BASIC ENGINEERING SCIENCES
TOPIC GROUP OF TRANSPORT PROCESSES AND MACHINES

Head of Doctoral School

Dr. Gabriella Bognár
DSc, Full Professor

Head of Topic Group

Dr. László Baranyi
Full Professor

Scientific Supervisor

Dr. Krisztián Hriczó
Associated professor

Miskolc
2026

CONTENTS

SUPERVISOR'S RECOMMENDATIONS

Mr. Aimen Tanougast has been pursuing his PhD studies at the István Sályi Doctoral School of Mechanical Engineering Sciences, Faculty of Mechanical Engineering and Informatics, under the Stipendium Hungaricum Scholarship Programme since September 2022.

During his doctoral studies, he has carried out research in the field of numerical modeling of fluid flow and heat transfer, with particular emphasis on the performance enhancement of heat exchangers and related thermal systems. His work involved extensive literature review, the development and application of computational fluid dynamics (CFD) models, and the analysis of various engineering configurations and operating conditions.

Throughout the research period, he has demonstrated the ability to conduct independent scientific work, analyze numerical results, and present his findings in a systematic manner. The research activities have resulted in scientific publications and contributed to the advancement of knowledge within the scope of his dissertation topic.

Based on my assessment, the dissertation reflects substantial research effort and meets the scientific and formal requirements expected for a doctoral thesis. The candidate has fulfilled the obligations of the doctoral program and completed the research objectives defined in the study plan.

Therefore, I support the submission of his doctoral dissertation and recommend that it be accepted for review and further evaluation within the PhD degree procedure.

Supervisor

Krisztian Hriczó, PhD
Associate Professor

ABSTRACT

This thesis investigates thermal enhancement in semi-circular corrugated channels using vortex generators (VGs). Improving heat transfer while limiting pressure losses is an important challenge in compact heat exchangers and thermal systems. Corrugated channels and VGs improve heat transfer by increasing flow mixing and disturbing the thermal boundary layer. However, the combined interaction between these enhancement techniques remains insufficiently studied, particularly for semi-circular corrugated channels. In addition, limited studies have investigated the influence of VG shape, size, and streamwise position in semi-circular corrugated channels or compared curved single-body vortex generators with conventional winglet-type and multi-pair configurations. Therefore, the novelty of the present work lies in the combined investigation and optimization of VG geometry, size, and position together within the same corrugated channel configuration.

A numerical investigation was performed under turbulent steady-state conditions using the SST k−ω turbulence model. Different VG geometries, sizes, and positions were examined to evaluate their influence on the flow structure and thermal–hydraulic performance.

The results showed that vortex generators changed the flow behavior inside the corrugated channel by reducing the recirculation zones near the walls and improving fluid mixing. The results showed that the concave-up vortex generator (CUVG) provided the best overall performance among the investigated geometries. The size and position of the VG had a strong influence on the thermal behavior, where a 5 mm VG placed near the corrugation entrance (d=-2) produced the highest heat-transfer enhancement of approximately 121%. However, this configuration also caused the largest pressure-drop increase, reaching nearly 12.5 times that of the baseline channel. The maximum performance evaluation criterion (PEC) reached approximately 0.96, indicating a good balance between heat-transfer enhancement and pressure loss. The comparison between single-body and two-pair VG arrangements also showed that the single-body configuration provided better overall thermal–hydraulic performance.

Overall, the study demonstrates that combining optimized vortex generators in semi-circular corrugated channels can significantly improve thermal performance while maintaining acceptable hydraulic losses, making these configurations promising for compact heat exchanger applications.

LIST OF SYMBOLS AND ABBREVIATIONS

	SYMBOLS
k	Turbulent kinetic energy $[\mathrm{m^2/s^2}]$
K	Thermal conductivity $[\mathrm{W/(m\ K)}]$
f	Friction factor
q_w	Heat flux $[\mathrm{W/m^2}]$
Re	Reynolds number
Nu	Nusselt number
h	Heat transfer coefficient $[\mathrm{W/(m^2\ K)}]$
P	Pressure [Pa]
T	Temperature [K]
u, v	Velocity components $[\mathrm{m/s}]$
x, y	Cartesian coordinates [mm]
G	The production term in various transport equations
Cp	Specific heat $[\mathrm{J/(kg\ K)}]$
	ABBREVIATIONS
VGs	Vortex generators
WVGs	Without vortex generators
CUVGs	Concave-up vortex generators
CDVGs	Concave-down vortex generators
SVGs	Straight vortex generators
	GREEK LETTERS
ω	Specific dissipation rate $[\mathrm{s^{-1}}]$
μ	Dynamic viscosity $[\mathrm{N\ m/s^2}]$
μ_t	Turbulent dynamic viscosity $[\mathrm{N\ m/s^2}]$
σ_k, σ_ω	Empirical constant for turbulence model
μ	Dynamic viscosity $[\mathrm{N\ m/s^2}]$
ρ	Density $[\mathrm{kg/m^3}]$
ΔP	Pressure drop [Pa]
τ	Shear stress [Pa]
ρ	Density $[\mathrm{kg/m^3}]$
	SUBSCRIPTS
i, j	Cartesian coordinates indices
w	Wall
av	Average

1. INTRODUCTION

Improving heat transfer performance while maintaining acceptable energy consumption and pressure losses has become a major challenge in modern thermal engineering applications [1,2]. Every aspect of our daily life depends on energy in various forms, from electricity and mechanical power to thermal energy. Among these, heat transfer plays a particularly vital role, as it is involved in numerous applications such as power generation, industrial processes, heating, and cooking. The growing global demand for energy, along with the need to improve energy efficiency, has made thermal energy management a key focus of current research.

Heat transfer plays a significant role in many engineering applications, including heating, ventilation, and air conditioning systems, heat exchangers, and cooling devices [3,4]. Methods for enhancing heat transfer performance are generally classified into three categories: active, passive, and compound techniques.

Passive heat transfer enhancement methods are widely used because they are simple, inexpensive, and capable of providing good performance [5]. These methods are applied to systems without the need for any external energy input, unlike active methods. One of the main challenges in thermal engineering is improving heat transfer while maintaining acceptable pressure losses and achieving high overall thermal–hydraulic performance, particularly in compact heat exchangers. Common passive techniques include the use of corrugated channels, and vortex generators (VGs). Each technique enhances heat transfer through different mechanisms such as flow recirculation, and vortex generation [6–9]. In many cases, two or more of these methods can be combined to achieve even greater heat transfer improvement. The main objective of combining these enhancement methods is to maximize the Performance Evaluation Criterion (PEC) by increasing heat transfer enhancement while minimizing the associated pressure-drop penalty. However, the combined interaction between these techniques and their overall thermal–hydraulic behavior is still not fully understood, which motivates the present study.

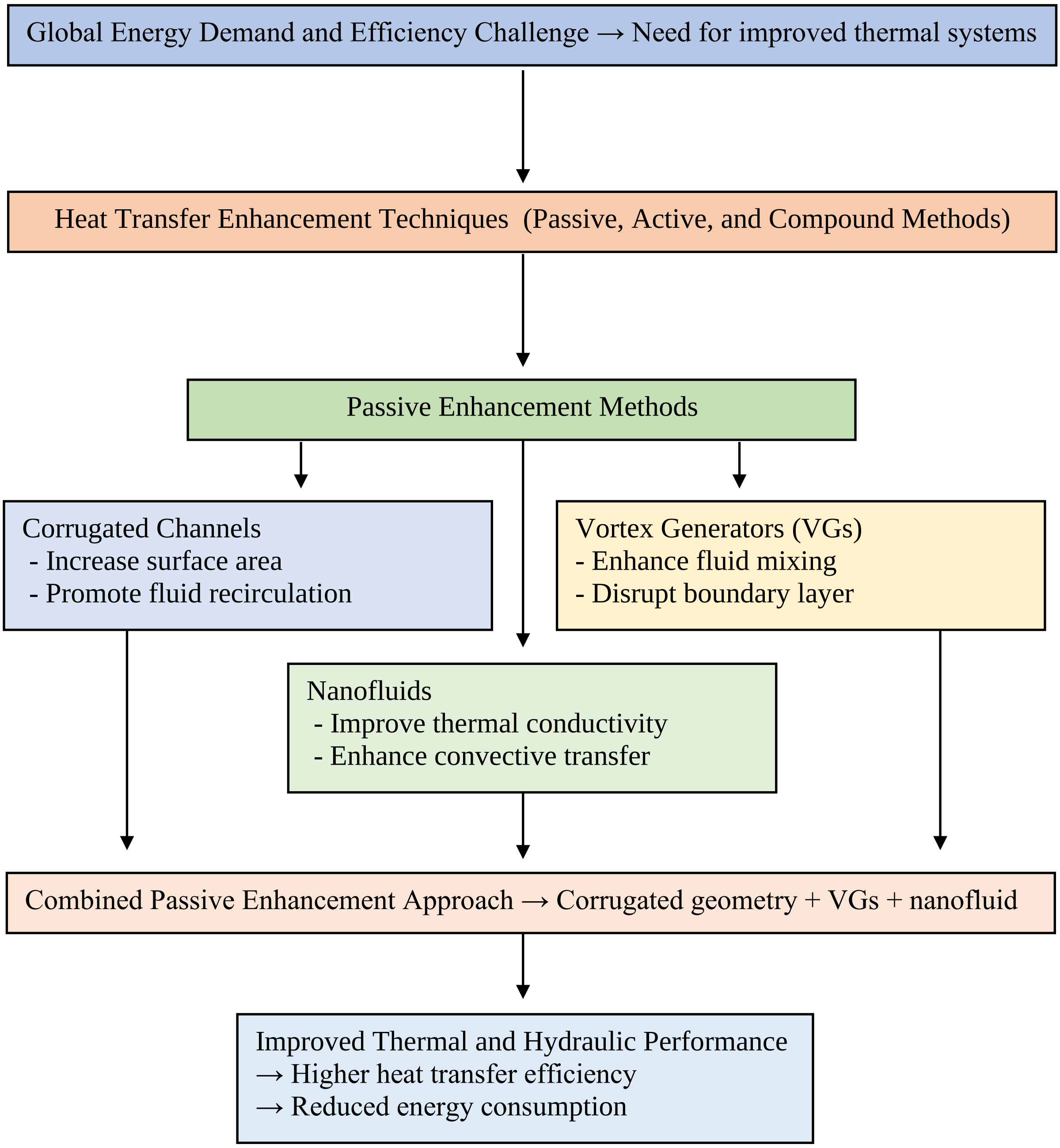

1.1 Corrugated channels

Corrugated channels are channels whose surfaces are modified with periodic shapes or surface patterns. The main goal of this design is to increase the contact area between the fluid and the surface and to promote better fluid mixing. Many studies have investigated this technique, and the number of related publications has increased significantly, especially in recent years (see Figure 1.1).

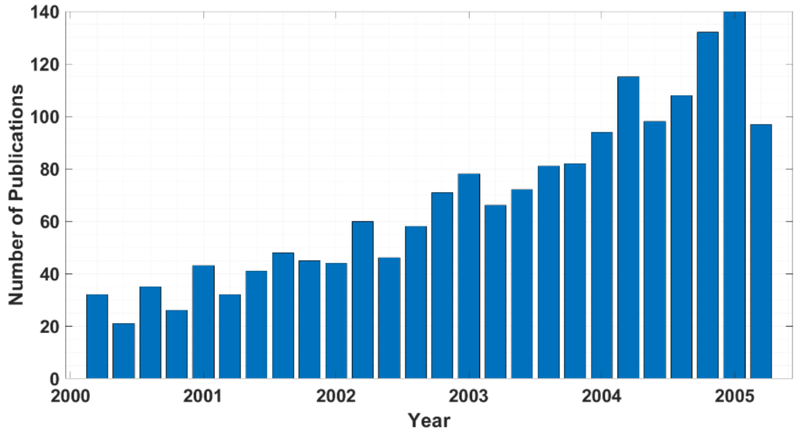

Figure 1.1 Number of publications on corrugated channels per year.

Corrugated channels are widely used for heat transfer enhancement because they significantly improve thermal performance. Many experimental and numerical studies have investigated their behavior, and the results consistently demonstrate that corrugated channels can effectively increase the heat transfer efficiency [10–16]. Ahmed et al. [17] investigated both numerically and experimentally three different corrugated channel designs trapezoidal, sinusoidal, and straight. Their results showed that the corrugated designs achieved better heat transfer performance compared to the straight channel, especially the trapezoidal shape, due to the stronger flow recirculation and enhanced near-wall mixing generated by the sharp corrugation geometry. Ajeel et al. [18] examined a half-sinusoidal corrugated design combined with nanoparticles through numerical and experimental analysis. When comparing corrugated and straight channels, they found that the corrugated geometry offered higher thermal performance, mainly because the corrugations promoted boundary-layer disruption and intensified fluid mixing near the heated surface. Alfellag et al. [19] reviewed recent advancements in compact heat exchangers using different corrugated designs, such as helical, wavy, zigzag, and converging-diverging patterns. According to their findings, heat transfer was enhanced but friction was also raised when helical and transverse corrugations were made wider and taller while the pitch ratio was decreased. This behavior was attributed to the stronger vortex formation and increased momentum losses caused by intensified flow disturbance. Performance was improved by zigzag and wavy designs, although pressure drops were increased. The enhanced thermal behavior was linked to repeated flow separation and reattachment along the corrugated walls, which simultaneously increased hydraulic resistance. Heat transfer in microchannels was more affected by wave amplitude than wavelength, and cross-corrugated surfaces outperformed V-corrugated ones. Pressure drop was lessened while retaining a high heat transfer efficiency due to perforated corrugated surfaces. Azman et al. [20] conducted a numerical study on sawtooth-shaped corrugated pipes with different pitch heights and distances. The findings demonstrated that significant recirculation, backflow, and a smaller boundary layer allowed corrugated pipes to perform better in heat transfer than smooth pipes. However, these same mechanisms increased wall friction and flow resistance, resulting in larger hydraulic losses. Because of the longer total pipe length, larger pitch gaps further exacerbated the pressure drop.

Table 1.1 Summary of previous studies on heat transfer enhancement in corrugated channels.

References	**Type of corrugations**	**Effect on performance**
Bahaidarah [21]	Arc and sinusoidal	The increase in the Nusselt number (*Nu*) corresponding to augmentation in Reynolds number (*Re*) is monotonic The average *Nu* is higher for arc-shaped corrugation configurations than that for sinusoidal configurations.
Islamoglu [22]	Sharp-edged and sinusoidal	The rounding off of the corrugation peaks resulted in the decrease in *Nu* due to the change in the fluid flow pattern (i.e. size and structure of separation region).
Naphon [23]	Arc-shaped, V-shaped, and trapezoidal	With a decrease in the wavy pitch of the arc-shaped channel the sharpness of the edges increases which augments the turbulent intensity of flow.
Ahmed et al. [24]	Sinusoidal, trapezoidal, and triangular	The performance of trapezoidal corrugated channel was found dominant over sinusoidal corrugated channel for Re<220, whereas at higher Re performance of sinusoidal corrugated channel was found dominant.

Tokgoz and Sahin [25]	Rectangular	The thermal boundary layer of the corrugated channel becomes thinner than that of the straight channel because of increased vorticity concentrations, flow separation, and flow reversal, which augments the heat transfer.
Dutta et al. [26]	V-corrugations	The *Nu* for the corrugated channel was found to be higher than that for a straight channel.
Ferhat et al. [27]	Rectangular, sinusoidal, triangular, and trapezoidal	The corrugated walls with artificial roughness in the heat exchanger helped in the improvement of the thermal–hydraulic performance and heat transfer rate.
Singh et al. [28]	Sinusoidal	The decrease in the wave length and *D* results in the increment of pressure drop and *Nu.*
Kurtulmus and Sahin [29]	Sinusoidal	The enhancement in the frequency of pulsation increases the average heat transfer rate.

Table 1.1 summarizes previous studies comparing corrugated and straight channels. Most studies reported that corrugated channels provide better heat transfer performance because the corrugated surfaces promote stronger fluid mixing and increase the effective heat transfer area. Ahmed et al. [17] reported that trapezoidal corrugations provide better thermal performance than sinusoidal geometries at low Reynolds numbers, whereas sinusoidal configurations become more effective at higher Reynolds numbers. Similarly, Naphon [23] showed that sharper corrugation edges intensify turbulence and heat transfer, while Islamoglu [22] demonstrated that smoothing the corrugation peaks reduces the enhancement because of weaker separation regions. Tokgoz and Sahin [25] and Dutta et al. [26] both concluded that corrugated channels outperform straight channels due to stronger recirculation and thermal boundary-layer disruption; however, Tokgoz

and Sahin emphasized the role of vorticity concentration, whereas Dutta et al. mainly associated the enhancement with V-shaped corrugation geometry. In addition, Ajeel et al. [18] showed that combining corrugated geometries with nanoparticles further enhances thermal performance due to improved thermal conductivity and intensified mixing near the corrugated walls. Alfellag et al. [19] and Azman et al. [20] also reported that increasing corrugation height or decreasing pitch ratio enhances thermal mixing, but they noted that stronger recirculation zones significantly increase hydraulic resistance. These comparisons indicate that the reported thermal–hydraulic behavior strongly depends on corrugation geometry and operating conditions. The corrugated geometry generates recirculation zones within the fluid, which promote mixing and enhance thermal exchange. This effect can be further strengthened by incorporating vortex generators (VGs), which induce stronger flow disturbances and improve overall thermal performance.

1.2Vortex generators

The vortex generator is a solid body that can be designed in multiple ways. They help control and redirect the fluid flow by directing it toward specific regions, increasing the contact between the fluid and the surface, and improving the thermal efficiency [30–36]. Figure 1.2 illustrates the number of publications related to vortex generators and how this number has increased over the past 25 years.

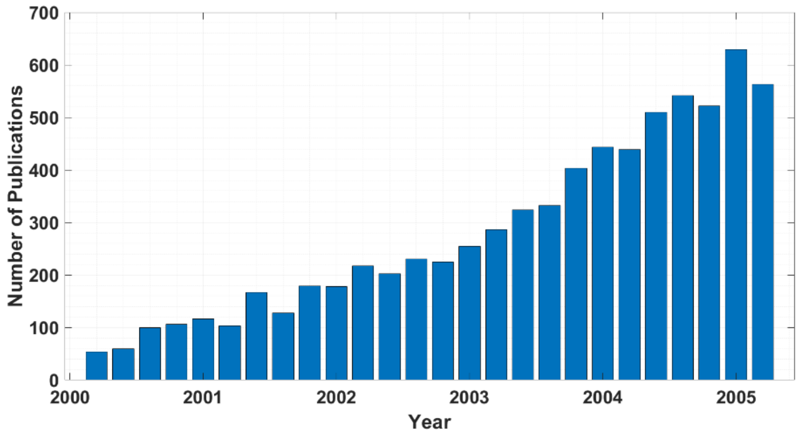

Figure 1.2 Number of publications on VGs per year.

Numerous studies have investigated the role and effect of VGs both numerically and experimentally. Ruifang et al. [37] examined the optimal design and inflow angle of the VG used for three-dimensional rotational effects. The VG showed improvement in the aerodynamic performance of the wind turbine by delaying airflow separation on the blade section. This improvement was associated with the ability of the VGs to control vortex formation and maintain attached flow over the blade surface. Xu et al. [38] conducted a numerical study on different VG shapes inside a rectangular channel to evaluate their impact on heat transfer and flow resistance. The half-cylinder VG produced the best thermohydraulic performance out of the five VG types examined in the study. Subsequent investigation showed that the best performance was achieved when these VGs were arranged in a side-lined row. Furthermore, efficiency was first increased by expanding the VG length, but it eventually decreased. The initial enhancement was attributed to stronger longitudinal vortex generation and improved near-wall mixing, whereas excessive VG size increased flow blockage and momentum losses, leading to higher hydraulic resistance and lower overall efficiency. Higher flow resistance and worse overall performance were the results of larger VG radii and smaller spacing. This behavior indicates that excessive vortex interaction can intensify frictional losses without providing proportional heat transfer enhancement. The application of vortex generators in corrugated channels to boost heat transfer and improve flow characteristics has been investigated by many researchers. By introducing VGs, they aimed to minimize the recirculation zones caused by the corrugated surface, leading to better fluid movement and more efficient thermal performance [39–41]. These studies specifically inserted VGs in curved or corrugated channels to redirect the flow, reduce dead zones, and enhance mixing near the walls, thereby significantly improving overall heat transfer efficiency.

Modi and Rathod [42] investigated three types of VGs: sinusoidal, wavy, and elliptical curved rectangular winglets inside a semi-circular corrugated channel. They found that the curved and wavy VGs enhanced heat transfer more effectively owing to the smoother guidance of the fluid toward the walls, which increased the fluid–surface contact and improved the thermal performance. The smoother curvature of these VGs also promoted more stable vortex structures and reduced abrupt flow separation compared with conventional straight winglets. Brodnianska and Kotsmíd [43] investigated cylindrical VGs in a novel wavy corrugated channel and found that they significantly enhanced heat transfer and thermal performance, although with a slight increase in pressure drop, achieving a maximum thermal performance factor of approximately 0.82. The pressure penalty was mainly caused by intensified vortex-induced mixing and increased wall friction near the corrugated surfaces. Akcay [44] studied the effects of different rectangular winglet VGs, both solid and perforated, on the hydraulic and thermal performance of a semi-corrugated channel under pulsating flow. The results showed that the thermal performance improved significantly as the pulsation amplitude and frequency increased, with only a small increase in the friction factor. The pulsating flow enhanced periodic boundary-layer disruption and strengthened vortex interaction, while the perforated winglets reduced resistance by allowing partial fluid passage through the VG body. Additionally, perforated winglets were found to reduce friction compared with solid winglets, making them more efficient under certain conditions. Tanougast and Hriczo [45] examined the effect of two-pair winglet VGs on a semi-circular corrugated channel. The VGs enhanced heat transfer by reducing the recirculation zones and thinning the thermal boundary layer, achieving a performance evaluation criterion (PEC) of 0.88. The improved performance was linked to stronger near-wall mixing generated by the interaction between the corrugation-induced flow structures and the longitudinal vortices produced by the VGs. In a related study, Tanougast et al. [46] investigated a single-body VG with three shapes (concave up, concave down, and straight) in the same channel. They found that the single-body VGs provided a higher PEC of 0.94, whereas the concave-up VGs offered slightly higher heat transfer, with a PEC of 0.93. This behavior suggests that VG geometry strongly affects vortex stability and the ability to direct high-momentum fluid toward the heated walls.

Table 1.2 Summary of previous studies on VGs.

References	**Type of VGs**
Gholami et al. [47]	Wavy rectangular winglet
Sawhney et al. [48]	Wavy delta winglet
Gong et al. [49], Lotfi et al. [50–52]	Curved Rectangular winglet
Wu et al. [53], Song et al. [54], Lu and Zhou [55], Lin et al. [56]	Curved Delta winglet
Esmaeilzadeh et al. [57]	Curved Trapezoidal winglet

Several studies have shown that vortex generators can improve heat transfer by enhancing fluid mixing and disturbing the thermal boundary layer. Xu et al. [38], Modi and Rathod [42], and Tanougast et al. [46] reported that curved VG geometries generally provide better thermal–hydraulic performance than straight winglets because they produce stronger and more stable vortices. Akcay [44] showed that perforated winglets can reduce pressure losses compared with solid VGs. Other studies [43,45] also reported improved performance in corrugated channels, although the PEC values varied depending on VG geometry, arrangement, and channel configuration. Overall, these studies indicate that the effectiveness of vortex generators strongly depends on their geometry and interaction with the channel flow.

Vortex generators enhance heat transfer mainly by increasing near-wall mixing and repeatedly disturbing the thermal boundary layer. However, stronger vortices also increase wall shear stress and pressure drop. Therefore, achieving good thermal–hydraulic performance requires balancing heat-transfer enhancement with hydraulic losses.

1.3Research Gap and Motivation

Previous studies generally agree that corrugated channels and vortex generators enhance heat transfer by increasing flow separation, vortex formation, and near-wall mixing. However, contradictions exist regarding the optimal geometry and configuration. Some studies report trapezoidal corrugations as the most effective design, while others show that sinusoidal or triangular profiles can provide better performance depending on Reynolds number and geometric ratios. Similarly, vortex generator studies report different optimal VG shapes and arrangements, since heat transfer enhancement is often accompanied by significant pressure penalties that strongly depend on VG size and placement. In many previous studies, the VG geometries were selected in a relatively conventional or random manner without considering geometric consistency with the corrugated channel profile or systematically evaluating the influence of VG size and streamwise position.

Although semi-circular corrugated channels have demonstrated promising thermal performance and have been experimentally validated in several previous studies, their combined interaction with vortex generators remains insufficiently explored. This channel configuration is also attractive for practical heat exchanger applications because it offers effective thermal enhancement while maintaining a relatively simple geometry that is easier to manufacture and implement compared with more complex enhanced surfaces commonly used in compact thermal systems. However, limited attention has been given to achieving geometric consistency between the vortex generator shape and the corrugated surface in order to maximize vortex generation, suppress recirculation zones near the walls, and improve fluid mixing. In addition, the effects of VG size and streamwise position on flow structure and thermal–hydraulic behavior in semi-circular corrugated channels remain insufficiently explored. Furthermore, most previous studies focused mainly on conventional winglet-type or multi-pair VG arrangements, while direct comparisons with optimized single-body VG configurations are still limited.

1.4Outline of the thesis

Previous studies have widely investigated corrugated channels, and vortex generators as passive heat transfer enhancement techniques. However, the combined interaction between corrugation-induced recirculation zones and vortex generator-induced longitudinal vortices has not been sufficiently examined in a systematic manner. In addition, limited attention has been given to the consistency between VG geometry and corrugated surface shape, and only few studies have reported a detailed optimization of VG type, size, and streamwise position in semi-circular corrugated channels. To address these gaps, this thesis provides a comprehensive numerical investigation of VG optimization modeling in a corrugated channel, for improved thermal–hydraulic performance and stability.

Chapter 1 introduces the importance of corrugated channels, and vortex generators in heat-transfer applications. It reviews previous research, highlights key findings reported in the literature, and identifies the main limitations and research gaps that motivate the present work. The chapter also presents the objectives and original contributions of the thesis.

Chapter 2 presents the mathematical and physical models used in this study. It describes the governing equations for fluid flow and heat transfer, and the turbulence model. The chapter also explains the evaluation parameters percentage enhancement, pressure-drop ratio, and performance evaluation coefficient which are essential for assessing thermal and hydraulic performance. The geometry, boundary conditions, and numerical procedure are discussed in detail, including the use of ANSYS Fluent for the simulations.

Chapter 3 focuses on the numerical verification process. It includes the mesh-independence study, the confirmation of steady-state behavior, and an evaluation of the geometry using a 3D model. The chapter then presents the validation of the numerical results against available experimental data for both thermal and hydraulic characteristics. Additional validation is performed against previous studies involving channels with vortex generators but different configurations.

Chapter 4 investigates three different VG shapes. The aim is to determine which geometry best fits the corrugated channel while providing an effective balance between hydraulic losses and heat-transfer enhancement. The chapter identifies the most suitable VG type for this configuration.

Chapter 5 examines the influence of VG size. Several dimensions are tested to understand their impact on boundary-layer disruption, vortex formation, pressure drop, and overall thermal performance. After evaluating the results, the optimal VG size is selected.

Chapter 6 analyzes the effect of VG position. Because VG position strongly affects both the flow structure and the heat-transfer rate, this chapter identifies the most effective location inside the corrugated channel.

Chapter 7 compares the performance of a single VG body (the chosen configuration) with two-pair VG arrangements, as many previous studies have focused on two-pair layouts. This comparison highlights the differences in thermal behavior, vortex interaction, and hydraulic cost.

2. NUMERICAL METHODOLOGY

In this chapter, the mathematical formulation used in the present study is introduced. It includes the governing equations such as the Navier–Stokes equations, the energy equation, the turbulence model, and evaluate key performance parameters. The geometry of the studied domain and its specific details, including boundary conditions, are also defined. In addition, the numerical procedure implemented in the ANSYS software is described, explaining how the computational setup was established to solve the governing equations within the defined domain.

2.1 Governing equations

The governing equations, which include the continuity, momentum, and energy equations, are derived by applying the basic conservation laws to a fixed small control volume that approaches zero in size. This method, known as the Eulerian approach, is used to describe the behavior of the fluid at each point in the domain. By applying the principles of mass conservation, Newton's second law for momentum, and energy conservation, the fundamental equations that govern fluid flow and heat transfer are obtained. The general form of these governing equations can be written as [58]:

$$\frac{\partial(\rho\Phi)}{\partial t} + div(\rho U\Phi) = div(\Gamma_{\Phi}\ grad\Phi) + S_{\Phi}. \qquad 1$$

In this formulation, Φ represents a general variable that can denote quantities such as *u*, *v*, *w*, or *T*, while Γ_{Φ} is the generalized diffusion coefficient associated with that variable. The first and second terms on the left-hand side of Equation (1) correspond to the unsteady and convective terms, respectively. On the right-hand side, the first term represents the generalized diffusion term, and the second term, S_{Φ}, is a generalized source term that accounts for all the remaining terms in the governing equations, excluding the unsteady, convective, and diffusion terms. The specific definitions of Γ_{Φ} and S_{Φ} are given in Table 2.1.

Table 2.1 Coefficient and source term of the general governing equations.

Equation	$\boldsymbol{\rho}$	$\boldsymbol{\Phi}$	$\Gamma_{\boldsymbol{\Phi}}$	$\boldsymbol{S_{\Phi}}$

Continuity	ρ	1	0	0
Momentum	ρ	u_i	μ	$\rho f_i - \frac{\partial P}{\partial x_i}$
Energy	ρ	T	$K/_{Cp}$	$S_T/_{Cp}$

In Table 2.1, x_i represents the spatial coordinates, while u_i denotes the corresponding velocity components. f_i refers to the body forces acting on the fluid. The symbols *P*, *ρ*, *μ*, *K*, and *Cp* represent pressure, density, dynamic viscosity, thermal conductivity, and specific heat capacity, respectively. S_T denotes the thermal source or sink term. This general formulation has been widely applied in numerical heat transfer to solve various practical engineering problems.

In this study, water was modeled as a viscous, Newtonian, and incompressible fluid with constant thermophysical properties. The flow was assumed to be steady [59] and turbulent. To simplify the analysis while capturing the essential flow characteristics, a two-dimensional (2D) simulation was carried out in the *x–y* plane. This approach allowed for a detailed investigation of the primary flow direction along the x-axis, the formation of recirculation zones, and the development of the thermal boundary layer, in accordance with previous two-dimensional studies [42,44,60]. The selected 2D approach was considered suitable for the present configuration because the vortex generators were extruded uniformly across the channel width, resulting in predominantly two-dimensional flow behavior with limited spanwise variation. Body forces were neglected because their influence on the flow field was considered insignificant. The governing equations for the conservation of mass, momentum, and energy in Cartesian coordinates are expressed as follows [61]:

- Mass conservation equation:

$$\frac{\partial(\rho u_i)}{\partial x_i} = 0. \tag{2}$$

The continuity equation ensures mass conservation throughout the computational domain and describes the incompressible nature of the flow inside the corrugated channel.

- Momentum conservation equation:

$$\frac{\partial(u_j \rho u_i)}{\partial x_j} = -\frac{\partial P}{\partial x_i} + \frac{\partial}{\partial x_j}\left(\mu\left(\frac{\partial u_i}{\partial x_j} - \rho\overline{u'_i u'_j}\right)\right). \tag{3}$$

The momentum equation governs the transport of fluid momentum and accounts for the effects of pressure gradients, viscous forces, and turbulence-induced momentum exchange generated by the corrugated geometry and vortex generators.

- Energy conservation equation:

$$\frac{\partial(\rho u_i T)}{\partial x_i} = \frac{\partial}{\partial x_i}\left(\left(\frac{\mu}{Pr} - \frac{\mu_t}{Pr_t}\right)\frac{\partial T}{\partial x_i}\right). \quad 4$$

The energy equation describes heat transport within the fluid domain and includes the combined effects of convection and thermal diffusion, which are strongly influenced by vortex-induced mixing near the heated walls.

Due to the presence of turbulence, the Reynolds-averaged Navier–Stokes (RANS) equations introduce additional unknown terms, known as Reynolds stresses, represented by $-\rho\overline{u'_i u'_j}$. These terms arise from the averaging process and require a turbulence model to close the system of equations. In the present study, the shear stress transport (SST) k–ω model was adopted to provide closure [62]. This model combines the advantages of the standard k–ω formulation near the wall and the k–ε model in the free-stream region, offering improved accuracy for flows involving strong adverse pressure gradients and separation [63]. The SST k–ω model is particularly suitable for corrugated channels equipped with vortex generators because it provides improved prediction of near-wall flow behavior, thermal boundary-layer development, adverse pressure gradients, and flow separation generated by the complex channel geometry.

$$-\rho\overline{u'_i u'_j} = \mu_t\left(\frac{\partial u_i}{\partial x_j} + \frac{\partial u_j}{\partial x_i}\right) - \frac{2}{3}\rho k \delta_{ij} - \frac{2}{3}\mu_t \frac{\partial u_k}{\partial x_k}\delta_{ij}, \quad 5$$

- The turbulent kinetic energy (k)

$$\frac{\partial u_i k}{\partial x_i} = \frac{\partial}{\partial x_i}\left[(\mu + \mu_t \sigma_k)\frac{\partial k}{\partial x_i}\right] + G_k - Y_k. \quad 6$$

- The specific dissipation rate (ω)

$$\frac{\partial u_i \omega}{\partial x_i} = \frac{\partial}{\partial x_j}\left(\Gamma_\omega \frac{\partial \omega}{\partial x_j}\right) + G_\omega - Y_\omega + D_\omega. \quad 7$$

In these equations, G_k denotes the rate of turbulent kinetic energy generation resulting from the mean velocity gradients, whereas G_ω represents the production rate of ω associated with the mean flow. The terms Y_k and Y_ω account for the dissipation of k and ω due to turbulence effects. The turbulent viscosity μ_t is incorporated into the momentum and energy equations, influencing the Reynolds stresses and enhancing the effective thermal diffusion. These transport equations enable the numerical model to capture the influence of turbulence on flow mixing and thermal boundary-layer development inside the corrugated channel.

2.2 Evaluation parameters

The pressure drop across the channel was determined using the following relation:

$$\Delta P = P_{in} - P_{out.} \tag{8}$$

The average Nusselt number (*Nu*) is obtained as follows [64]:

$$Nu = \frac{h\, D_h}{K}, \tag{9}$$

where h represents the convective heat transfer coefficient (W/(m²·K)), K is the thermal conductivity of the working fluid (W/(m·K)), and D_h denotes the hydraulic diameter (m) of the corrugated passage, expressed as [65]:

$$D_h = H + h. \tag{10}$$

The friction factor (*f*) is calculated using the following equation [66]:

$$f = \frac{2\, D_h\, \Delta P}{L\, \rho\, u^2}. \tag{11}$$

To quantify the increase in pressure loss caused by the VGs relative to that of a plain wavy channel, the pressure drop ratio (PR) is defined as [67]:

$$PR = \frac{\Delta P_{VGs}}{\Delta P_{WVGs}}, \tag{12}$$

where ΔP_{VGs} and ΔP_{WVGs} are the pressure drops in channels with and without VGs, respectively.

The percentage enhancement (PE) quantifies the improvement in heat transfer when VGs are applied and is given by [68]:

$$PE\ (\%) = \frac{(Nu_{VGs} - Nu_{WVGs})}{Nu_{WVGs}} 100, \tag{13}$$

where Nu_{VGs} and Nu_{WVGs} denote the Nu for channels with and without VGs.

The overall thermal–hydraulic performance was assessed using the Performance Evaluation Criterion (PEC) [69]:

$$PEC = \frac{Nu_{VGs}/Nu_{WVGs}}{\left(\Delta P_{VGs}/\Delta P_{WVGs}\right)^{(\frac{1}{3})}}. \quad 14$$

2.3 Physical Model

The semi-circular corrugated channel used in this study is illustrated in Figure 2.1. The channel has a total length of 500 mm and consists of an inlet section (*L1* = 200 mm), a test section (*L2*= 200 mm), and an outlet section (*L3* = 100 mm). To ensure fully developed flow and prevent backflow, the inlet and outlet sections (*L1* and *L3*) were designed with a height greater than the main channel height (*H*) [60]. The maximum and minimum heights of the channel are 10 mm and 5 mm, respectively. The corrugated geometry follows a wavy profile characterized by a wavelength (*P*) of 10 mm and a pitch diameter (*D*) of 5 mm.

In the first stage of the study, three different types of vortex generators (VGs) were examined: concave-up vortex generators (CUVGs), concave-down vortex generators (CDVGs), and straight vortex generators (SVGs). Each VG has a width (*S*) and length (*B*) of 5 mm and is positioned at the entrance of each corrugation section to enhance flow mixing and heat transfer. The vortex generators were extruded uniformly across the full channel width, resulting in a spanwise-constant geometry without localized side-edge effects. Therefore, the dominant flow structures were primarily governed by streamwise recirculation and near-wall mixing within the x–y plane. Based on the results of this comparison, the configuration that exhibited the best overall thermal–hydraulic performance was selected for further analysis.

In the second stage, the influence of VG size and placement position was investigated using the selected VG type. Three VG sizes (2, 4, and 6 mm) and three positions relative to the corrugation entrance (*d* = −2 mm, 0 mm, and +2 mm) were analyzed to assess their impact on the flow structure and heat transfer enhancement.

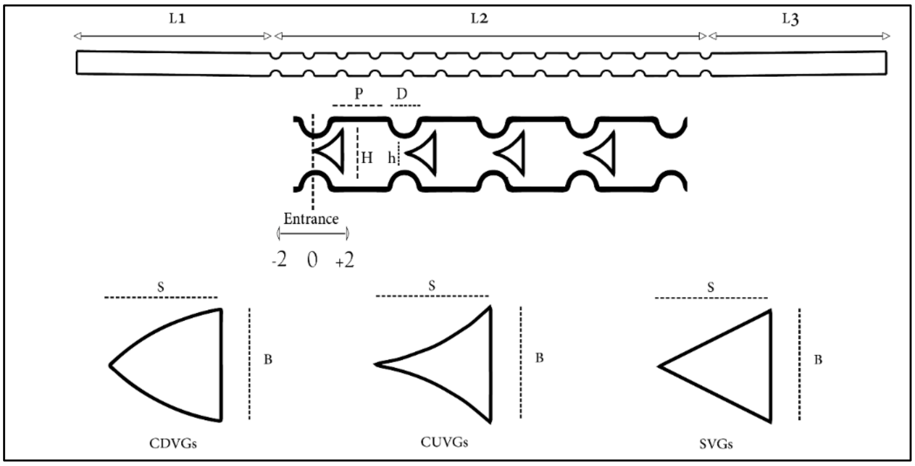

Figure 2.1 The physical model.

2.4 Boundary conditions

The following boundary conditions are imposed in solving the Navier–Stokes equations:

- At the entrance to the channel

The fluid enters with a temperature of T = 298 K at a flow velocity determined by the Reynolds number (10000-30000), the inlet turbulence intensity was set to 5%, a typical value for internal channel flows, to provide a physically realistic representation of the inflow conditions

$$u = \frac{Re\mu}{\rho D_h}. \quad 15$$

- Near smooth and corrugated walls

The no-slip and impermeability conditions (u = v =0) were applied at all solid surfaces, including the smooth and corrugated walls as well as the channel boundaries in the height direction. The channel walls are made of copper with a thermal conductivity of 387.6 W/m·K. The upstream and downstream smooth channel walls are assumed to be adiabatic, while a constant heat flux of 10000 $\mathrm{W/m^2}$ is applied at the corrugated section

$$-k\frac{\partial T}{\partial y} = q_w. \quad 16$$

- To the output

The flow is assumed to occur under atmospheric conditions and to be fully developed, leading to a zero normal gradient for all physical quantities governed by differential transport equations

$$\frac{\partial u}{\partial x} = 0; \quad \frac{\partial v}{\partial x} = 0; \quad \frac{\partial T}{\partial x} = 0; \quad P = P_{atm}. \tag{17}$$

2.5 Numerical procedure

This study was carried out using ANSYS Fluent, a commercial computational fluid dynamics (CFD) software that employs the Finite Volume Method (FVM) to discretize and solve the governing equations of mass, momentum, and energy. In the FVM, the computational domain is divided into a finite number of small control volumes, and the integral form of each conservation equation (2) is applied to every cell. This ensures that the conservation of mass, momentum, and energy is maintained over the entire solution domain [70]. The fluxes through the cell faces are evaluated and balanced, resulting in a set of algebraic equations that approximate the behavior of the flow field.

The Pressure-Based Coupled Solver (PBCS) was adopted in this study. This solver provides a fully coupled approach in which all governing equations (continuity, momentum, and energy) are solved simultaneously as a single system [71]. This method improves stability and convergence, particularly for complex, highly coupled flow problems such as turbulent and mixed convection flows.

The discretization of the governing equations (2, 3, and 4) was performed using a second-order upwind scheme for pressure, momentum, energy, and turbulence quantities to ensure higher numerical accuracy and minimize false diffusion [72]. Spatial gradients were computed using the least-squares cell-based method, which provides accurate gradient estimation for unstructured and irregular meshes.

Convergence was monitored based on the residuals of the governing equations (2, 3, and 4). The solution was considered converged when the residuals of the energy equation dropped below 10^{-6}, while those of the momentum, continuity, and turbulence transport equations (6 and 7) were below 10^{-4}. In addition to the residual criteria, overall mass and energy balances were checked to ensure global solution consistency.

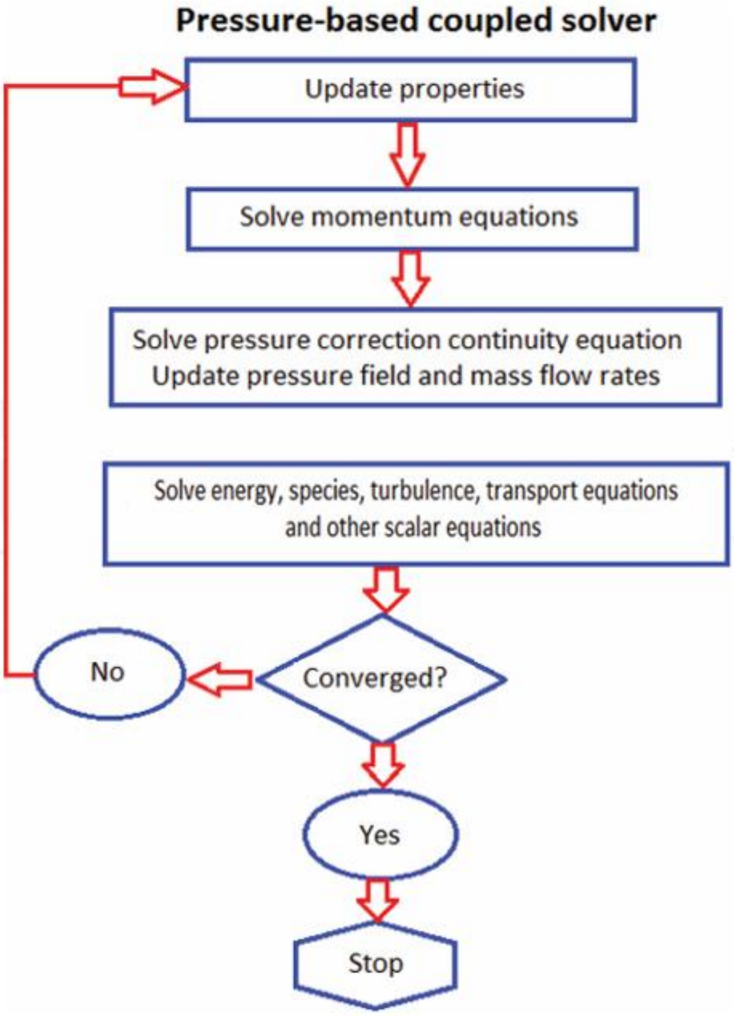

Figure 2.2 Schematic representation of the pressure-based coupled solver (PBCS) scheme used in ANSYS Fluent.

3. MESH INDEPENDENCE AND MODEL VALIDATION

In this chapter, the steady-state verification and evaluation of the 3D model are presented. The assumptions made in this study are supported by references from previous research and further validated through our own numerical investigations. To ensure the accuracy and reliability of the results, a grid independence test was conducted, followed by an analysis of the convergence behavior of the model within the simulation software. Furthermore, the numerical model was validated by comparing its results with those from previous experimental and numerical studies, both for cases without VGs and for cases incorporating VGs. This comprehensive verification process confirms the robustness of the computational setup and strengthens the confidence in the results obtained in the subsequent chapters.

3.1Steady-state verification

To verify the steady-state assumption in this study, two monitoring points were selected one located at the wall of the channel and the other at the centerline. The velocity and temperature variations with time were recorded at these points to examine how the hydrodynamic and thermal fields evolved during the simulation.

Figure 3.1 presents the velocity and temperature profiles at the channel wall. It can be observed that the velocity remains nearly constant over time, with only a minor fluctuation at the very beginning of the simulation. The velocity value at the wall is essentially zero, which confirms the validity of the no-slip boundary condition; this is expected since viscous effects cause the fluid velocity to vanish at the wall. The temperature, on the other hand, shows a slight transient variation during the first second due to the imposed wall heat flux, but the difference is less than 1 K. After this initial adjustment, it stabilizes and remains constant throughout the rest of the simulation period.

Figure 3.2 shows the same profiles at the midline of the channel. Here, the velocity initially varies by about 0.2 m/s during the first second before reaching a steady value, while the temperature fluctuates by approximately 0.06 K before becoming stable. This small transient behavior occurs as the flow develops and the solver begins to converge toward a steady solution.

In the numerical setup, each time step was set to 0.1 s with 20 iterations per step. During the initial time steps, the residuals of the governing equations (2, 3, and 4) had not yet reached their convergence criteria, resulting in minor variations in the monitored parameters. Once the residuals dropped below the predefined thresholds (after approximately the first second), both velocity and temperature remained constant with time. This confirms that the flow and heat transfer fields are independent of time, and therefore the system can be accurately treated as steady-state in the subsequent analysis.

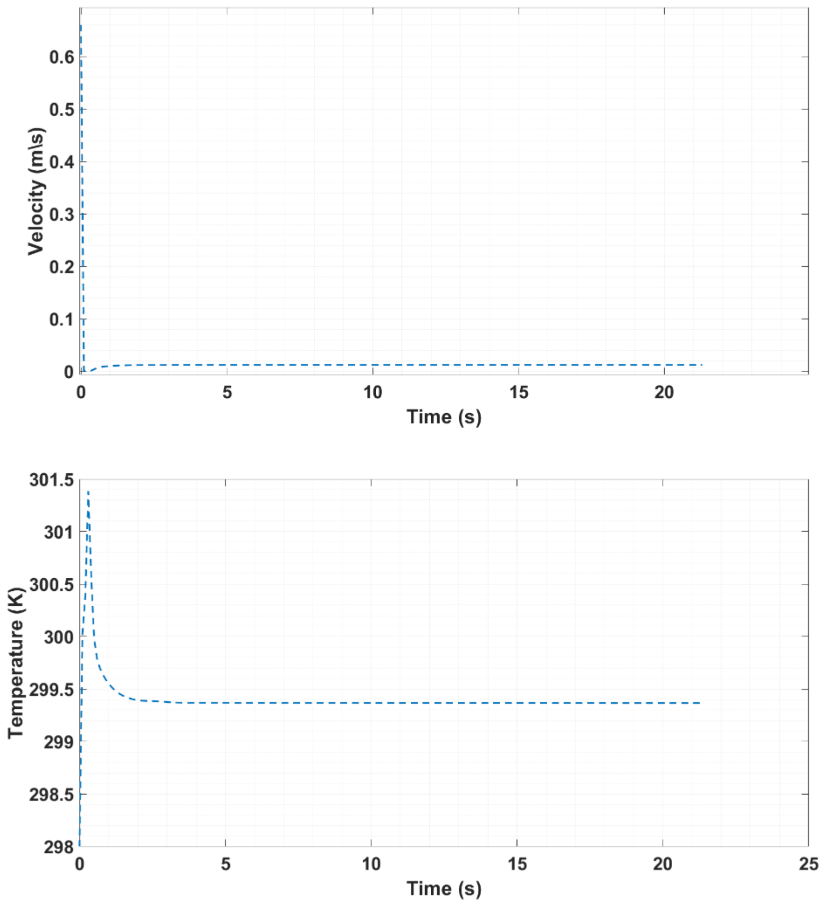

Figure 3.1 Velocity and temperature profiles with time at the wall of the corrugated channel.

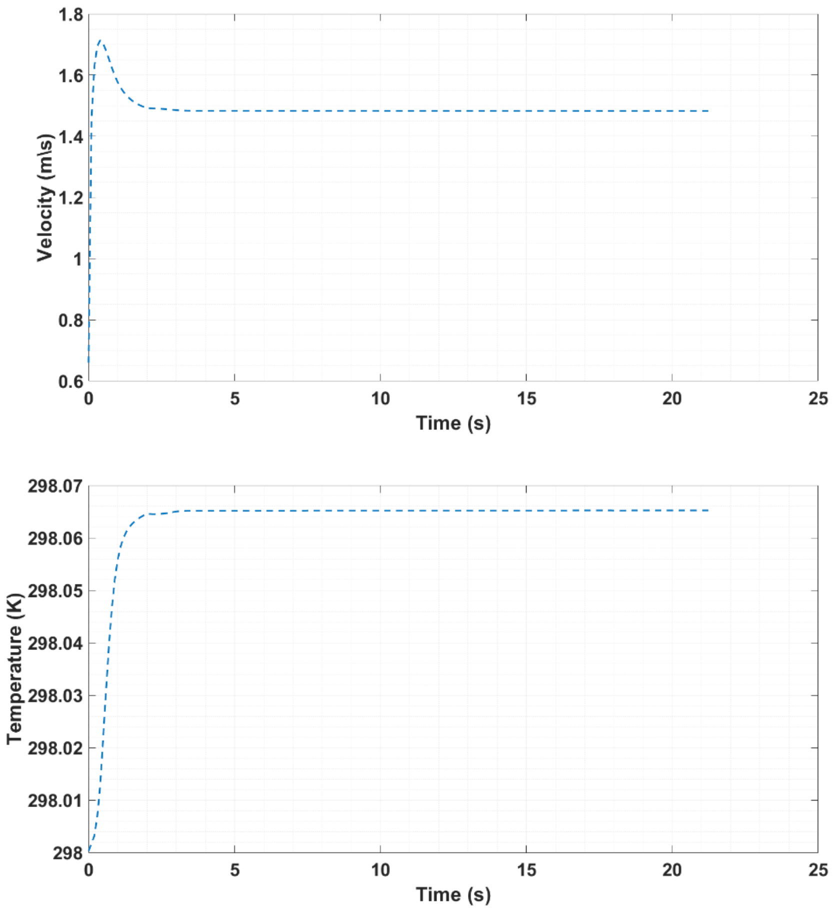

Figure 3.2 Velocity and temperature profiles with time at the centerline of the corrugated channel.

3.2Evaluation of 3D model effects

To evaluate whether a full three-dimensional analysis was necessary, an additional 3D simulation was performed by extruding the channel 50 mm along the *z*-axis, as shown in Figure 3.3. The main flow direction remained along the *x*-axis. Velocity contours were examined at several cross-sectional planes located at z = 10, 20, 30, and 40 mm. The results showed very similar flow patterns to those obtained from the 2D model, with no significant variation along the *z*-direction, indicating a uniform flow throughout the channel depth. A slight difference was observed at the channel centerline, where the 3D model exhibited slightly higher velocity concentration due to the influence of four confining walls, whereas the 2D model was limited to interaction with only two walls.

It should also be noted that the vortex generators investigated in the present study were extruded across the full channel width rather than being localized winglets with finite spanwise dimensions.

Consequently, the generated flow structures were predominantly two-dimensional, and the dominant enhancement mechanism was associated with suppression of recirculation zones, boundary-layer disruption, and near-wall flow acceleration within the x–y plane. Since the primary objective of the study was to investigate the influence of VG geometry, size, and position on the thermal–hydraulic behavior and recirculation characteristics of the corrugated channel, the 2D approach was considered sufficient to capture the dominant flow physics with substantially lower computational cost. Nevertheless, it is acknowledged that the 2D model cannot fully resolve detailed three-dimensional secondary vortices and complex spanwise flow interactions, which represents a limitation of the present study.

Similar two-dimensional approaches have also been adopted in previous investigations of corrugated channels and vortex-generator-enhanced flows [42,44,60]. These studies demonstrated that 2D simulations can reasonably capture the dominant thermal–hydraulic behavior and recirculation characteristics while significantly reducing computational cost.

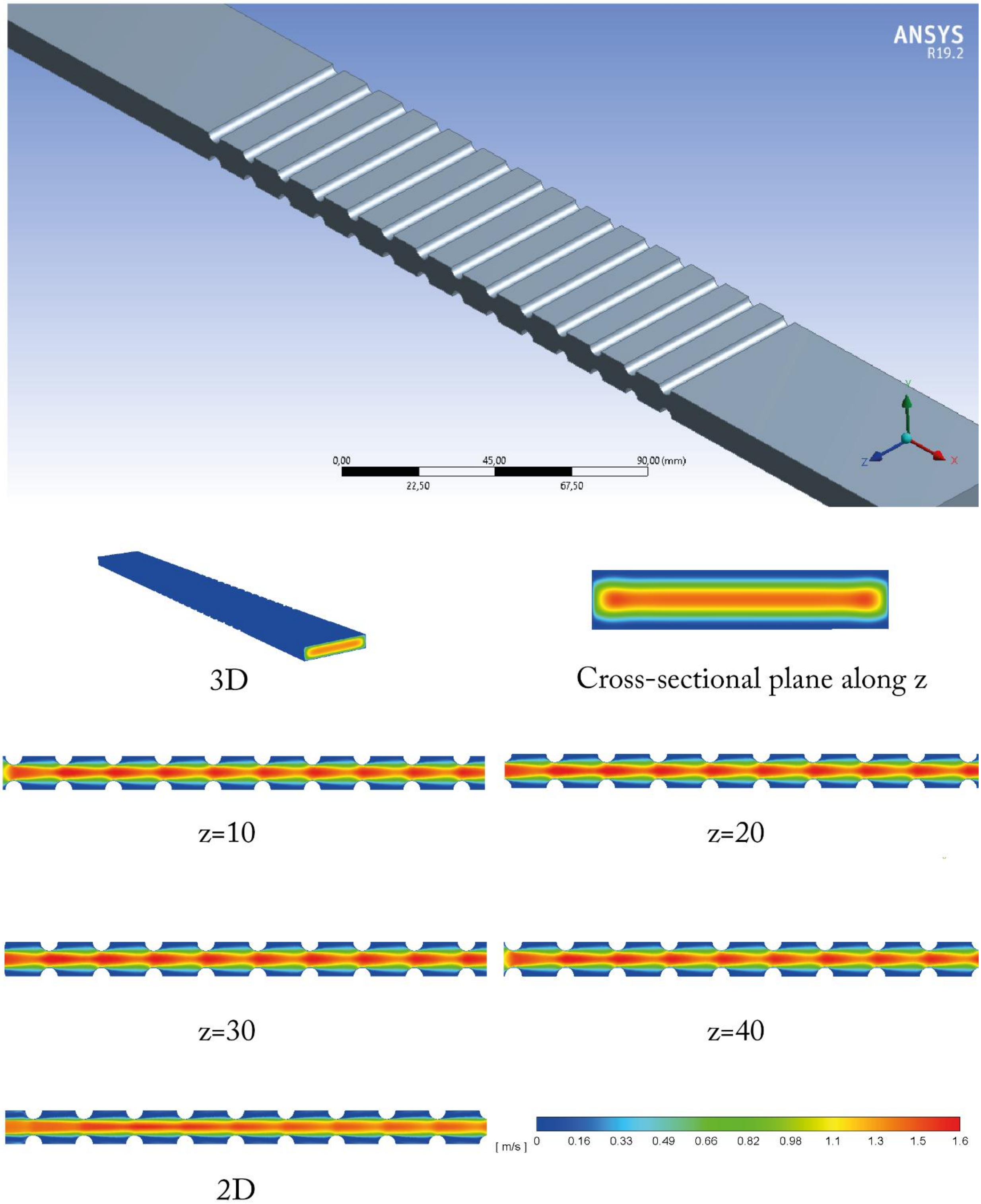

Figure 3.3 Three-dimensional model of the corrugated channel extruded along the z-axis for comparison with the 2D simulation.

3.3Mesh Independence Study

The mesh plays a crucial role in determining the accuracy of the numerical results. A mesh independence test was conducted to identify the coarsest grid capable of producing reliable and accurate results. Five different mesh configurations were examined, with the total number of nodes varying between 98,037 and 557,168. To better capture the near-wall effects, ten inflation layers were generated adjacent to the channel walls (Figure 3.4) and around the VGs to capture the boundary layer development and local velocity gradients with high precision in these regions. The relative error between successive meshes was calculated using Equation (18) as described in [18], where M_{i+1} denotes the current result and M_{i} represents the preceding *Nu* value

$$Error(\%) = \left|\frac{M_{i-}M_{i+1}}{M_i}\right| * 100. \qquad 18$$

To further assess the numerical uncertainty associated with mesh refinement, the Grid Convergence Index (GCI) method proposed by Roache [73] was also considered. Three representative meshes (coarse, medium, and fine) containing 98,037, 226,732, and 557,168 nodes, respectively, were selected for the analysis. Based on the average Nusselt number, the calculated fine-grid GCI was approximately 2.12%, indicating low mesh-related numerical uncertainty and confirming mesh-independent behavior of the numerical solution.

A notable reduction in error was observed with progressive mesh refinement. Although the finest mesh provided slightly lower numerical variation, the difference in the average Nusselt number between the meshes containing 392,205 and 557,168 nodes was only approximately 0.51%. Therefore, the mesh comprising 392,205 nodes (Figure 3.5) was selected for the numerical simulations because it provides a satisfactory balance between numerical accuracy and computational cost.

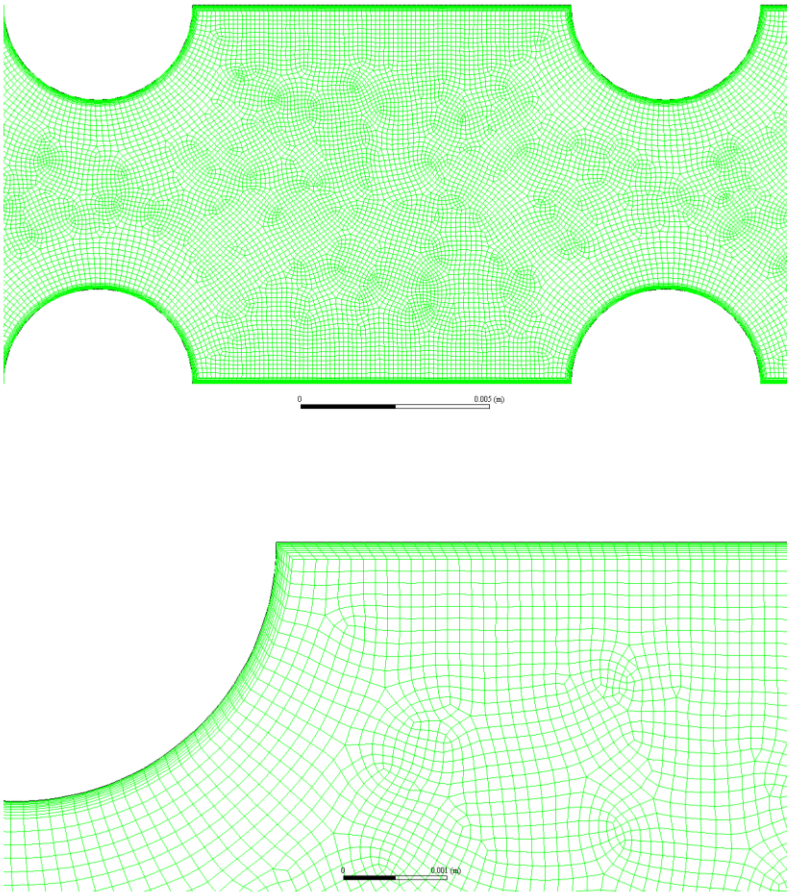

Figure 3.4 Computational mesh.

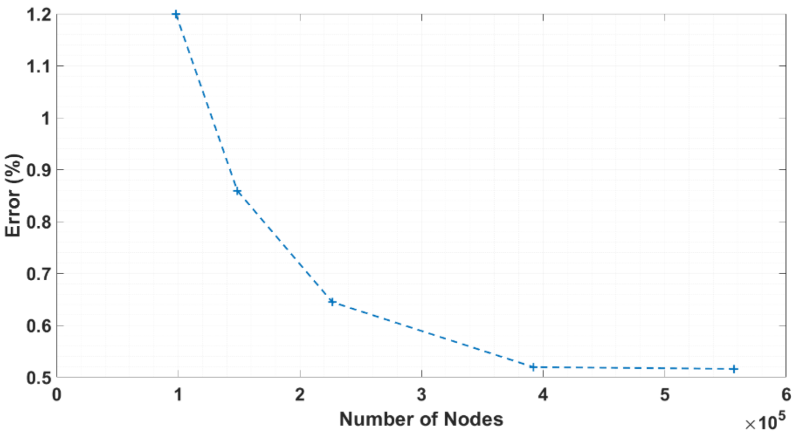

Figure 3.5 Variation of the relative error with the number of nodes.

3.4Convergence Behavior

The convergence behavior of the solver was tracked using the residuals of the continuity, momentum, and energy equations (2, 3, and 4). As illustrated in Figure 3.6, the residual plots for a representative simulation confirm that all residuals declined to adequately low magnitudes, ensuring the accuracy and stability of the numerical solutions. Furthermore, the stability of the solution was verified by tracking the h and ΔP, which showed consistent relative variations over the iterations, guaranteeing dependable values for the Nu and f.

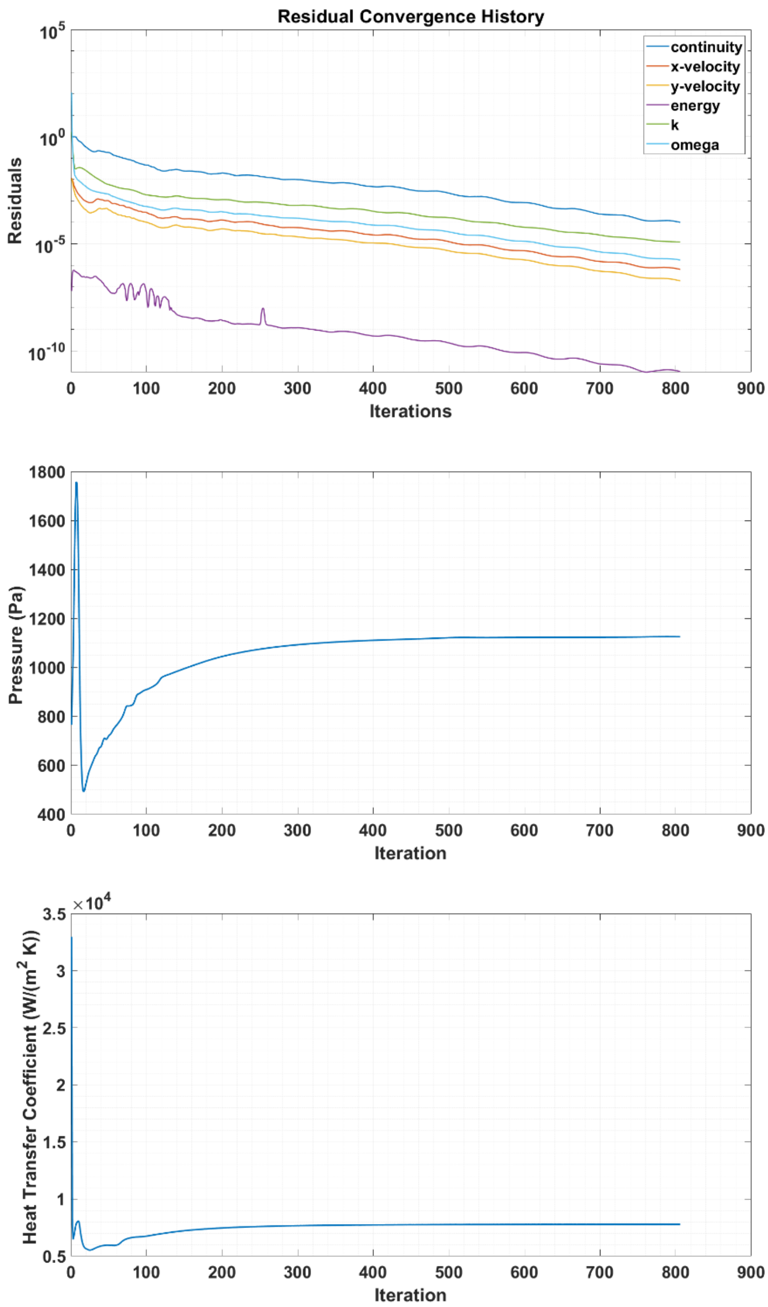

Figure 3.6 Convergence of residuals during the simulation.

3.5Validation

To ensure the reliability of the simulation results, a validation study was conducted prior to the main analysis. The model was compared with the experimental work of Ajeel et al. [18], who investigated a semi-circular corrugated channel under similar conditions. Figure 3.7 shows the variation in the average *Nu* over a *Re* range of 10,000–30,000, indicating that the numerical predictions are in good agreement with the experimental data. The average relative error between the numerical and experimental Nusselt number values was approximately 5.31%, while the maximum deviation remained below 8.55%, confirming the reliability of the present numerical methodology for predicting heat-transfer behavior in the corrugated channel without VGs. This close agreement validates the precision of the numerical setup and the suitability of the selected modeling method for estimating heat transfer in corrugated channels. It is important to note that this validation was conducted for the baseline case (channel without VGs). An additional comparison with a numerical study incorporating VGs [60] The comparison showed good agreement in the predicted thermal–hydraulic trends and heat transfer enhancement, indicating that the present numerical methodology can reasonably capture the dominant flow structures and vortex-induced mixing generated by the VGs, and further confirmed the robustness of the proposed numerical methodology. The comparison with the numerical study involving VGs showed an average relative error of approximately 4.04%, while the maximum deviation remained below 6.18%, further confirming the capability of the present numerical methodology to predict the thermal–hydraulic behavior of corrugated channels equipped with vortex generators. Moreover, the ΔP results obtained from the simulation were validated against experimental data [74], with deviations remaining below 13%, demonstrating the reliability of the hydraulic performance prediction (Table 3.1).

Overall, the validation procedure included thermal and hydraulic comparisons for the baseline corrugated channel, as well as additional verification for configurations involving vortex generators. The good agreement obtained in all cases confirms the capability of the present numerical methodology to predict the dominant thermal–hydraulic behavior of corrugated channels equipped with vortex generators within the investigated operating conditions. In addition, mesh-independence assessment and Grid Convergence Index (GCI) analysis were performed to further evaluate the numerical uncertainty and reliability of the computed results in cases where direct validation data were unavailable.

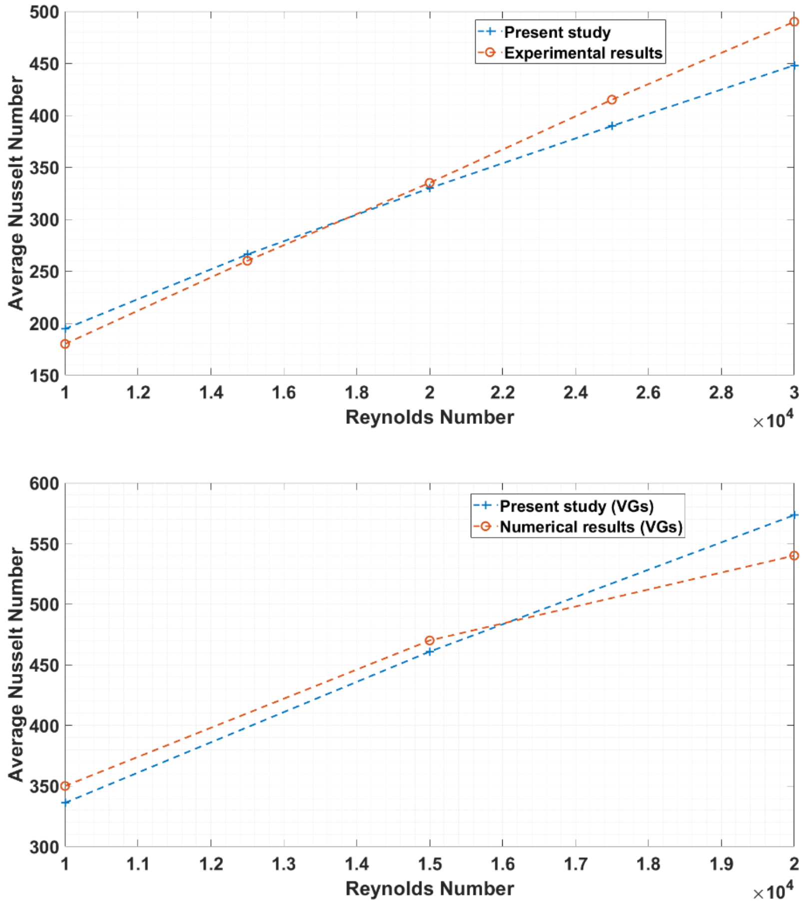

Figure 3.7 Validation of present CFD results against literature data: average Nu for channels with and without VGs.

Table 3.1 Validation of CFD pressure drop against experimental data for the baseline channel, showing percentage deviations.

Re	**Friction Factor *f***	***ΔP* Numerical (Pa)**	***ΔP* Experimental (Pa)**	**Difference %**
10000	0.0204	148	132	12.1%
20000	0.0153	450	400	12.5%
30000	0.0131	872	800	9.0%

4. EFFECT OF VORTEX GENERATOR TYPE

Chapter 4 presents a detailed analysis of the numerical results obtained for the corrugated channel equipped with VGs. Although vortex generators are widely recognized as effective passive heat-transfer enhancement devices, the influence of VG shape on the interaction between vortex-induced flow structures and the natural recirculation zones inside semi-circular corrugated channels remains insufficiently understood. In particular, limited attention has been given to achieving geometric consistency between the vortex-generator shape and the corrugated surface in order to improve fluid mixing while minimizing pressure losses. Therefore, this chapter investigates the effect of different VG geometries on the thermal–hydraulic behavior of the corrugated channel. The discussion begins with qualitative flow visualization, including velocity contours, streamlines, and vortex structures, to illustrate the fundamental flow mechanisms induced by different VG configurations. These observations are then supported by quantitative results through velocity profiles, wall shear stress, local heat transfer coefficients, and turbulent kinetic energy distributions. Finally, the thermal–hydraulic performance is evaluated using global parameters such as the Nusselt number, pressure drop, percentage enhancement, pressure ratio, and the performance evaluation criterion. This step-by-step analysis allows a clear understanding of how VGs influence the flow behavior and heat transfer characteristics in corrugated channels [P1].

Figure 4.1 presents the semi-circular corrugated channel equipped with the investigated vortex-generator geometries. Three VG configurations were considered: concave-up vortex generators (CUVGs), concave-down vortex generators (CDVGs), and straight vortex generators (SVGs). The VG dimensions and channel geometry were maintained identical to those described in Chapter 2 unless otherwise specified. The VG height and geometric dimensions were kept constant for all configurations to isolate the effect of the VG shape on the thermal–hydraulic performance. The vortex generators were positioned at the entrance of the corrugation section for all investigated cases. A uniform inlet velocity corresponding to Reynolds numbers between 10,000 and 30,000 was applied at the channel inlet, while a constant heat flux was imposed along the heated corrugated wall. The outlet was defined using a pressure-outlet boundary condition.

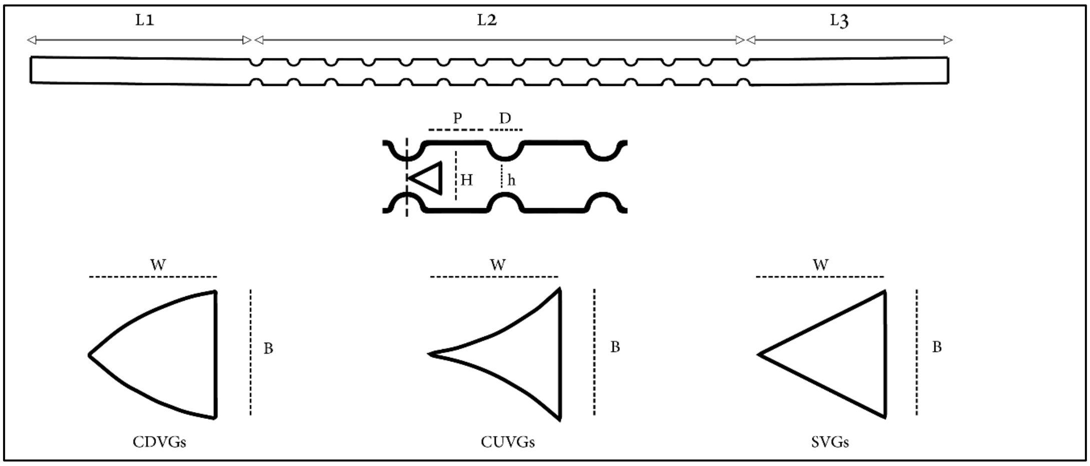

Figure 4.1 Schematic of the investigated vortex-generator geometries in the corrugated channel.

4.1Flow field characteristics

Figure 4.2 presents the velocity contours and streamlines for various VGs geometries. The fluid flow is concentrated in the middle of the channel, where recirculation zones, also known as dead zones, are observed. This behavior is primarily due to the pitch of the corrugated section. The introduction of VGs alters the flow direction, directing the fluid toward the channel walls and thereby enhancing the contact between the fluid and the wall surface. Each VGs geometry influences the flow differently. The CUVGs guide the flow more smoothly along the corrugated wall, while still showing small recirculation zones in the corners of the corrugation. This smoother flow guidance promotes stronger near-wall mixing and more effective thermal boundary-layer disruption. The CDVGS, on the other hand, creates larger recirculation zones in the corners and boosts the velocity within the pitch region. However, the larger corner vortices reduce the effectiveness of fluid interaction near the heated wall compared with the CUVGs. The SVGs provides a balanced performance between the CUVGs and CDVGs. In contrast, the VGs in general tend to generate an additional recirculation region in the channel core, which contributes to a higher pressure drop. These VGs induce secondary flows and swirling motion, which intensify mixing in the channel and disrupt the thermal boundary layer along the walls. This enhancement of fluid-wall interaction promotes convective heat transfer, leading to higher local and overall heat transfer rates. The regions of increased velocity and turbulent kinetic energy downstream of the VGs further confirm the mechanism by which heat transfer is improved, despite the accompanying pressure drop penalty [P1].

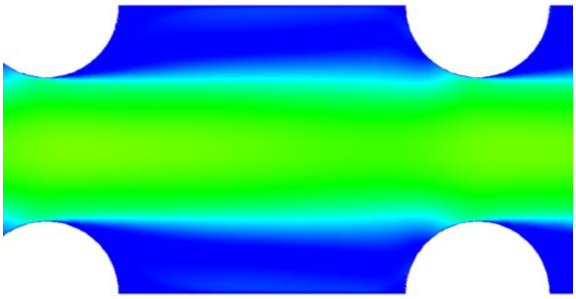

WVGs

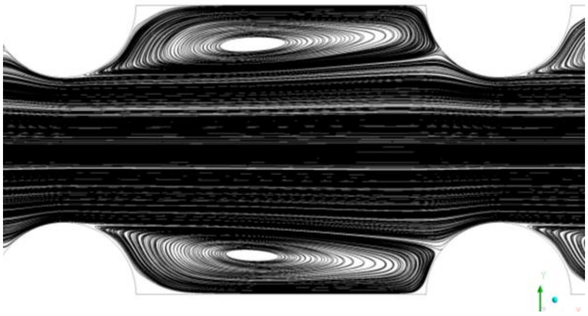

WVGs

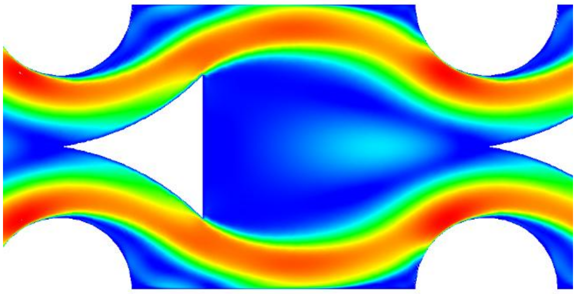

CUVGs

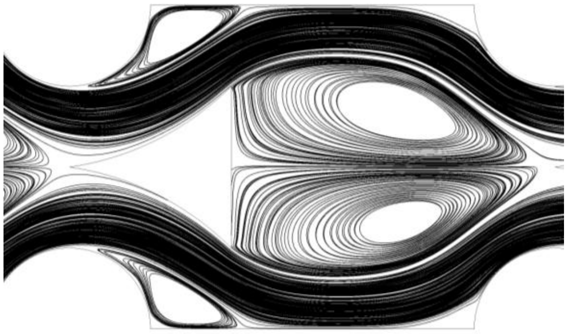

CUVGs

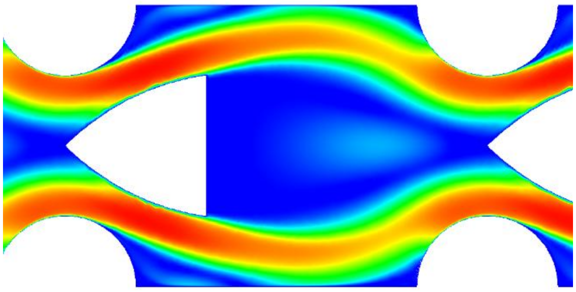

CDVGs

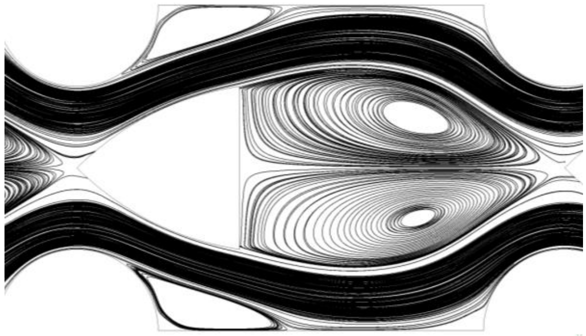

CDVGs

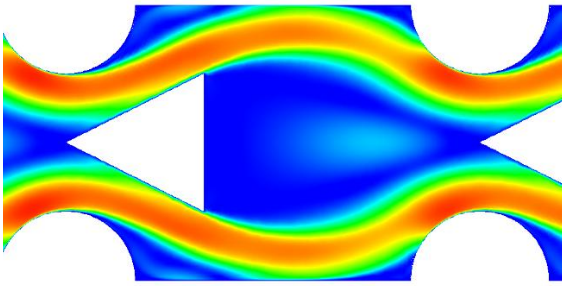

SVGs

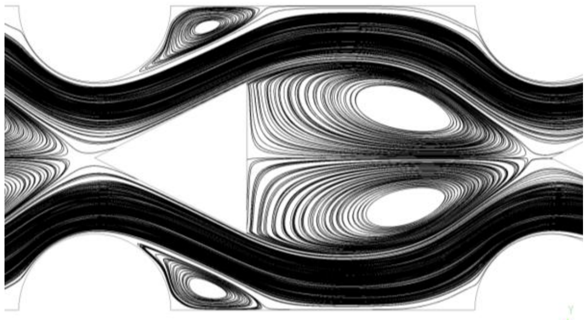

SVGs

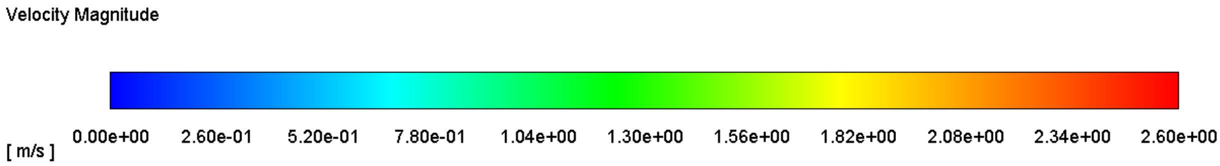

Figure 4.2 Velocity contours and streamlines for different VG types [P1].

4.2Vortex structure analysis

Figure 4.3 presents the vorticity magnitude contours for the different VG shapes. The vorticity inside the channel is generally higher at the pitch of the corrugated section, which leads to the formation of recirculation zones near the walls. The insertion of VGs increases the vorticity further, while simultaneously redirecting the fluid toward the heated walls and generating additional vortical structures around the VG corners. The CUVGs exhibit higher vorticity values at their corners, resulting in a larger recirculation zone downstream of the VG. These stronger vortical structures enhance near-wall mixing and contribute to more effective disruption of the thermal boundary layer. In contrast, the CDVGs intensify the vorticity at the pitch of the corrugated section, which explains why the recirculation zone at the corrugated corner (see Figure 4.2) is larger for CDVGs compared to the other configurations. This indicates that part of the flow energy in the CDVG configuration is concentrated within the corner recirculation regions rather than being utilized for near-wall heat transfer enhancement [P1].

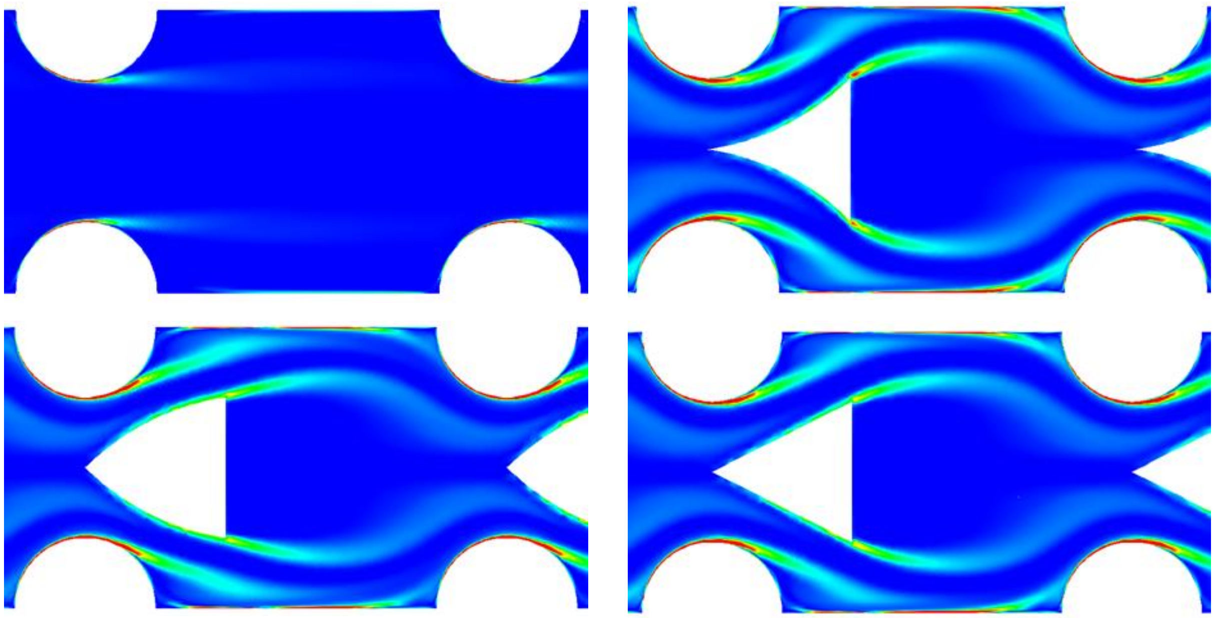

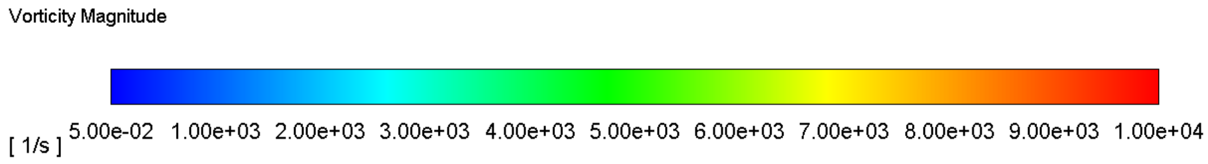

Figure 4.3 Vorticity magnitude contours for different VG types [P1].

Figure 4.4 shows the vorticity distribution along the channel height at three representative streamwise locations: the entrance, middle, and exit of the corrugation. In the channel without VGs, the highest vorticity occurs at the entrance of the corrugation, primarily due to the pitch, which induces a strong recirculation zone. When VGs are installed, the vorticity increases significantly, especially at the middle of the corrugation where the VGs are located, indicating stronger vortex generation and enhanced momentum exchange within the channel core. At the entrance, the vorticity is elevated due to the combined effects of the pitch and upstream flow, while at the exit, the vorticity decreases as the flow relaxes downstream. The streamlines in Figure 4.2 clearly illustrate the formation of secondary flows induced by the VGs, and the corresponding heat transfer coefficient at the wall shows enhancement in regions of elevated vorticity, confirming that secondary flows contribute directly to thermal performance improvements. Other VG types show similar behavior, which is why only the CU-VG type is presented here for clarity [P1].

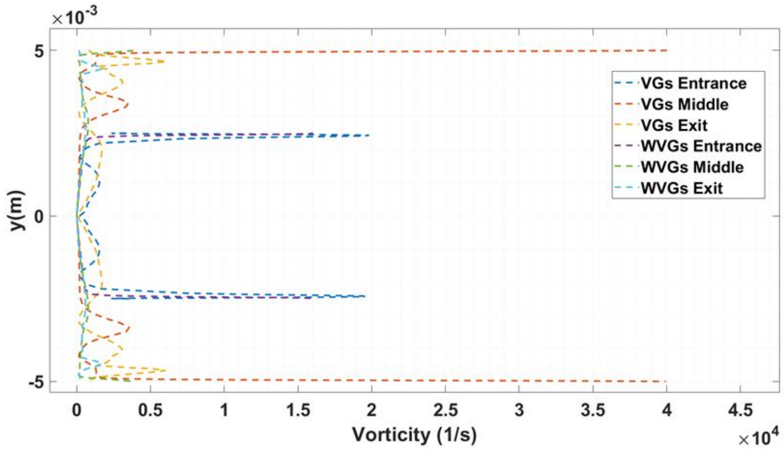

Figure 4.4 Vorticity distribution along the channel height at the entrance, middle, and exit of the corrugation [P1].

4.3Near-wall flow behavior

Figure 4.5 presents the wall shear stress along the bottom corrugated section as a function of *x* (m). For the channel without VGs, the shear stress is highest near the entrance, then decreases, reaching its lowest values at the corners after the pitch, which can be considered dead zones. The use of VGs increases the shear stress, especially at the middle of the channel. This increase is caused by stronger near-wall flow acceleration and enhanced momentum exchange generated by the vortical structures. This behavior is directly related to the local *h*: greater fluid contact with the wall produces higher shear stress, which enhances heat transfer (Figure 4.6). Higher wall shear stress also indicates thinning of the viscous and thermal boundary layers, allowing more efficient heat transfer between the wall and the fluid. The CUVGs increase the shear stress mainly at the middle of the corrugation, while the CDVGs produce higher shear stress near the entrance of each corrugation section (Table 4.1). This difference reflects the distinct vortex distribution generated by each VG geometry and explains the variation in their thermal–hydraulic performance. [P1].

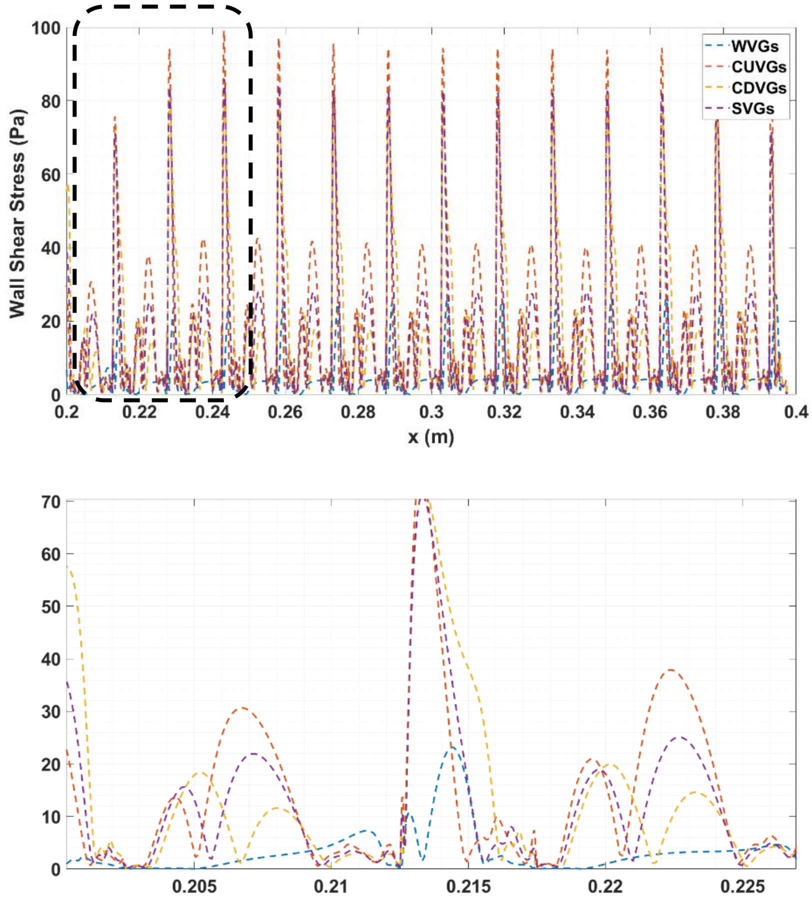

Figure 4.5 Distribution of wall shear stress along the corrugated section [P1].

Table 4.1 Peak wall shear stress and average trend for different VG types [P1].

Case	Peak wall shear stress (Pa)	Average trend (approx.)
WVGS	~20–25	~1.0
CUVGs	~90–100	~2.5–2.7
CDVGs	~80–85	~2.2–2.3

SVGs	~70–75	~2.0–2.1

Figure 4.6 shows the local *h* along the lower corrugated wall for the different VG geometries, plotted against the streamwise distance (x-axis). This representation highlights how the coefficient varies along the channel length and how the VG shapes influence the local distribution. In the case of the channel WVGs, the local *h* is highest at the entrance of each corrugation (the pitch) and decreases toward the middle of the corrugated wall. The use of VGs increases the heat transfer coefficient at the center of the corrugated wall, resulting in more uniform heat transfer along the corrugated section. The peak of the *h* occurs at the middle of the corrugation, which corresponds to the region of increased vorticity induced by the VGs, as shown in Figure 4.4. This behavior confirms that stronger vortical structures enhance momentum exchange and continuously disrupt the thermal boundary layer near the heated wall. The CDVGs improves the *h* notably around the pitch, while the CUVGs enhances it just after the entrance of the corrugation, where the geometry redirects the flow more effectively toward the wall. The smoother curvature of the CUVGs promotes stronger near-wall mixing and more stable vortex development, which explains their superior local heat transfer performance. The SVGs provides average values, with values falling between those of the other two types. This enhancement in heat transfer is supported by the hydraulic effect observed in the velocity contours and streamlines, where the increased contact between the fluid and the wall is evident. The local *h* values were extracted from the profiles (Figure 4.6) and summarized in Table 4.2. It is evident that CUVGs achieve the highest local peaks (~2.7×10^4 W/m²K), followed by CDVGs and SVGs, while the baseline case remains significantly lower (~1.9×10^4 W/m²K) [P1].

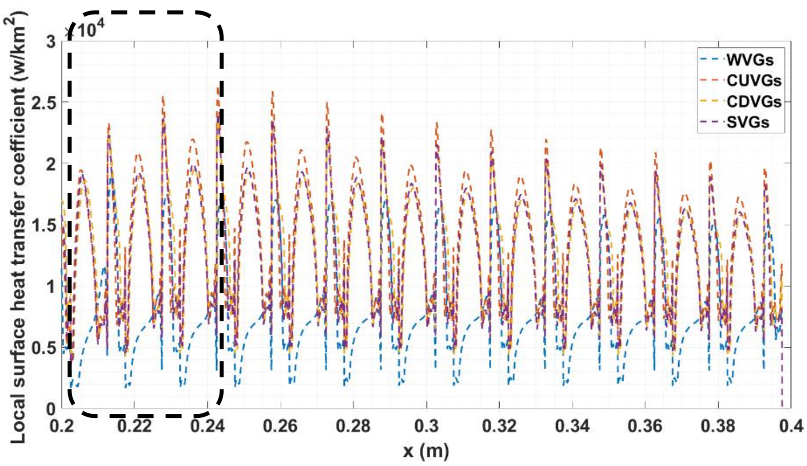

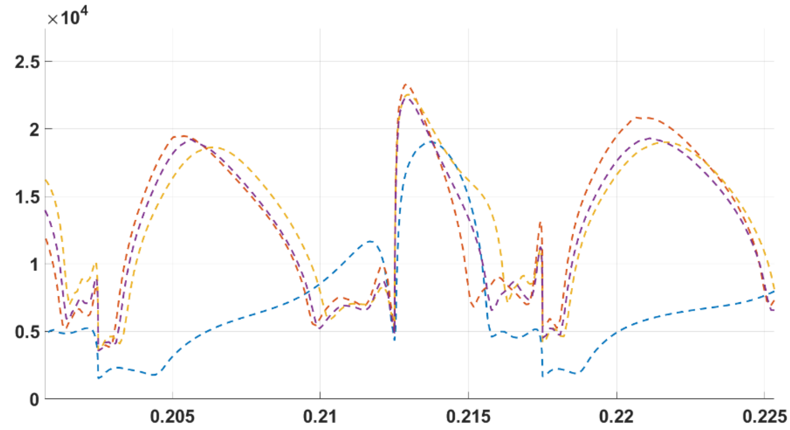

Figure 4.6 Distribution of local heat transfer coefficient along the corrugated section [P1].

Table 4.2 Peak local heat transfer coefficient and average trend for different VG types [P1].

Case	Peak local h (×10⁴ W/m²K)	Average trend (approx.)
WVGS	~1.9	~1.0
CUVGs	~2.6–2.7	~1.7–1.8
CDVGs	~2.3–2.4	~1.5–1.6
SVGs	~2.1–2.2	~1.4–1.5

4.4Velocity and turbulence characteristics

Figure 4.7 presents the x-velocity profile and turbulent kinetic energy along a vertical line located at the mid-length of the corrugated section (y-axis direction). This illustrates how the flow develops across the channel height and how VGs affect the velocity distribution and turbulence intensity. The velocity is higher at the center of the channel where the fluid flow is concentrated. The presence of VGs alters the velocity profile, reducing the velocity in the center and increasing it near the walls. This redistribution of velocity indicates that the VGs redirect part of the core flow toward the heated surfaces, which enhances fluid–wall interaction and weakens the low-velocity regions near the corrugated walls. All three types exhibit similar effects, with slight differences. Notably, the CUVGs shows higher velocity values compared to the other configurations. This behavior is associated with the smoother flow guidance produced by the concave-up geometry, which accelerates the flow more effectively along the corrugated wall.

The VGs also increases the turbulent kinetic energy within the channel, thereby enhancing heat transfer. The CDVGs generates more turbulence near the walls due to the difference in movement between the wall and the fluid. At the same time, the CUVGs increases turbulence in the central region, specifically in the layer between the recirculation zone and the main fluid flow. This interaction region promotes stronger momentum exchange between the recirculating flow and the high-velocity core flow, leading to more effective thermal boundary-layer disruption. This comparison is made at the middle of the corrugated wall. The SVGs generates less turbulence compared to the other two types [P1].

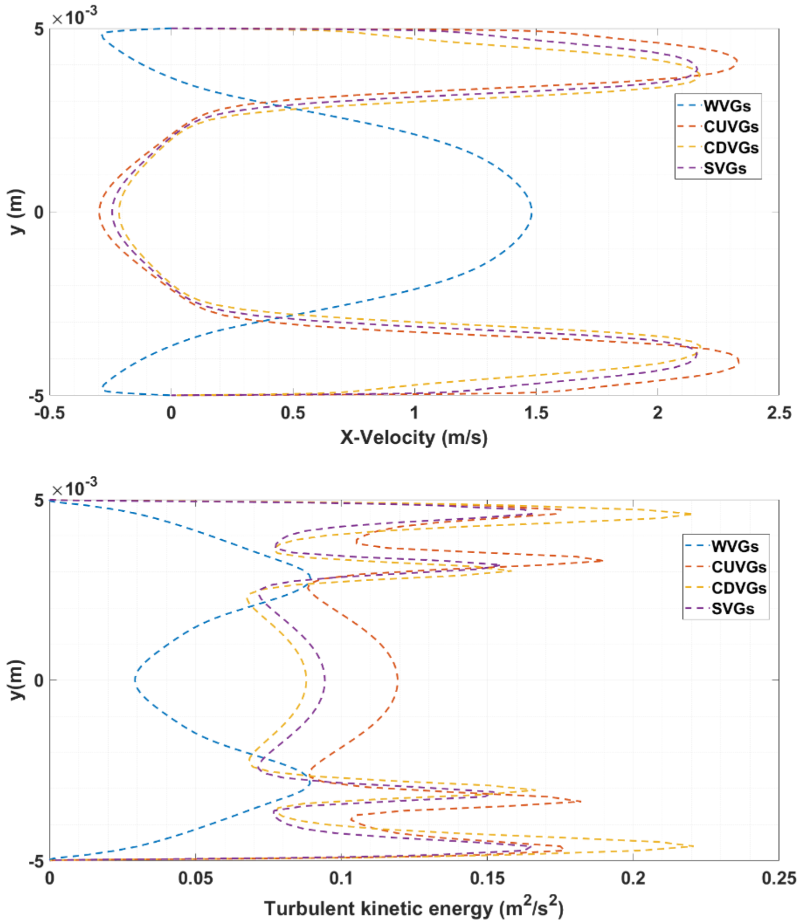

Figure 4.7 Profiles of x-velocity and turbulent kinetic energy along a vertical line at the mid-length of the corrugated section [P1].

4.5Global thermal and hydraulic performance

Table 4.3 Overview of average Nu and pressure drop for various VG types across different Re [P1].

	Nu				**Δ*P***			
Re	WVGs	CUVGs	CDVGs	SVGs	WVGs	CUVGs	CDVGs	SVGs
10000	194.45	336.1	326.56	318.3	1123.93	8191.48	7432.96	6625.37
15000	266.09	460.78	446.34	435.95	2503.78	17921.05	16200.42	14432.04

20000	329.86	573.39	565.94	541.76	4336.47	30374.9	27663.45	24575.09
25000	389.69	680.64	659.49	643.91	6637.79	45502.82	41990.26	37097.41
30000	448.08	791.71	765.35	746.15	9457.5	63726.09	59362.92	52307.76

Figure 4.8 illustrates the variation of the average *Nu* and ΔP with the *Re* in the corrugated section. This representation highlights how both thermal and hydraulic performance change with increasing flow rates. The *Nu* (Equation (9)) and ΔP (Equation (8)) both rise with increasing *Re* due to higher velocities, which improve heat transfer, while viscosity has a greater effect. The use of VGs increases the average *Nu*, which can be explained by the rise in local heat transfer coefficient. The CUVGs exhibits the highest Nusselt number, followed by the CDVGs and then the SVGs. This superior performance of the CUVGs is associated with their ability to generate stronger and more stable vortices while directing the flow more effectively toward the heated corrugated wall. The ΔP shows a similar trend, increasing with *Re*. As seen earlier, the fluid interacts with the VGs and creates recirculation zones behind them, which is the main reason for the rise in ΔP [P1].

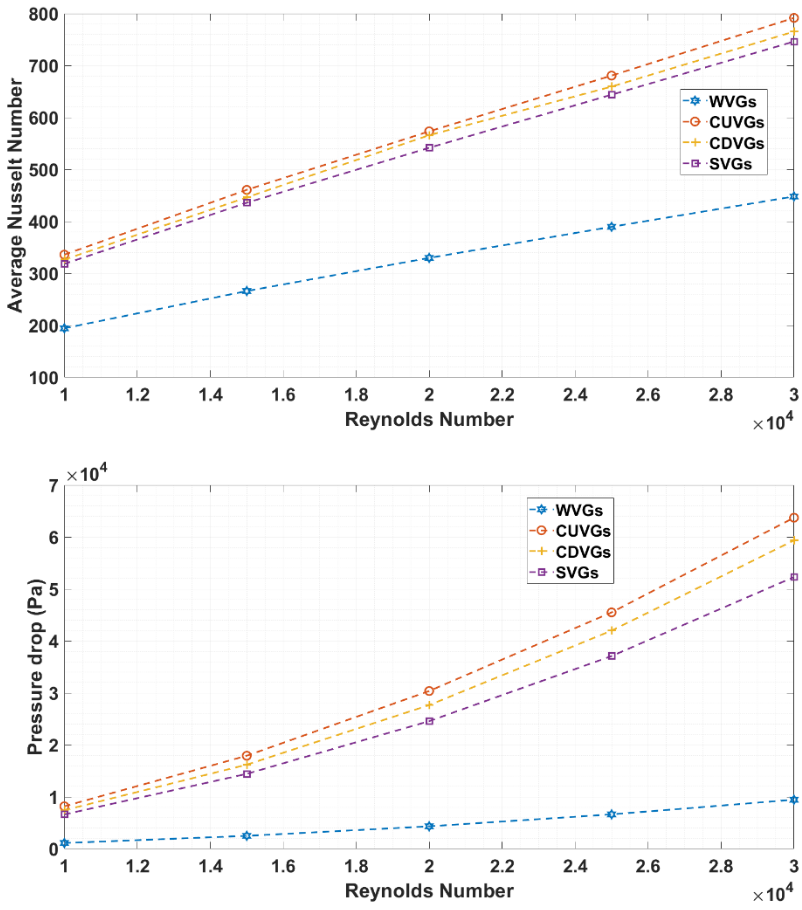

Figure 4.8 Variation of the average Nu and pressure drop with Re for different VG types [P1].

4.6Performance enhancement and pressure ratio

We compare the Nusselt number enhancement and pressure drop increase caused by using VGs relative to the case without VGs. The results are expressed as percentage enhancement (Equation (13)) for *Nu* and as a pressure drop ratio (Equation (12)), plotted against the *Re*, as shown in Figure 4.9. Heat transfer is improved by the use of VGs, with CUVGs showing the greatest enhancement, reaching up to 77%, followed by CDVGs and SVGs, with the lowest improvement reaching around 63%. The superior enhancement obtained with the CUVGs is attributed to the stronger vortex structures and improved near-wall flow redirection generated by the concave-up geometry, which intensify thermal boundary-layer disruption along the corrugated wall. The pressure drop increases by about 7 times with CUVGs, about 6.5 times with CDVGs, and less than 6 times with SVGs. This increase is mainly associated with stronger flow blockage, vortex formation, and momentum dissipation generated by the VGs inside the corrugated section. The enhancement in heat transfer comes with the cost of increased pressure drop. The baseline Nusselt number without VGs is moderate for the corrugated channel in this *Re* range, providing a meaningful reference for assessing the absolute improvement [P1].

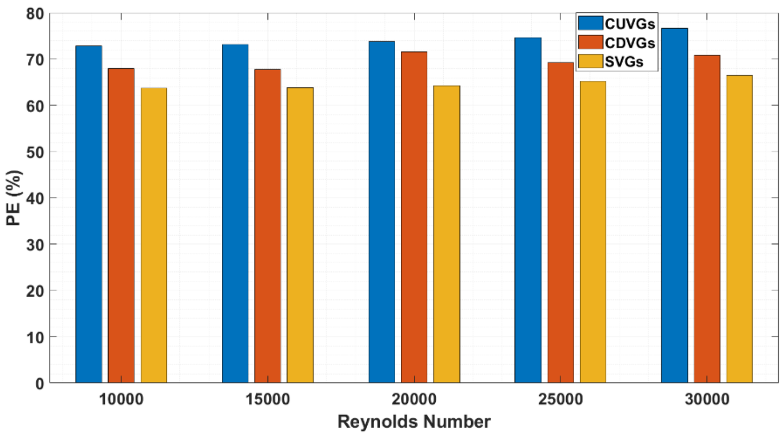

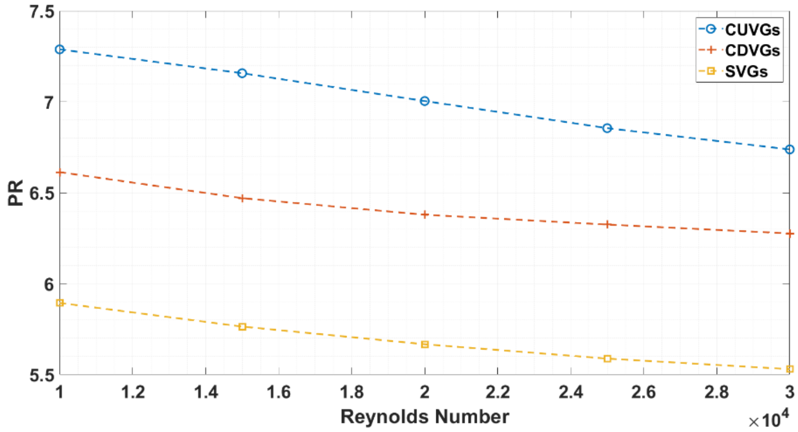

Figure 4.9 Variation of PE and PR with Re for different VG types [P1].

4.7Overall performance evaluation

Figure 4.10 illustrates the variation of the PEC with *Re* for different VG geometries. This representation highlights the balance between heat transfer enhancement and pressure drop increase, showing how each VG type performs across the range of *Re* according to Equation (14). The PEC rises with increasing *Re*, which means that the VGs offer better enhancement relative to the pressure drop at higher *Re*. At higher Re, the generated vortical structures become stronger and more effective in disrupting the thermal boundary layer, while the relative influence of viscous losses decreases. The PEC values are between 0.89 and 0.94, which is close to one. These values are considered good for keeping balance between the gain in heat transfer and the loss in pressure drop. In practical heat exchanger design, a PEC above 0.9 is generally considered worthwhile, indicating significant thermal performance improvement without excessive hydraulic penalty. The SVGs shows greater balance compared to the other types, except at one point where the CDVGs is higher at *Re* = 20,000. This behavior suggests that the SVG configuration generates moderate vortex intensity with lower flow resistance, whereas the CUVGs and CDVGs produce stronger vortical structures accompanied by larger hydraulic losses. If we just consider the heat transfer enhancement, the CDVGs gives better effect in the range *Re* = 10,000–24,000, and the CUVGS in the range 24,000–30,000 [P1].

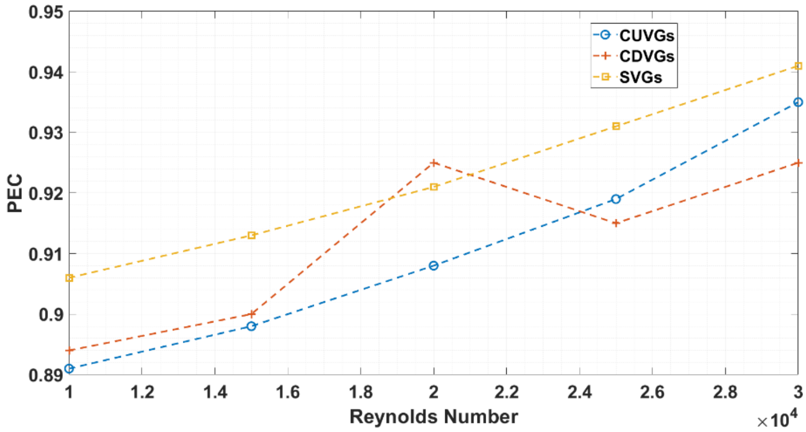

Figure 4.10 Variation of PEC with Re for different VG types [P1].

These findings demonstrate that vortex generators can significantly improve the thermal performance of semi-circular corrugated channels by enhancing fluid mixing and disrupting the thermal boundary layer. Among the investigated configurations, the CUVGs provided the highest heat-transfer enhancement because their geometry directed the flow more smoothly toward the corrugated wall, increasing fluid–wall interaction and generating stronger secondary vortices near the heated surface. This behavior reduced the thermal boundary-layer thickness and improved convective heat transfer more effectively than the CDVG and SVG configurations. The study also showed that achieving geometric consistency between the vortex-generator profile and the corrugated wall can improve vortex-induced mixing and thermal performance in compact corrugated channels. These observations provide useful guidance for the design of enhanced compact heat exchangers where thermal performance and pressure-drop balance are important considerations.

5. EFFECT OF VORTEX GENERATOR SIZE

Although vortex generators are widely used to improve heat transfer, the effect of VG size on the interaction between vortex-induced flow structures and the recirculation zones inside semi-circular corrugated channels remains insufficiently understood. In particular, increasing the VG size may enhance fluid mixing and wall interaction, but it can also produce a considerable pressure-drop penalty. Therefore, identifying an appropriate VG size that provides effective thermal enhancement while maintaining acceptable hydraulic performance is still an important challenge. This chapter investigates the influence of VG size on the thermal and hydraulic behavior of the corrugated channel. After identifying the most suitable VG shape in the previous chapter, the size is treated here as a key geometric parameter controlling flow disturbance and boundary layer development. The analysis begins with isotherm contours and streamlines to illustrate how different VG sizes modify the flow structure and thermal fields. This is followed by a detailed examination of wall shear stress, local heat transfer coefficient, velocity distribution, and turbulent kinetic energy. Finally, the global performance is evaluated using the average Nusselt number, pressure drop, percentage enhancement, pressure ratio, and performance evaluation criterion (PEC), allowing a clear assessment of the trade-off between heat transfer enhancement and hydraulic penalty associated with increasing VG size [P10].

Figure 5.1 presents the semi-circular corrugated channel equipped with vortex generators of different sizes. The VG size parameter S was varied while maintaining the remaining geometric dimensions and operating conditions identical to those described in Chapter 2. Three VG sizes (S=2, 4, and 6 mm) were investigated to evaluate the influence of the VG dimension on the flow structure and thermal–hydraulic performance. A uniform inlet velocity corresponding to Reynolds numbers between 10,000 and 30,000 was applied at the channel inlet, while a constant heat flux was imposed along the heated corrugated wall. The outlet was defined using a pressure-outlet boundary condition.

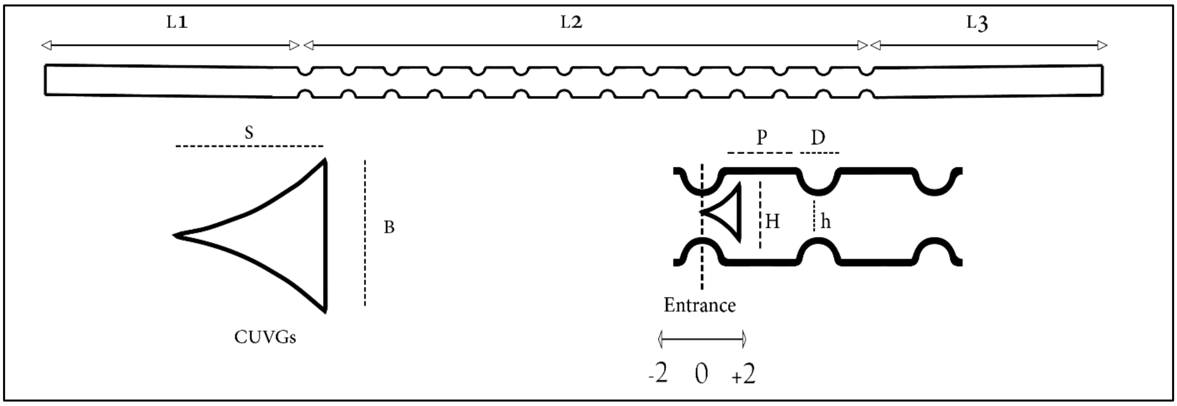

Figure 5.1 Definition of the vortex-generator size parameter S.

5.1Isothermal and flow visualization

Figure 5.2 shows the isotherm contours and streamlines for different VG sizes. In the corrugated section without VG. The channel pitch generated a recirculation zone in the channel. which acts as a dead zone for the fluid. This region was clearly visible in the isotherm contours as a thick, thermal boundary layer. This behaves like an insulating layer and reduces the heat transfer efficiency of the system. When VGs is introduced. The thermal boundary layer becomes thinner, leading to better heat transfer. Even at the smallest size (S = 2 mm). The effect on the thermal boundary layer can be observed. and as the size increases. The layer became progressively thinner (S = 6 mm). This behavior indicates that larger VGs generate stronger vortical structures and promote greater momentum exchange between the core flow and the near-wall region. The VGS redirect the flow direction by disrupting the large recirculation zone attached to the wall. However, they simultaneously create new recirculation zones downstream of VGS. These downstream vortices intensify mixing and continuously refresh the fluid near the heated surface, but they also increase momentum dissipation inside the channel. For small VG sizes. the induced recirculation occurs mainly in the middle of the channel. leaving a larger stagnant zone at the corrugation corners. As the VG size increases, the central recirculation becomes stronger, while the dead zones near the corrugated corners are reduced. This demonstrates that larger VGs interact more effectively with the natural recirculation generated by the corrugated geometry, resulting in stronger suppression of low-velocity regions and more uniform thermal behavior along the wall. [P10].

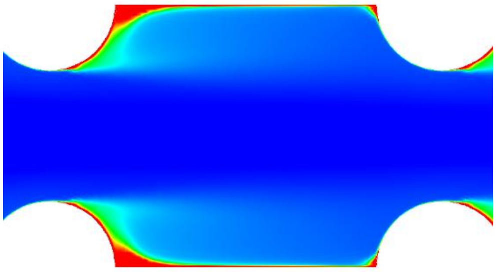

WVGs

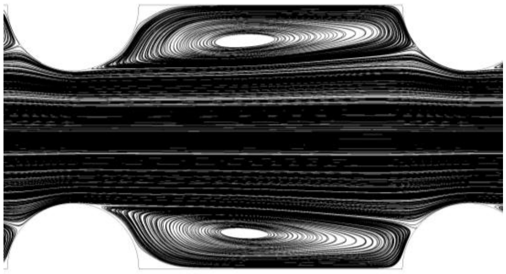

WVGs

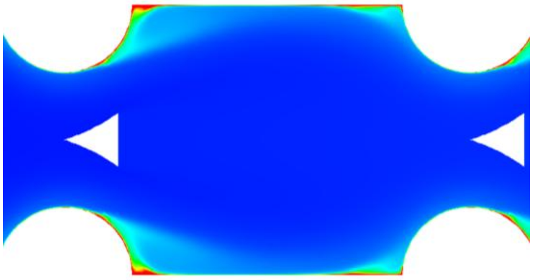

***S*=2**

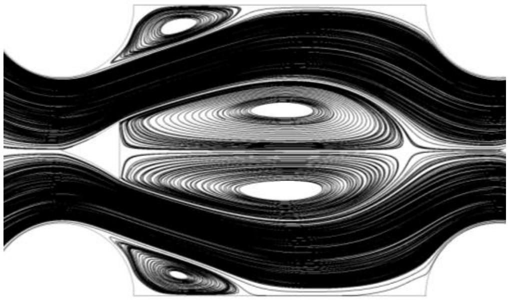

***S*=2**

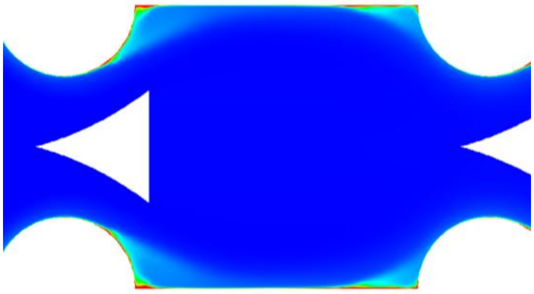

***S*=4**

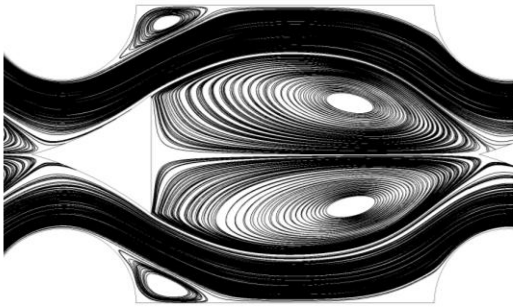

***S*=4**

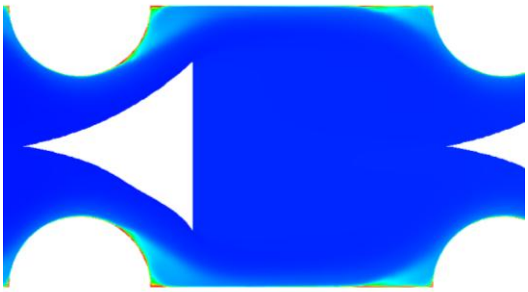

***S*=6**

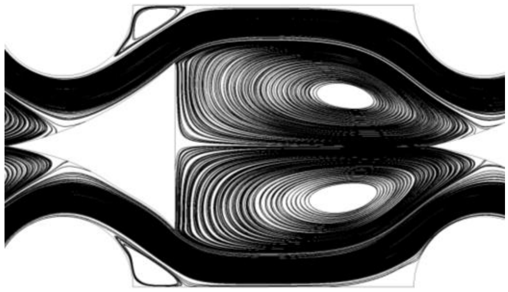

***S*=6**

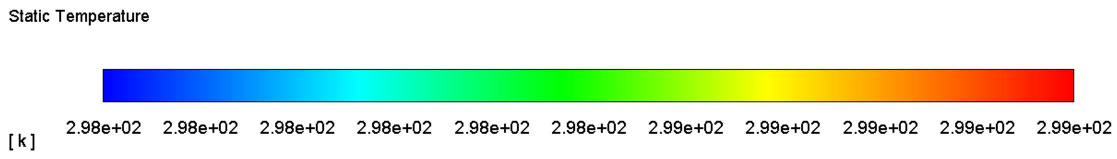

Figure 5.2 Isotherm contours and streamlines showing the effect of different VG sizes [P10].

5.2Near-wall flow characteristics

Figure 5.3 shows the variation in the wall shear stress along the bottom corrugated section as a function of *x*. In the case without VGs. The shear stress follows a wave-like distribution and reaches its highest value at the corrugation pitch. When VGs is introduced. The shear stress increased and became more uniform along the corrugated wall as the VG size increased. This behavior is associated with stronger near-wall flow acceleration and improved fluid–wall interaction. For small VG sizes, the effect was more localized near the pitch region, indicating limited influence over the middle of the corrugated wall. As the VG size increases. The shear stress increased significantly along the entire wall. This shows that larger VGs affect a wider portion of the flow field and interact more effectively with the corrugation-induced recirculation. The peak shear stress values for each case are summarized in Table 5.1 [P10].

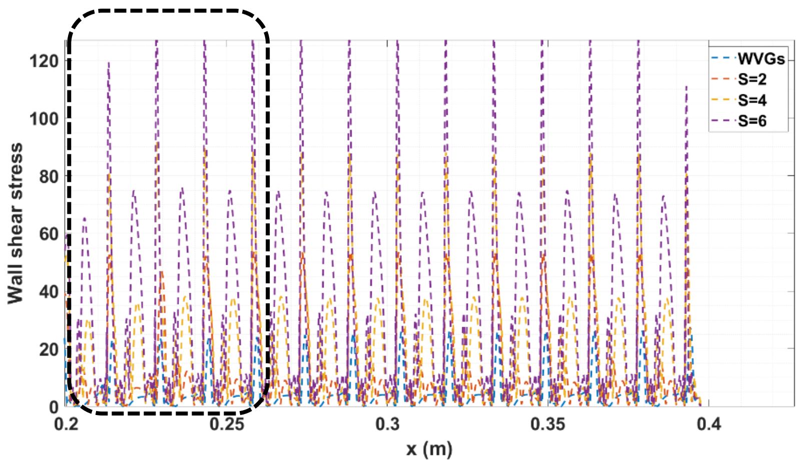

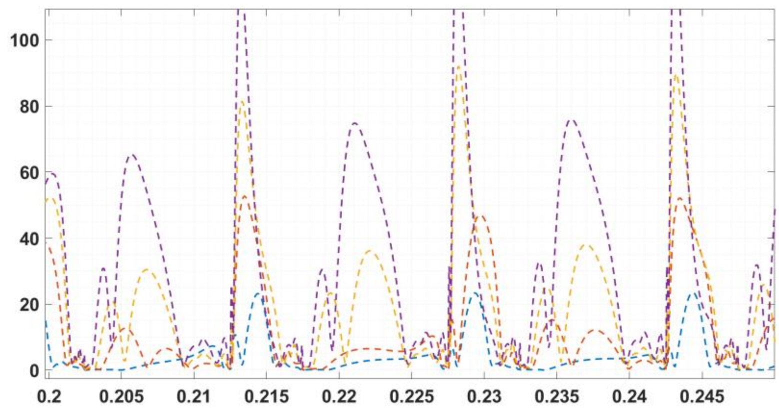

Figure 5.3 Distribution of wall shear stress along the corrugated section [P10].

Table 5.1 Peak wall shear stress along the corrugated wall [P10].

Case	Peak shear stress (Pa)	Average trend (approx.)
WVGS	~20–25	Localized at corrugation pitch
***S* = 2**	~40–50	Higher near pitch. limited spread
***S* = 4**	~70–80	Increased along wall. more uniform
***S* = 6**	~110–120	Strong and nearly uniform along wall

Figure 5.4 shows the local *h* along the lower corrugated section as a function of *x*. The local *h* exhibited a trend similar to that of wall shear stress, confirming the strong relationship between near-wall flow behavior and local heat transfer enhancement. In the case without VGs. The coefficient reaches higher values only at the pitch of the corrugation. where the flow had a better contact with the wall. When the VGs was introduced, the *h* increased not only at the pitch but also in other parts of the corrugated wall. This demonstrates the key role of the VGs, which made the heat transfer distribution more uniform. This significantly improves the overall thermal performance. The size of VGs also plays an important role. A smaller VGs primarily enhanced the heat transfer near the pitch. A larger VGs increases the effect along almost the entire corrugated wall. This indicates that larger VGs generate a wider flow interaction region and suppress low-velocity zones more effectively. However. One limitation is that the VGs cannot fully eliminate blind spots at the corrugation corners. where it is difficult to achieve peak heat-transfer efficiency. The peak local heat transfer coefficients for the different cases are summarized in Table 5.2 [P10].

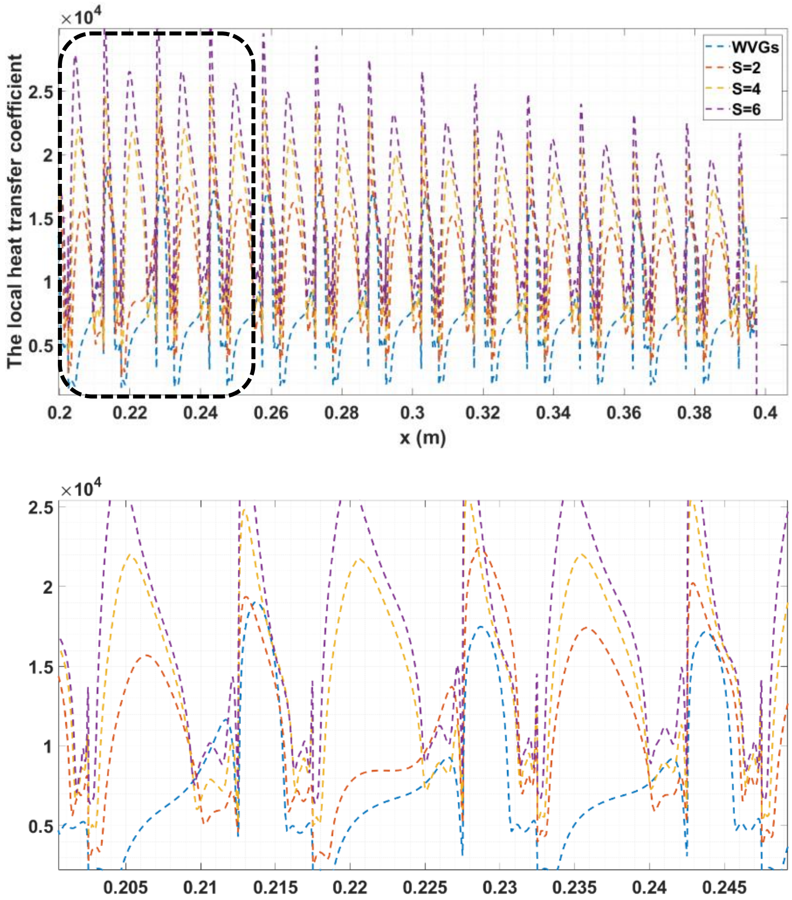

Figure 5.4 Distribution of the local heat transfer coefficient along the corrugated section [P10].

Table 5.2 Peak local heat transfer coefficient along the corrugated wall [P10].

Case	**Peak local *h* (×10⁴ W/m²K)**	**Average trend (approx.)**
WVGS	~0.9–1.0	Peaks only at pitch. weak elsewhere
***S* = 2**	~1.6–1.7	Localized near pitch. limited spread
***S* = 4**	~2.0–2.1	Higher along wall. moderate uniformity
***S* = 6**	~2.6–2.7	Strong. nearly uniform along wall

5.3Velocity and Turbulence Characteristics

Figure 5.5 shows the x-velocity and turbulent kinetic energy (TKE) profiles along the vertical line at the center of the corrugated section. Before adding VGs. the x-velocity profile was parabolic. with the flow concentrated at the channel center. After introducing VGs. The flow separated near the top and bottom walls of the channel. This increased the velocity near the wall. This redistribution of the flow weakens the stagnant regions near the corrugated surfaces and promotes stronger fluid–wall interaction. However, it simultaneously increased the shear stress. Negative velocity values appeared in the profiles owing to recirculation zones. This indicates that the fluid moved in the opposite direction. As the VG size increases. The velocity near the walls also increased. providing a greater contact surface for heat transfer, but also intensifying the shear effects. The turbulent kinetic energy was much lower in the case without VGs than in the cases with VGs. The presence of the VGs significantly increased the turbulence. This is particularly evident when comparing the turbulence profiles with the streamlines shown in Figure 5.2. Larger VG sizes resulted in higher turbulence levels because of the stronger vortical structures generated within the channel. These stronger vortices enhance momentum exchange and thermal boundary-layer disruption more effectively, which explains the improved thermal performance obtained with larger VG sizes. [P10].

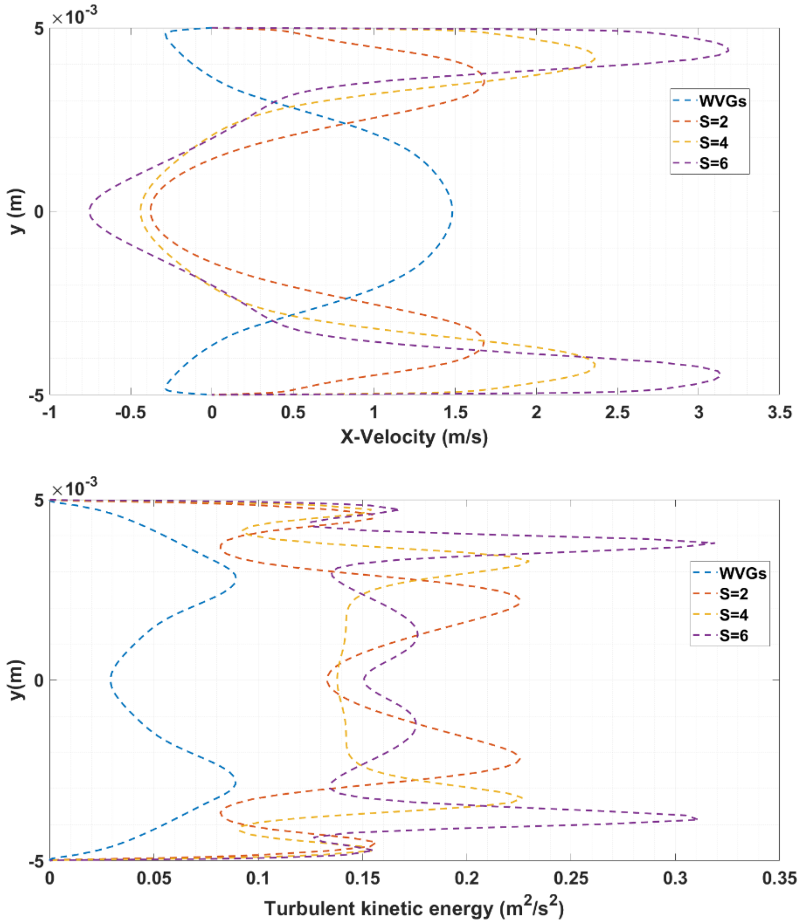

Figure 5.5 Profiles of x-velocity and turbulent kinetic energy along the vertical line at the mid-length of the corrugated section [P10].

5.4Global Thermal and Hydraulic Performance

Table 5.3 Overview of average Nu and pressure drop for various VG sizes across different Re [P10].

	Nu				**Δ*P***			
Re	WVGs	S=2	S=4	S=6	WVGs	S=2	S=4	S=6
10000	194.45	282.238	342.99	395.8	1123.93	5167.289	8536.781	14323.97
15000	266.09	385.66	472.27	550.82	2503.78	11535.48	18784.33	31347.72
20000	329.86	478.77	589.47	695.04	4336.47	19880.08	32225.44	53480.68
25000	389.69	569.4	703.97	839.29	6637.79	30370.92	48969.57	80970.46
30000	448.08	659.28	821.41	986.5	9457.5	43325.36	69414.89	114600

Figure 5.6 shows the variation in the average *Nu* and Δ*P* as a function of the *Re*. The *Nu* is directly related to the heat transfer coefficient (see Equation 9). This is because the VGs enhances the local *h*. They also increased the average *Nu*. As the VG size increases. the average *Nu* increased accordingly. Larger VGs generate stronger flow disturbances and wider vortex interaction regions, which improve near-wall mixing and thermal boundary-layer disruption. In addition. the *Nu* increases with the *Re.* reflecting the effect of the higher flow velocity on strengthening the heat transfer. On the other hand. The Δ*P* was also significantly affected by VGs. Compared to the case without VGs. The Δ*P* was significantly higher, particularly at large *Re*. This difference is mainly due to the viscous effects and recirculation zones generated by the VGs (see Figure 5.2). As the VG size increases, the intensified vortical structures produce greater momentum dissipation inside the channel, leading to larger hydraulic losses. The key results are presented in Table 5.3 [P10].

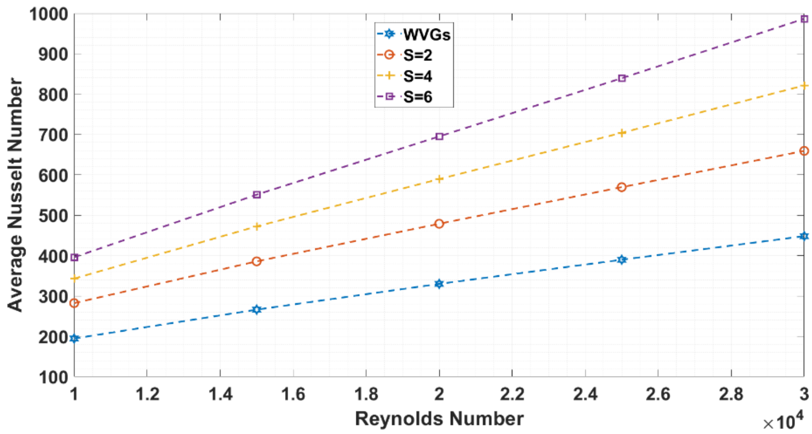

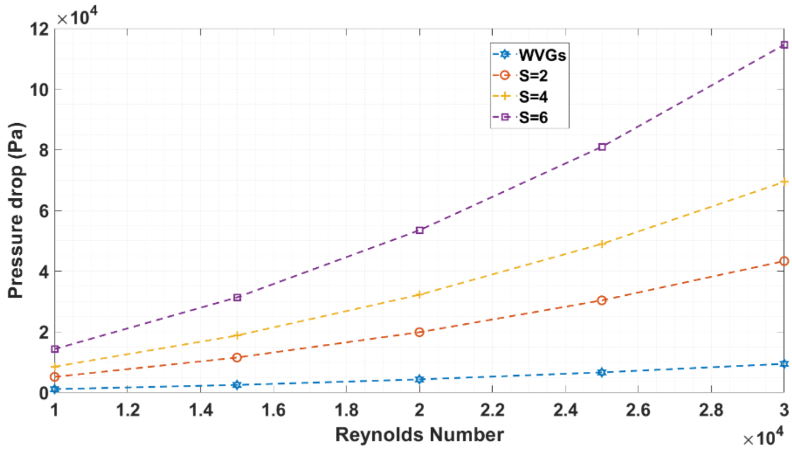

Figure 5.6 Variation of average Nu and pressure drop with Re for different values of VG size [P10].

5.5Performance Enhancement and Pressure Ratio

Figure 5.7 presents the PE (Equation (13)) of heat transfer and PR (Equation (12)) as functions of the *Re*. The enhancement yielded promising results. The smallest size (*S* = 2 mm) provided the lowest level of improvement. reaching about 47%. whereas *S* = 4 mm achieved approximately 83%. and *S* = 6 mm provided the highest enhancement of up to 120%. In all cases. The enhancement was more pronounced at higher *Re* than at lower ones. The improved performance at larger VG sizes is associated with the stronger flow disturbance and wider wall-interaction region observed previously. However, the pressure drop ratio highlights the cost of this improvement in performance. The case with *S* = 2 mm increased the pressure drop by approximately five times compared to the baseline. When *S* = 4 mm, a 7.5-fold increase was noted. and *S* = 6 mm led to a pressure increase of approximately 12.5 times. This behavior is mainly attributed to the larger frontal area and stronger flow blockage generated by larger VGs, which increase momentum dissipation and wall shear stress inside the channel. Thus. A larger VG size provided a stronger heat transfer enhancement. They also impose a significantly higher pressure penalty on the system [P10].

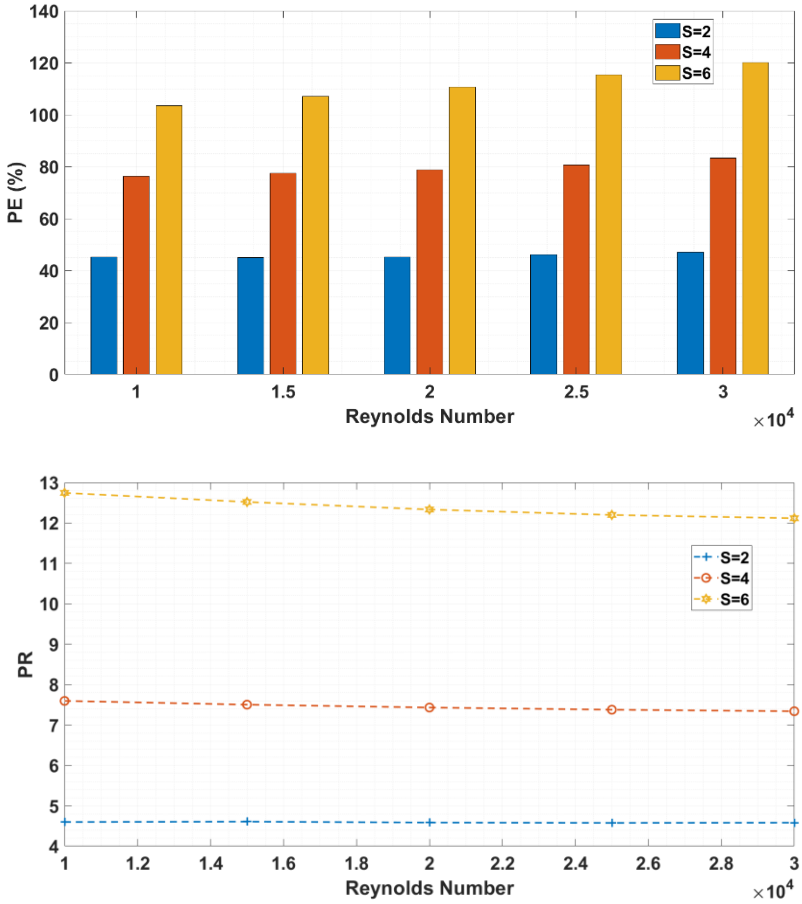

Figure 5.7 Variation of PE and PR with Re for different values of VG size [P10].

5.6Overall performance evaluation

To evaluate the trade-off between the heat transfer gain and pressure drop penalty. The PEC (Equation (14)) was calculated as a function of the *Re* (Figure 5.8). The results showed that the PEC increased with the *Re*. This indicates that the balance between the enhancement and pressure loss improved at higher flow rates. For the smallest size (*S* = 2 mm). The maximum PEC was ~ 0.88. This was lower than that in the other cases. The medium size (*S* = 4 mm) exhibited higher PEC values across the entire range of *Re*, indicating a more balanced thermal–hydraulic performance over a wide operating range. The large size (*S* = 6 mm) performed better in the higher *Re* range (22.000–30.000), where the stronger flow momentum reduced the relative effect of the hydraulic penalty. The maximum PEC was obtained with *S* = 6 mm. reached 0.95, which is the closest value to unity, representing the most favorable balance between thermal performance and pressure loss [P10].

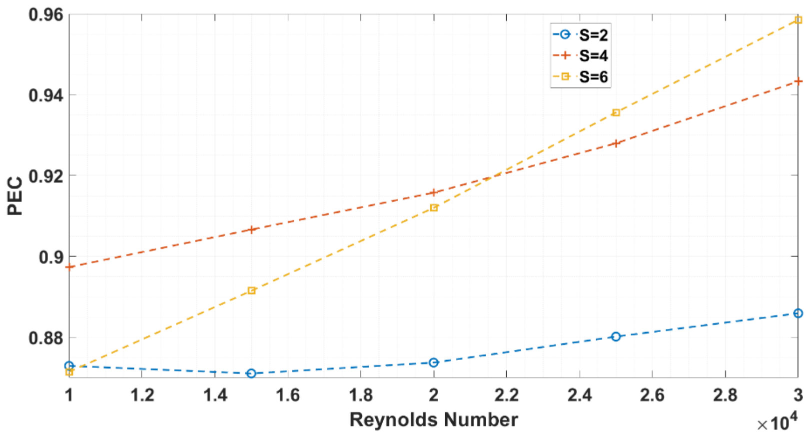

Figure 5.8 Variation of PEC with Re for different VG sizes [P10].

These findings demonstrate that the VG size strongly controls the interaction between the generated vortices and the recirculation zones inside the corrugated channel. Increasing the VG size intensified the flow disturbance, reduced the thermal boundary-layer thickness, and improved fluid mixing near the heated wall, leading to higher local and average heat-transfer rates. The results also showed that larger VGs produced a more uniform distribution of wall shear stress and local heat transfer along the corrugated surface. However, this enhancement was accompanied by a significant increase in pressure loss owing to stronger recirculation and viscous effects. The study therefore highlights the importance of selecting an appropriate VG size to achieve an effective balance between thermal enhancement and hydraulic performance in corrugated heat exchangers.

PEC was considered together with the PE and PR. Both S = 4 mm and S = 6 mm exhibited good overall performance. Each of these methods has distinct advantages. For this reason. the VG size was fixed at 5 mm in the next stage of the study to investigate the effect of the VG positions inside the corrugated channel.

6. EFFECT OF VORTEX GENERATOR POSITION

The streamwise position of vortex generators plays a major role in determining the interaction between vortex-induced flow structures and the recirculation zones formed by the corrugated geometry. Different VG positions can significantly modify the turbulence distribution, wall–fluid interaction, and pressure losses inside the channel. However, the influence of VG placement relative to the corrugation entrance and pitch remains insufficiently explored for semi-circular corrugated channels. Therefore, identifying an appropriate VG position that maximizes heat-transfer enhancement while maintaining acceptable hydraulic performance is an important aspect of thermal system optimization. This chapter focuses on the effect of VG position within the corrugated channel on flow structure and heat transfer performance. With the VG size fixed based on the findings of Chapter 5, different streamwise locations are examined to understand how placement relative to the corrugation geometry influences recirculation zones, turbulence intensity, and wall–fluid interaction. The discussion starts with isotherm and streamline contours to visualize the impact of VG position on thermal boundary layer disruption. Subsequently, wall shear stress, local heat transfer coefficient, velocity profiles, and turbulent kinetic energy are analyzed in detail. The chapter concludes with an evaluation of the average Nusselt number, pressure drop, percentage enhancement, pressure ratio, and PEC, providing a comprehensive comparison of the thermal–hydraulic performance for each VG position [P11].

Figure 6.1 presents the semi-circular corrugated channel equipped with vortex generators placed at different streamwise positions. The VG position parameter d was varied while maintaining the remaining geometric dimensions and operating conditions identical to those described in Chapter 2. The vortex-generator configuration was maintained at the optimized size of 5 mm. Three VG positions (d=0, -2, and +2 mm) were investigated to evaluate the influence of the VG location on the flow structure and thermal–hydraulic performance. A uniform inlet velocity corresponding to Reynolds numbers between 10,000 and 30,000 was applied at the channel inlet, while a constant heat flux was imposed along the heated corrugated wall. The outlet was defined using a pressure-outlet boundary condition.

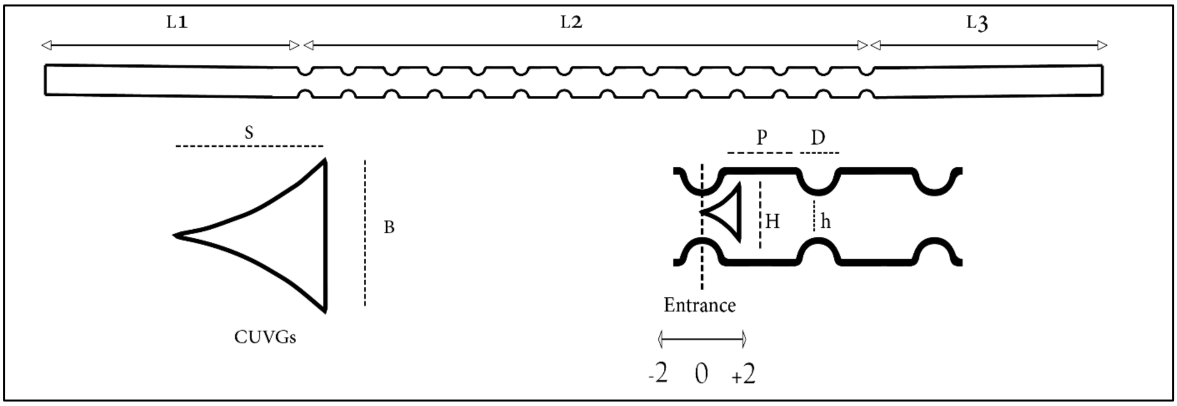

Figure 6.1 Definition of the vortex-generator position parameter d.

6.1 Isothermal and flow visualization

Figure 6.2 presents the isotherm contours and streamlines for the different VG positions. The position of the VGs plays a crucial role in the thermal–hydraulic performance of the channel. At *d* = –2. the VGs position of the VGs eliminated much of the thermal boundary layer, especially near the corrugation corners. This was also evident in the streamlines. where the recirculation zone at the corner almost disappeared. Positioning the VGs near the corrugation entrance allows the generated vortices to interact earlier with the developing recirculation region, resulting in stronger suppression of the stagnant zones. However. when the VGs was moved to the middle (*d* = 0) or further downstream (*d* = +2). The effect gradually weakened thereafter. and larger recirculation zones appeared at the corrugation corners. Placing the VGs at *d* = –2 also generated a larger recirculation zone in the center of the channel. This enhanced fluid mixing and increased the turbulence. This improved the heat transfer. On the other hand. This configuration significantly increased the pressure drop across the reactor. Conversely, moving the VGs to *d* = +2 reduced the central recirculation. leading to a lower pressure penalty, less mixing, and weaker thermal performance [P11].

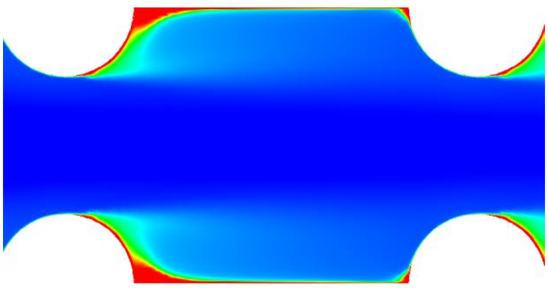

WVGs

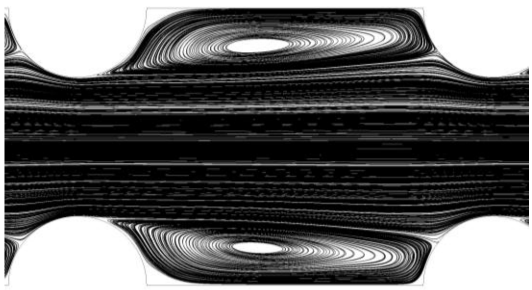

WVGs

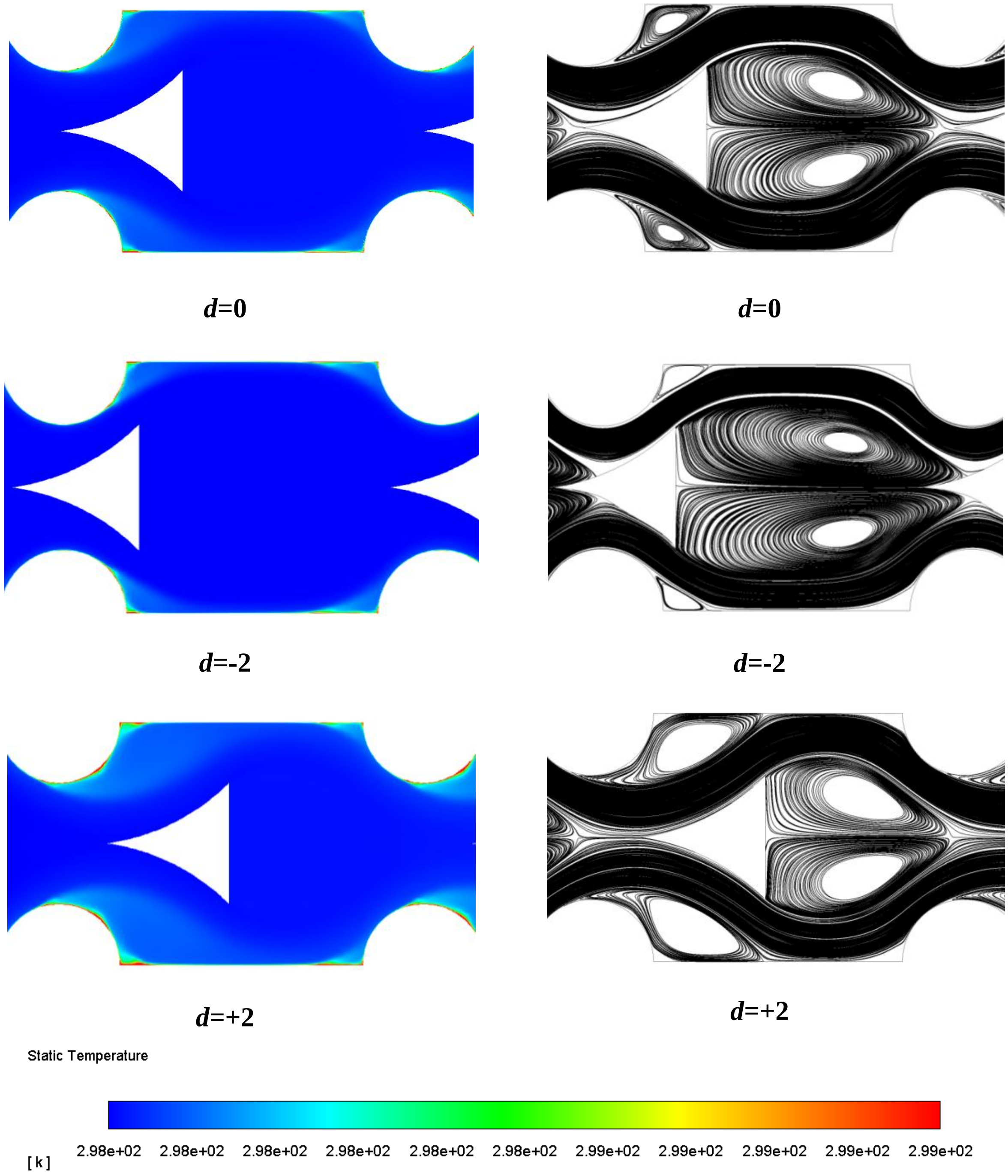

Figure 6.2 Isotherm contours and streamlines showing the effect of different VG positions [P11].

6.2Near-wall flow characteristics

Figure 6.3 shows the shear stress distribution along the bottom corrugated wall for different VG positions. For d = 0. The shear stress reached its peak value at the middle of the corrugated wall. In contrast, at d = –2. The highest values were observed near the corners. This is consistent with the streamline and velocity behavior discussed previously. The upstream placement (d = –2) redirects the flow toward the wall earlier, increasing near-wall momentum exchange in the corner regions. Each position has its own influence. enhancing wall–fluid contact in different regions of corrugation. Case d = +2 exhibited the weakest overall shear stress. indicates a reduced interaction between the fluid and wall compared with the other cases. The corresponding peak values are listed in Table 6.1 [P11].

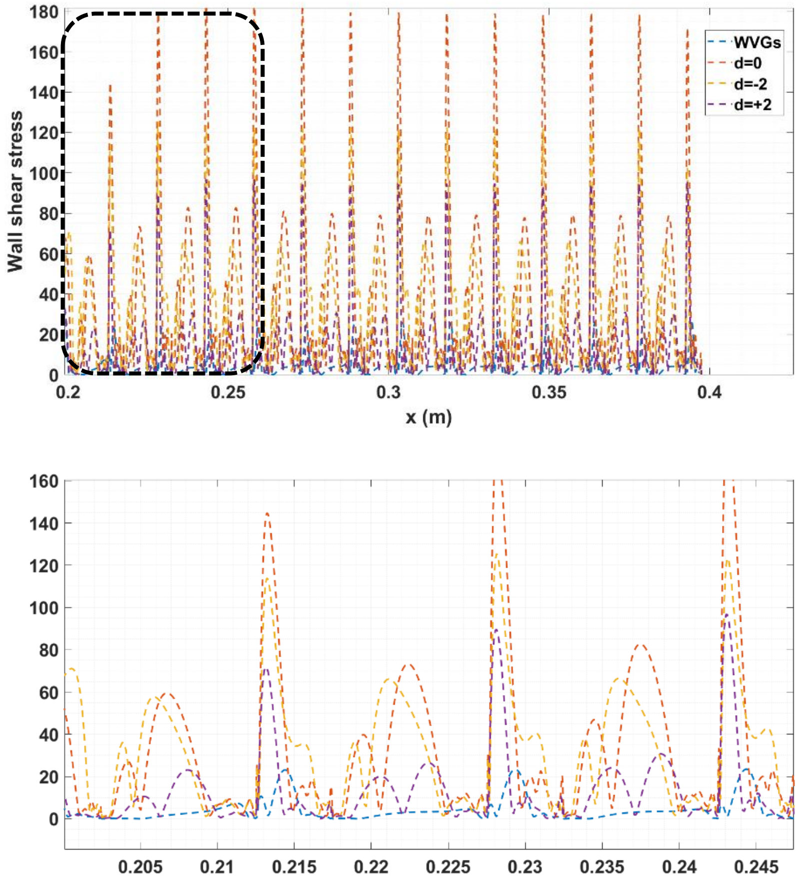

Figure 6.3 Distribution of wall shear stress along the corrugated section [P11].

Table 6.1 Peak wall shear stress along the corrugated wall [P11].

Case	Peak shear stress (Pa)	Average trend (approx.)
WVGS	~40–50	Low; peaks mainly at pitch
***d* = –2**	~150–160	High at corners; strong wall contact
***d* = 0**	~170–180	Highest in middle; strong uniformity
***d* = +2**	~120–130	Moderate; weaker overall effect

Figure 6.4 shows the local h along the bottom wall of the corrugated section for different VG positions. At d = –2. The VGs significantly increased the h at the corrugation corners compared with other cases. This behavior indicates more effective suppression of the low-velocity regions in these areas. In contrast, at d = 0. The enhancement was higher in the middle of the corrugated wall but was less pronounced at the corners. The case with d = +2 shows the weakest overall performance. due to low turbulence and reduced velocity near the wall. This prevents the fluid from being effectively driven into these areas. The peak values for each configuration are listed in Table 6.2 [P11].

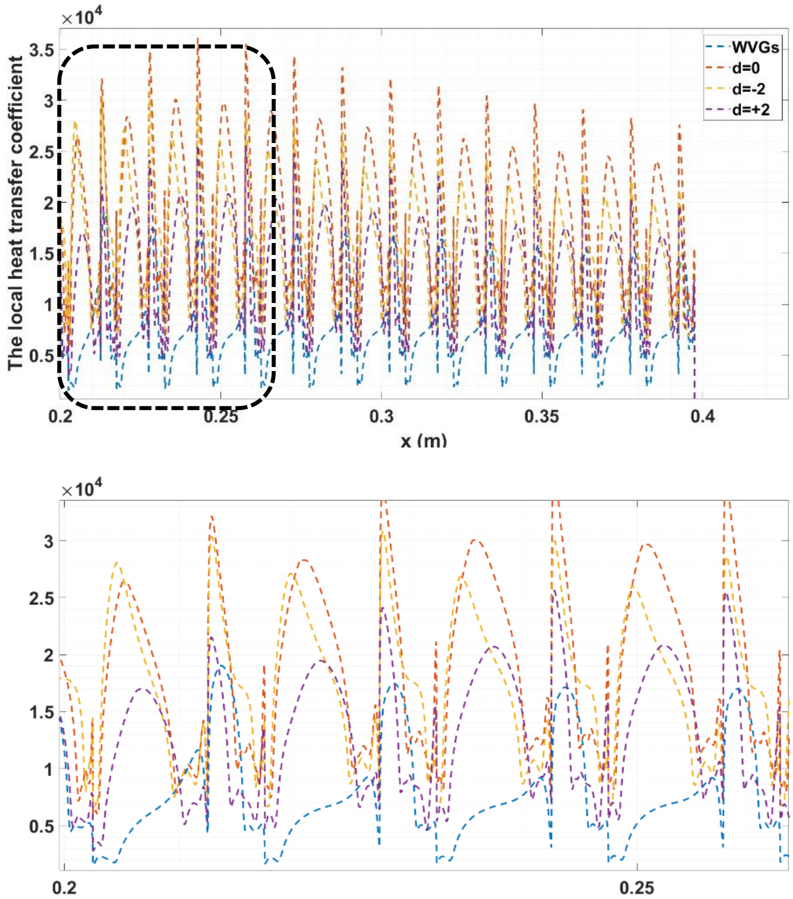

Figure 6.4 Distribution of the local heat transfer coefficient along the corrugated section [P11].

Table 6.2 Peak local heat transfer coefficient along the corrugated wall [P11].

Case	Peak local *h* ($\times 10^4$ W/m^{2}K)	Average trend (approx.)
WVGS	~0.9–1.0	Peaks only at pitch; weak elsewhere
***d* = –2**	~3.2–3.4	Strong at corners; enhanced spread along wall
***d* = 0**	~3.6	Higher in middle; weaker at corners

***d* = +2**	~2.3–2.4	Moderate; weaker overall due to low turbulence

6.3Velocity and Turbulence Characteristics

Figure 6.5 shows the x-velocity and turbulent kinetic energy (TKE) profiles along the vertical line at the middle of the corrugated section for various VG positions. When VGs is placed at *d* = 0. The velocity near the walls exhibited the greatest increase. Along the middle line of the channel, the velocity becomes negative owing to the influence of the central recirculation. In contrast. at *d* = –2. The velocity along this line also decreased to a negative value. However, the effect was stronger because of the larger recirculation zone formed upstream (Figure 6.2). For *d* = +2. Recirculation was still observed. However, the line passes through the center of the recirculation zone. The velocity captured along that line was close to zero rather than negative values. The turbulent kinetic energy profiles further highlight this effect. Both *d* = –2 and d = 0 produced significantly higher turbulence than *d* = +2. where a weaker recirculation zone results in much lower turbulence. Along the middle line. *d* = 0 exhibited the highest turbulence intensity. This is because the flow is forced to divide and concentrate more strongly around the VGs at this location. This concentrated flow interaction increases local momentum exchange and promotes stronger mixing within the channel core [P11].

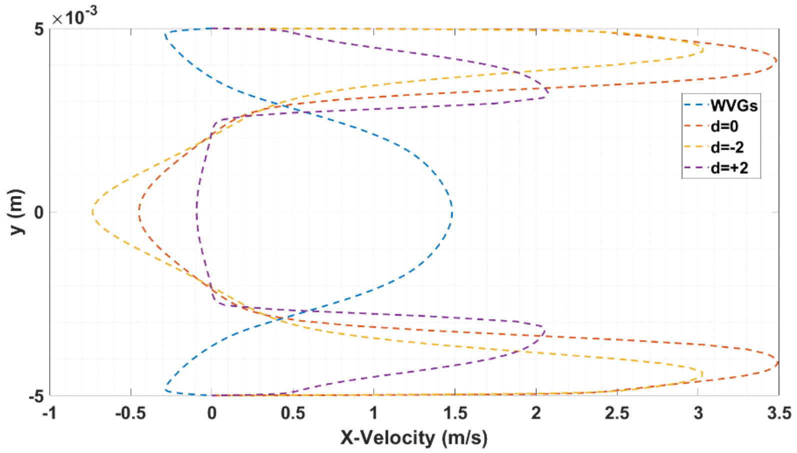

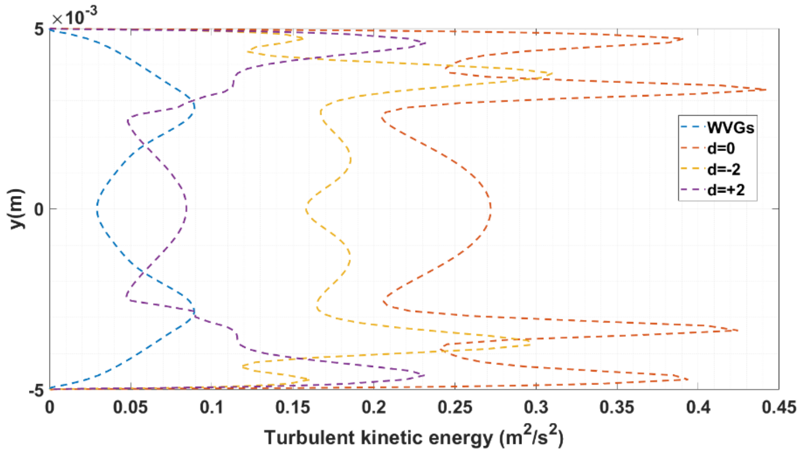

Figure 6.5 Profiles of x-velocity and turbulent kinetic energy along the vertical line at the mid-length of the corrugated section [P11].

6.4Global Thermal and Hydraulic Performance

Table 6.3 Overview of average Nu and pressure drop for various VG positions across different Re [P11].

	Nu				**Δ*P***			
Re	WVGs	d=0	d=-2	d=+2	WVGs	d=0	d=-2	d=+2
10000	194.45	336.1	399.09	323.59	1123.93	8191.48	14394.38	7966.91
15000	266.09	460.78	555.01	460.43	2503.78	17921.05	31703.37	17928.72
20000	329.86	573.39	700.26	572.15	4336.47	30374.9	54411.41	30392.25
25000	389.69	680.64	845.48	680.06	6637.79	45502.82	82593.7	45527.93
30000	448.08	791.71	993.64	789.9	9457.5	63726.09	117250.8	63767.62

Figure 6.6 shows the variation in the average *Nu* (Equation (9)) and Δ*P* (Equation (8))with the *Re* for different VG positions. The results indicate a clear difference in the heat transfer when the VGs is inserted. The case with *d* = –2 achieved the highest average *Nu*. was significantly higher than that of the other positions. This improvement is associated with the stronger suppression of the recirculation zones near the corrugation corners, resulting in more effective utilization of the heated wall area. This improvement is linked to the stronger enhancement at the corrugation corners. This is reflected in the overall average performance. The cases with *d* = 0 and *d* = +2 show similar results. with *d* = +2 slightly lower and *d* = 0 slightly higher. However, the differences are relatively small compared to the gap with *d* = –2. For Δ*P*. The position at *d* = –2 again shows the highest penalty for the same reason as above. as the VGs near the entrance created a large

recirculation zone that strongly resisted flow. In contrast. *d* = 0 and *d* = +2 resulted in lower pressure drops. with *d* = +2 being slightly higher than that for *d* = 0. This behavior is attributed to the proximity of the VG to the next corrugation entrance, which locally restricts the flow passage and increases resistance**.** The corresponding values are listed in Table 6.3 [P11].

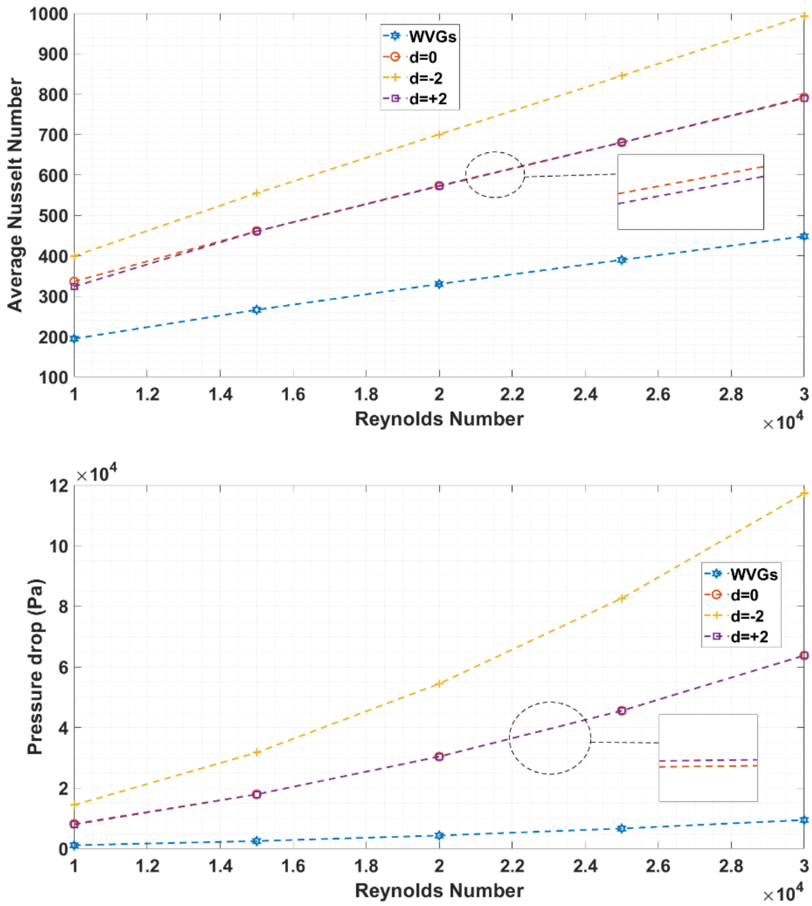

Figure 6.6 Variation of average Nu and pressure drop with Re for different values of VG position [P11].

6.5Performance Enhancement and Pressure Ratio

Figure 6.7 presents the PE (Equation (13)) and PR (Equation (12)) as functions of the *Re* for different VG positions. The heat transfer enhancement reached approximately 121% for *d* = –2. compared to 77% and 76% for *d* = 0 and *d* = +2, respectively. The superior performance of *d* = –2 is consistent with the stronger interaction between the generated vortices and the corrugation-induced recirculation observed in the previous flow visualizations. The enhancement was more pronounced at higher *Re* than at lower ones. highlighting that the use of VGs is especially effective in higher-flow regimes. On the other hand. The PR exhibited the highest penalty at *d* = –2. reaching nearly 12.5 times the baseline. This was significantly higher than that of the other positions. which is approximately seven times. As the *Re* increased, the difference in the PR between the cases decreased. This suggests that the influence of the VG-induced flow resistance becomes less dominant relative to the overall flow momentum at higher *Re* [P11].

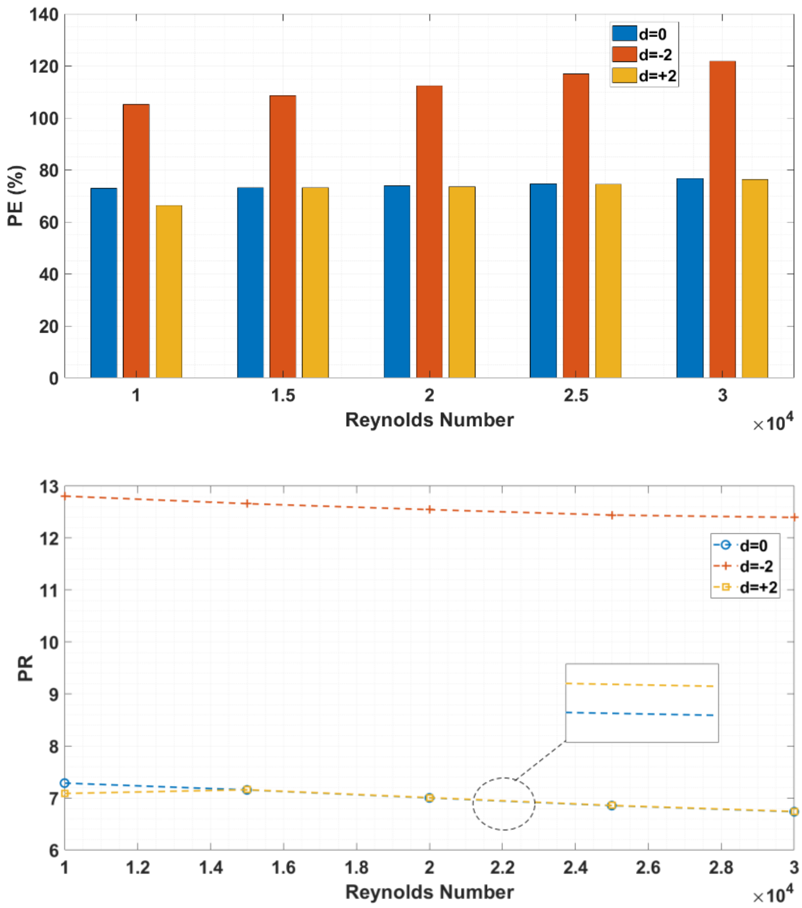

Figure 6.7 Variation of PE and PR with Re for different VG positions [P11].

6.6 Overall performance evaluation

Figure 6.8 presents the PEC (Equation (14)) as a function of the *Re* for different VG positions. The configuration with $d = 0$ showed higher PEC values only in the *Re* range of 10000–15000. In contrast, the $d = -2$ configuration achieves higher PEC values overall, particularly at $Re = 30000$, where it reaches 0.96, which is very close to the ideal value of 1, indicating an excellent balance between heat transfer enhancement and pressure drop. This behavior confirms that positioning the VG near the corrugation entrance allows more effective utilization of the generated vortical structures over the entire corrugated section. This configuration also exhibited favorable PE results, suggesting that a VG with spacing $S = 5$ mm represents an optimal position and size. Such a VG can be implemented in real-world applications, such as heat exchangers, to significantly improve thermal performance while maintaining acceptable pressure losses. The key results are presented in [46] [P11].

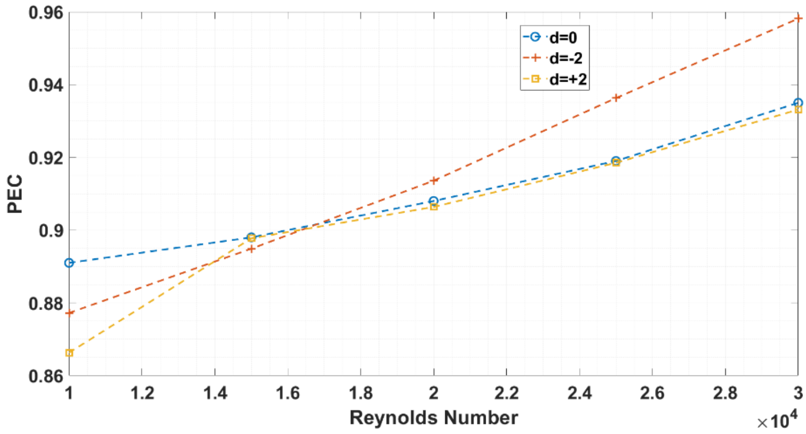

Figure 6.8 Variation of PEC with Re for different VG positions [P11].

These findings demonstrate that the streamwise position of the vortex generator strongly influences the interaction between the generated vortices and the natural recirculation zones inside the corrugated channel. Placing the VG near the corrugation entrance (d = -2) promoted stronger fluid mixing and significantly reduced the recirculation regions near the corrugation corners, leading to a thinner thermal boundary layer and improved wall–fluid interaction. This configuration produced the highest heat-transfer enhancement and PEC among the investigated cases, indicating a more favorable thermal–hydraulic balance. The results also showed that the location of the VG controls the distribution of turbulence and wall shear stress along the corrugated surface, which directly affects the local and average heat-transfer behavior. These observations provide useful design guidance for optimizing vortex-generator placement in compact corrugated heat exchangers.

7. SINGLE VG VS. TWO-PAIR VG CONFIGURATION

The use of additional VG pairs can enhance vortex interaction and fluid mixing inside corrugated channels; however, it may also increase pressure losses because of the stronger flow obstruction. Direct comparisons between single-body and two-pair VG configurations in semi-circular corrugated channels remain limited, particularly when both arrangements are positioned inside the corrugated section. Furthermore, the influence of vortex interaction between VG pairs on the overall thermal–hydraulic balance is still not fully understood. Therefore, evaluating whether a two-pair arrangement provides meaningful advantages over a single optimized VG configuration is important for the design of compact heat exchangers. This chapter presents a comparative analysis between a single VG configuration and a two-pair VG arrangement within the corrugated channel. The objective is to assess how increasing the number of vortex generators influences the flow structure and overall thermal–hydraulic performance. The discussion begins with velocity contours and streamlines to highlight differences in flow interaction, vortex development, and mixing intensity between the two configurations. The comparison is then extended to global performance indicators, including the percentage heat transfer enhancement, pressure ratio, and performance evaluation criterion. This focused analysis provides insight into whether the use of multiple VGs offers additional benefits compared to a single VG configuration, considering both heat transfer improvement and the associated pressure loss [P5].

Figure 7.1 presents the geometry with the same dimensions described in Section 2. It also illustrates the configuration of the two-pair winglet-type VGs. In this arrangement, each VG pair is attached at the midpoint of the semi-circular corrugation wall. The VGs extend from the surface with an extrusion height (F) of 2 mm, a length (L) of 4 mm, and a thickness (E) of 0.5 mm. Three different spacings between the two winglets were examined, with distances (A) of 2, 4, and 6 mm [P5].

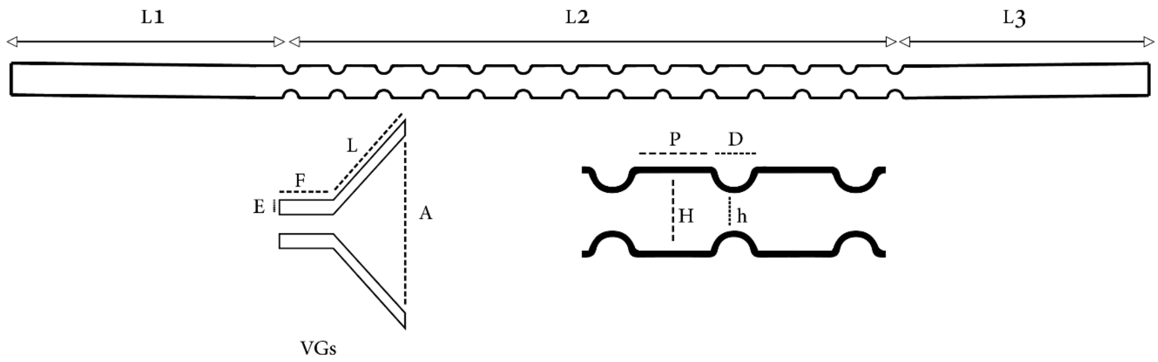

Figure 7.1 Geometry of the corrugated channel showing the two-pair vortex generator arrangement.

7.1Flow field visualization

Figure 7.2 shows the velocity contours. The velocity is concentrated in the middle of the channel, while dead zones appear near the corrugation corners because of the corrugation pitch. The use of VGs redirects the flow toward the walls, increasing the near-wall velocity and improving fluid–wall interaction. As the distance between the VGs increases, the velocity near the walls becomes higher. This indicates that wider VG spacing allows the generated vortices to develop more effectively before interacting with adjacent flow structures. At A = 6 mm, the near-wall velocity is the highest, resulting in better contact between the fluid and the wall [P5].

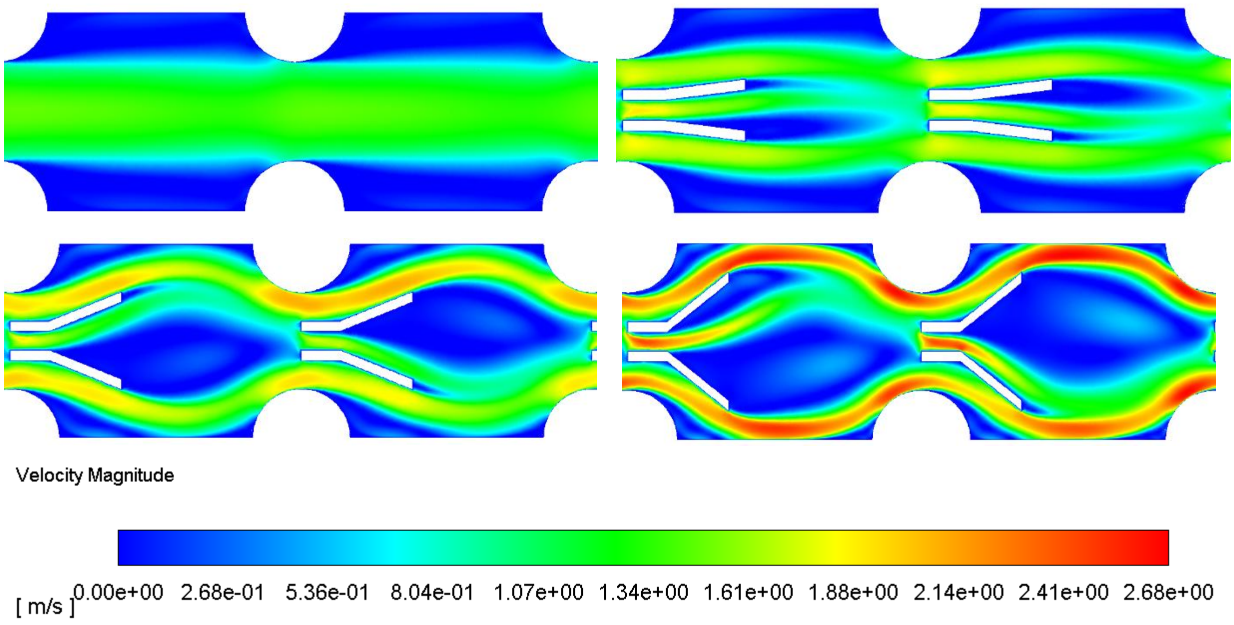

Figure 7.2 Velocity contours for the two-pair VG configuration [P5].

Figure 7.3 presents the velocity streamlines. The dead zones correspond to fluid recirculation regions that reduce the local heat transfer efficiency near the corrugated walls. The VGs reduce the recirculation zones near the wall but generate a larger recirculation region in the middle of the channel, which contributes to additional pressure loss. The spacing between the VGs also affects the flow structure. Increasing the VG distance reduces the recirculation near the corrugated wall while enlarging the central recirculation region. This behavior suggests that wider spacing allows stronger vortex development in the channel core, leading to enhanced mixing but also greater momentum dissipation [P5].

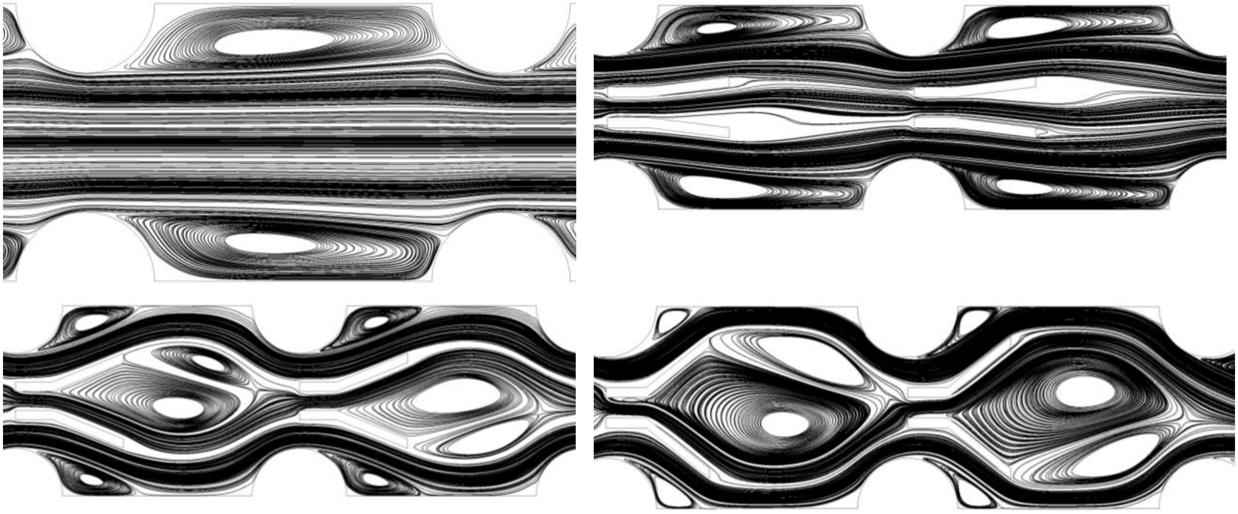

Figure 7.3 Streamlines for the two-pair VG configuration [P5].

7.2Heat transfer enhancement and pressure ratio

Figure 7.4 present the PE (Equation (13)) and PR (Equation (12)) varying with *Re*. The VGs show a good effect on heat transfer enhancement, which increases respectively with the increase of the distance. The highest value is for *A* = 6 mm, about 86%, while the lowest is for *A* = 2 mm, about 22%. *A* = 4 mm shows average performance. The improved enhancement at larger spacing is associated with stronger development of the generated vortices and a wider interaction region between the flow core and the heated walls. The pressure drop increases more than 9 times at the largest distance, while it is about 5 times and 4 times for *A* = 4 mm and *A* = 2 mm, respectively.

For comparison, the best configuration of the single-body VGs (CUVGs) yielded a higher heat-transfer enhancement of around 121%, though with a larger pressure penalty of nearly 12.5 times. This indicates that the single-body VG produces stronger and more concentrated flow disturbance than the two-pair configurations, resulting in greater thermal enhancement but also higher momentum loss [P5].

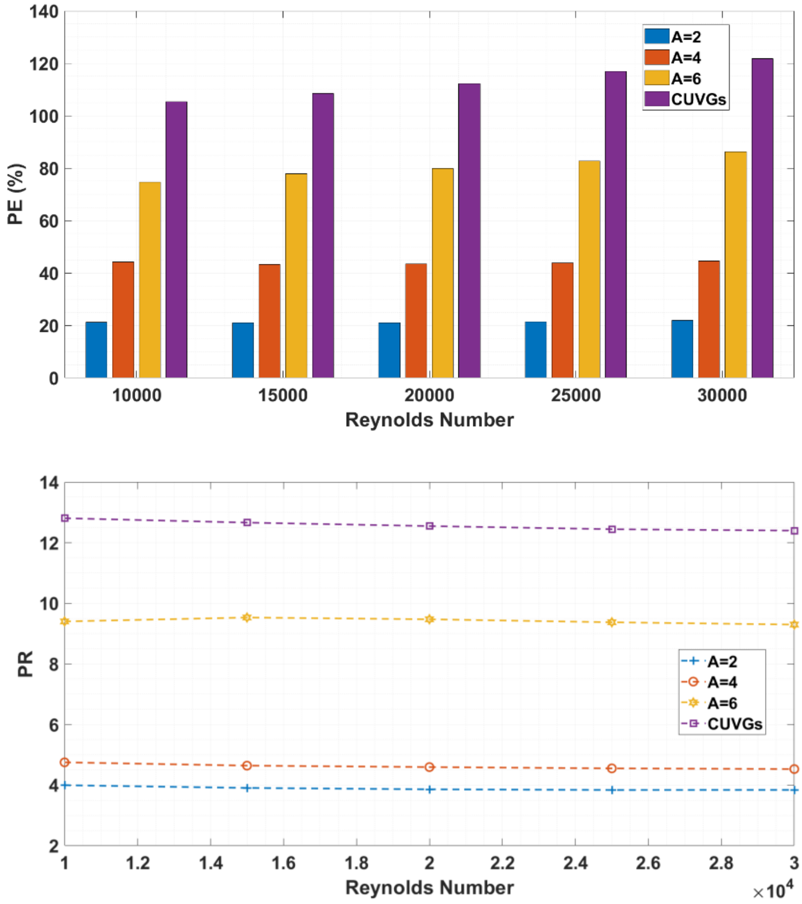

Figure 7.4 Variation of PE and PR with Re for the two-pair VG configuration.

7.3Overall Performance Evaluation

To balance between heat transfer enhancement and pressure drop, the thermal hydraulic performance coefficient was measured (Equation (14)), as shown in Figure 7.5. The smallest distance has a lower PEC compared to the other two distances. The cases A = 4 mm and A = 6 mm range between 0.83 and 0.88, which is close to one, with each having an advantage within a specific Reynolds number range. A = 4 mm shows higher values for *Re* between 10,000 and 26,000, while A = 6 mm performs better above 26,000. This indicates that larger spacing becomes more effective at high flow rates, where the stronger flow momentum supports better vortex development with a relatively lower hydraulic penalty.

For comparison, the single-body configuration exhibits higher PEC values across most *Re*. At *Re* = 30,000, the PEC reaches approximately 0.96, which is very close to the ideal value of one, indicating a stronger overall balance between heat-transfer enhancement and pressure drop than the two-pair cases. This behavior is consistent with its higher heat-transfer performance reported earlier. Based on these results, the single-body VG (CUVGs) provides the best overall thermal–hydraulic performance among the configurations studied.

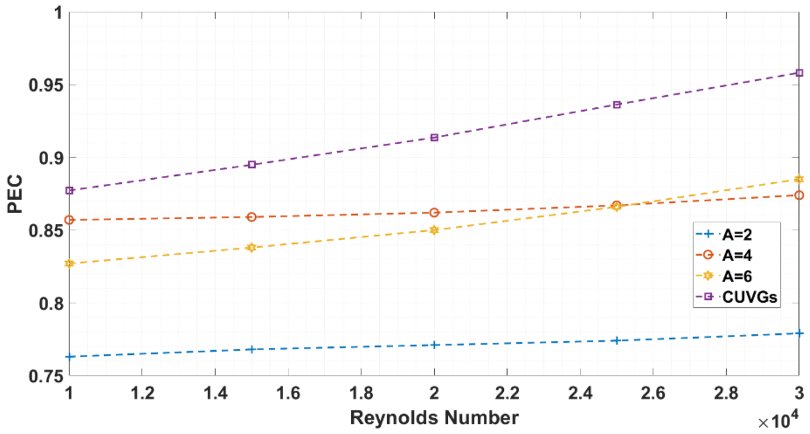

Figure 7.5 Variation of PEC as a function of Re for the two-pair VG configuration.

These findings demonstrate that using two VG pairs does not necessarily improve the overall thermal–hydraulic performance of the corrugated channel. Although the two-pair arrangement intensified vortex interaction and flow disturbance, the additional vortices generated strong flow interference and larger recirculation regions inside the channel, leading to a significant increase in pressure losses. In comparison with the optimized single CUVG configuration (S = 5 mm and d = -2), the two-pair arrangement produced less favorable thermal–hydraulic behavior because the excessive vortex interaction weakened the overall flow organization and reduced the performance balance. The results therefore indicate that a properly positioned single VG can provide more efficient enhancement than two VG pairs, highlighting the importance of controlled vortex generation rather than increasing the complexity of the VG arrangement.

A comparison with previous study involving two-pair winglet vortex generators further highlights the effectiveness of the present optimized configuration. For example, previous investigations employing different paired rectangular winglet vortex generators in compact heat exchangers reported maximum heat-transfer enhancements of approximately 112%. In the present study, the optimized single-body concave-up vortex generator combined with the selected size and position achieved a higher enhancement of approximately 121%. This improvement indicates that geometric consistency between the vortex generator shape and the corrugated channel profile plays an important role in strengthening near-wall mixing and improving thermal–hydraulic performance.

8. THESES-NEW SCIENTIFIC RESULTS

This thesis presented a comprehensive numerical investigation of heat transfer enhancement in a semi-circular corrugated channel using combined passive enhancement techniques, including vortex generators. The study systematically examined the influence of VG geometry, size, and streamwise position. The main original contributions and findings of the thesis are summarized as follows:

T1. A novel contribution of this thesis is that I investigated three different vortex generator geometries in relation to the corrugated channel shape, which has received limited attention in previous studies. The geometry of the vortex generators strongly influences the flow behavior and heat transfer characteristics in corrugated channels. Concave-up vortex generators generate stronger and more stable vortical structures, which enhance fluid mixing and effectively disrupt the thermal boundary layer, resulting in the highest heat transfer enhancement among the investigated designs. Concave-down and straight vortex generators also improve heat transfer compared to the baseline configuration, but with relatively weaker vortex intensity. These findings demonstrate that VG geometry plays a key role in controlling vortex strength and heat transfer performance [P1] [P2].

T2. This thesis demonstrates the influence of vortex generator size on the thermal–hydraulic performance of corrugated channels. In this work, I investigated the effect of VG size on flow disturbance, thermal boundary-layer development, and pressure-drop behavior. The results demonstrate that increasing the vortex generator size significantly enhances heat transfer in corrugated channels by intensifying flow disturbance, thinning the thermal boundary layer, and promoting stronger fluid mixing. This leads to higher local and average Nusselt numbers. However, the thermal improvement is accompanied by an increase in wall shear stress and pressure drop. Among the investigated configurations, moderate VG sizes (S = 4–6 mm) provide the most favorable thermal–hydraulic compromise, achieving PEC values close to unity, which indicates efficient performance without excessive hydraulic penalties. This finding highlights the importance of VG size optimization in corrugated channels, which has received limited attention in previous studies [P10] [P2].

T3. This thesis demonstrates the importance of vortex generator streamwise position on the flow structure and thermal–hydraulic performance in a corrugated channel. In particular, I studied the influence of VG placement relative to the corrugation geometry. The position of the vortex generator plays a critical role in determining overall performance. Locating the VG near the corrugation entrance (d = –2) produces the highest heat transfer enhancement due to stronger mixing and suppression of recirculation zones, resulting in a maximum PEC of approximately 0.96. Although this configuration induces a higher pressure drop, it offers the best overall thermal–hydraulic balance. This confirms that strategic placement of VGs is as important as their size in achieving optimal heat exchanger performance. This result highlights that accurate VG positioning within corrugated channels is a key design parameter, and its systematic assessment has received less attention compared to VG geometry and size in previous studies [P11].

T4. Another contribution of this thesis is the direct comparison between a two-pair vortex generator configuration with a single-body concave-up vortex generator (CUVG) to determine which arrangement provides better thermal–hydraulic performance in a corrugated channel. In this part of the work, I compared the thermal enhancement produced by paired and single-body VG configurations under identical operating conditions. Many previous studies have employed two-pair vortex generator configurations in corrugated channels. The results show that although the two-pair configuration enhances heat transfer, its maximum improvement (approximately 86%) remains lower than that achieved by the single-body CUVG, which reaches about 121%. This indicates that a properly designed single-body VG can outperform more complex multi-VG configurations. This demonstrates that a well-designed single VG can outperform more complex multi-VG configurations while avoiding unnecessary geometric complexity [P5] [P2].

ACKNOWLEDGEMENTS

First and foremost, I would like to express my deepest gratitude to my supervisor, Dr. Krisztián Hriczó, whose guidance, support, and encouragement have been invaluable throughout my PhD journey. Over the past four years, he introduced me to this fascinating research field and provided continuous academic and personal support. His knowledge, patience, constructive feedback, and dedication have played a fundamental role in my development as a researcher. I am truly grateful for the countless discussions, advice, and encouragement that helped me overcome challenges and remain focused on my goals. Beyond academia, I deeply appreciate his kindness, understanding, and the positive working environment he created.

I would also like to thank my friends and colleagues for their support, encouragement, and friendship throughout this journey. Your presence made the challenges easier to overcome and the successes more meaningful.

My deepest gratitude goes to my family, whose unconditional love, belief, and support have been the foundation of everything I have achieved. To my mother, my father, my brothers, and my sisters, thank you for always believing in me and encouraging me to pursue my dreams. I would like to express special appreciation to my eldest brother, Mohammed, who has been a source of strength, guidance, and support throughout my life. His encouragement and belief in me have had a profound impact on my personal and academic journey.

I dedicate this thesis to my family. This achievement would not have been possible without your sacrifices, patience, and unwavering support.

I am also grateful for the opportunity to be part of an outstanding research university that has provided an excellent environment for learning, discovery, and professional growth. Completing this PhD represents one of the most significant milestones of my life and marks an important step in my academic and professional career.

Finally, I hope that the work presented in this thesis contributes, even in a small way, to the advancement of knowledge in this field. I remain motivated to continue learning, exploring, and contributing to future research. I am sincerely thankful to everyone who has supported me along this journey, and I look forward to the opportunities and challenges that lie ahead.

LIST OF PUBLICATIONS RELATED TO THE TOPIC OF THE RESEARCH FIELD

(P1) Tanougast, A., Bessaih, R., & Hriczó, K. (2025). Comparative study of different vortex generator designs in corrugated channels for turbulent heat transfer enhancement. *Results in Physics*, 108450.

(P2) Tanougast, A., & Hriczó, K. (2025). Enhanced heat transfer in wavy channels with vortex generators: A CFD investigation. *International Journal of Thermofluids, 30*, 101405.

(P3) Tanougast, A., & Hriczó, K. (2025). Advancements in Heat Exchangers for Improved Engine Cooling: A Comprehensive Literature Review. *Periodica Polytechnica Transportation Engineering*, *53*(4), 431-439.

(P4) Tanougast, A., Omle, I., & Hriczó, K. (2025). Turbulent Hybrid Nanofluid Flow in Corrugated Channels with Vortex Generators: A Numerical Study. *Fluids*, *10*(10), 249.

(P5) TANOUGAST, A., & HRICZÓ, K. (2025). Effect of Winglet-Designed Vortex Generators on Heat Transfer Performance in Corrugated Channels. *Applied Scientific Research*, *5*(2), 5-14.

(P6) Tanougast, A., & Hriczó, K. (2025, September). Numerical modeling of unsteady heat convection in turbulent flow. In *AIP Conference Proceedings* (Vol. 3315, No. 1, p. 180006). AIP Publishing LLC.

(P7) Tanougast, A., & Hriczó, K. (2025). Comparison of Turbulence Models in the Simulation of Fluid Flow in Corrugated Channel. *Advances in Science and Technology*, *165,* 53-64.

(P8) Tanougast, A., & Hriczó, K. (2023). Numerical study of the vortex generators effects in a corrugated channel for turbulent flow. *MULTIDISZCIPLINÁRIS TUDOMÁNYOK: A MISKOLCI EGYETEM KÖZLEMÉNYE*, *13*(4), 30-41.

(P9) TANOUGAST, A., Hriczo, K. (2023). Numerical simulation of nanofluid flow through a corrugated channel with vortex generator - In: Gép, ISSN 0016-8572, 2023. (vol. 74), 2-3. no., 72-77 p.

(P10) Tanougast, A., Bessaih, R., & Hriczó, K. Effect of vortex generator size on thermal–hydraulic performance in a corrugated channel. Pollack Periodica. **Accepted**

(P11) Tanougast, A., & Hriczó, K. Numerical Investigation of Vortex Generator Position Effects on Thermal–Hydraulic Performance in a Corrugated Channel. Design of Machines and Structures. **Accepted**

REFERENCES

[1] M. Siddique, A.-R.A. Khaled, N.I. Abdulhafiz, A.Y. Boukhary, Recent Advances in Heat Transfer Enhancements: A Review Report, Int. J. Chem. Eng. 2010 (2010) 106461. https://doi.org/10.1155/2010/106461.

[2] S. Bhattacharyya, M.M. Ardekani, R. Biswas, R.C. Mehta, Inverse Heat Conduction and Heat Exchangers, BoD – Books on Demand, 2020.

[3] S.A. Marzouk, M.M. Abou Al-Sood, E.M.S. El-Said, M.M. Younes, M.K. El-Fakharany, A comprehensive review of methods of heat transfer enhancement in shell and tube heat exchangers, J. Therm. Anal. Calorim. 148 (2023) 7539–7578. https://doi.org/10.1007/s10973-023-12265-3.

[4] E.K. Simpeh, J.-P.G. Pillay, R. Ndihokubwayo, D.J. Nalumu, Improving energy efficiency of HVAC systems in buildings: a review of best practices, Int. J. Build. Pathol. Adapt. 40 (2022) 165–182. https://doi.org/10.1108/IJBPA-02-2021-0019.

[5] R.B. C., K. P., S. Roy, R. Ganesan, A comprehensive review on compound heat transfer enhancement using passive techniques in a heat exchanger, Mater. Today Proc. 54 (2022) 428–436. https://doi.org/10.1016/j.matpr.2021.09.541.

[6] M.A. Alfellag, H.E. Ahmed, M.G. Jehad, A.A. Farhan, The hydrothermal performance enhancement techniques of corrugated channels: a review, J. Therm. Anal. Calorim. 147 (2022) 10177–10206. https://doi.org/10.1007/s10973-022-11247-1.

[7] K. Kumar, R. Kumar, R.S. Bharj, P.K. Mondal, Irreversibility analysis of the convective flow through corrugated channels: a comprehensive review, Eur. Phys. J. Plus 136 (2021) 402. https://doi.org/10.1140/epjp/s13360-021-01388-x.

[8] R.V. Pinto, R.M.D. Duarte, W.G. Ferreira, D.J. Dezan, Thermal–hydraulic performance evaluation of solar air heaters containing longitudinal vortex generators: review and meta-analysis, J. Braz. Soc. Mech. Sci. Eng. 47 (2025) 160. https://doi.org/10.1007/s40430-025-05474-4.

[9] L. Yidie, L. Gongli, N.S. Bennett, L. Zhen, M. Adnan, M.S. Islam, Heat Transfer Enhancement in Heat Exchangers by Longitudinal Vortex Generators: A Review of Numerical and Experimental Approaches, Energies 18 (2025) 2896. https://doi.org/10.3390/en18112896.

[10] H. Shafiei, M.H. Hekmat, S. Saharkhiz, Comprehensive study of heat transfer enhancement in turbulent nanofluid flow in skewed corrugated channels, J. Braz. Soc. Mech. Sci. Eng. 44 (2022) 599. https://doi.org/10.1007/s40430-022-03901-4.

[11] H. Pehlivan, I. Taymaz, Y. İslamoğlu, Experimental study of forced convective heat transfer in a different arranged corrugated channel, Int. Commun. Heat Mass Transf. 46 (2013) 106–111. https://doi.org/10.1016/j.icheatmasstransfer.2013.05.016.

[12] E.A.M. Elshafei, M.M. Awad, E. El-Negiry, A.G. Ali, Heat transfer and pressure drop in corrugated channels, Energy 35 (2010) 101–110. https://doi.org/10.1016/j.energy.2009.08.031.

[13] P. Naphon, Heat transfer characteristics and pressure drop in channel with V corrugated upper and lower plates, Energy Convers. Manag. 48 (2007) 1516–1524. https://doi.org/10.1016/j.enconman.2006.11.020.

[14] R.K. Ajeel, W.S.-I.W. Salim, K. Hasnan, Thermal performance comparison of various corrugated channels using nanofluid: Numerical study, Alex. Eng. J. 58 (2019) 75–87. https://doi.org/10.1016/j.aej.2018.12.009.

[15] N. Kurtulmuş, B. Sahin, A review of hydrodynamics and heat transfer through corrugated channels, Int. Commun. Heat Mass Transf. 108 (2019) 104307. https://doi.org/10.1016/j.icheatmasstransfer.2019.104307.

[16] E.A.M. Elshafei, M.M. Awad, E. El-Negiry, A.G. Ali, Heat transfer and pressure drop in corrugated channels, Energy 35 (2010) 101–110. https://doi.org/10.1016/j.energy.2009.08.031.

[17] M.A. Ahmed, M.Z. Yusoff, K.C. Ng, N.H. Shuaib, Numerical and experimental investigations on the heat transfer enhancement in corrugated channels using SiO2–water nanofluid, Case Stud. Therm. Eng. 6 (2015) 77–92. https://doi.org/10.1016/j.csite.2015.07.003.
[18] R.K. Ajeel, W.S.-I. Salim, K. Sopian, M.Z. Yusoff, K. Hasnan, A. Ibrahim, A.H.A. Al-Waeli, Turbulent convective heat transfer of silica oxide nanofluid through corrugated channels: An experimental and numerical study, Int. J. Heat Mass Transf. 145 (2019) 118806. https://doi.org/10.1016/j.ijheatmasstransfer.2019.118806.
[19] M.A. Alfellag, H.E. Ahmed, M.G. Jehad, A.A. Farhan, The hydrothermal performance enhancement techniques of corrugated channels: a review, J. Therm. Anal. Calorim. 147 (2022) 10177–10206. https://doi.org/10.1007/s10973-022-11247-1.
[20] A. Azman, A. Mukhtar, M.Z. Yusoff, P. Gunnasegaran, N. Khai Ching, A.S.H. Md Yasir, Numerical investigation of flow characteristics and heat transfer efficiency in sawtooth corrugated pipes with Al2O3-CuO/Water hybrid nanofluid, Results Phys. 53 (2023) 106974. https://doi.org/10.1016/j.rinp.2023.106974.
[21] H.M.S. Bahaidarah, A Numerical Study of Fluid Flow and Heat Transfer Characteristics in Channels with Staggered Wavy Walls, Numer. Heat Transf. Part Appl. 51 (2007) 877–898. https://doi.org/10.1080/10407780600939644.
[22] Y. Islamoglu, Effect of rounding of protruding edge on convection heat transfer in a converging–diverging channel, Int. Commun. Heat Mass Transf. 35 (2008) 643–647. https://doi.org/10.1016/j.icheatmasstransfer.2007.11.002.
[23] P. Naphon, Effect of wavy plate geometry configurations on the temperature and flow distributions, Int. Commun. Heat Mass Transf. 36 (2009) 942–946. https://doi.org/10.1016/j.icheatmasstransfer.2009.05.007.
[24] M.A. Ahmed, M.Z. Yusoff, K.C. Ng, N.H. Shuaib, Effect of corrugation profile on the thermal–hydraulic performance of corrugated channels using CuO–water nanofluid, Case Stud. Therm. Eng. 4 (2014) 65–75. https://doi.org/10.1016/j.csite.2014.07.001.
[25] N. Tokgoz, B. Sahin, Experimental studies of flow characteristics in corrugated ducts, Int. Commun. Heat Mass Transf. 104 (2019) 41–50. https://doi.org/10.1016/j.icheatmasstransfer.2019.03.003.
[26] P. Dutta, P.P. Dutta, P. Kalita, Thermohydraulic investigation of different channel height on a corrugated heat exchanger, AIP Conf. Proc. 2091 (2019) 020011. https://doi.org/10.1063/1.5096502.
[27] R. Ferhat, A.Z. Dellil, K. Boualem, M.-K. Hamidou, Thermal Performance of a Corrugated Wall With Artificial Roughness, J. Heat Transf. 141 (2019). https://doi.org/10.1115/1.4043729.
[28] S. Singh, A. Singh, S. Chander, Thermal performance of a fully developed serpentine wavy channel solar air heater, J. Energy Storage 25 (2019) 100896. https://doi.org/10.1016/j.est.2019.100896.
[29] N. Kurtulmuş, B. Sahin, Experimental investigation of pulsating flow structures and heat transfer characteristics in sinusoidal channels, Int. J. Mech. Sci. 167 (2020) 105268. https://doi.org/10.1016/j.ijmecsci.2019.105268.
[30] S. Asaadi, H. Abdi, Numerical investigation of laminar flow and heat transfer in a channel using combined nanofluids and novel longitudinal vortex generators, J. Therm. Anal. Calorim. 145 (2021) 2795–2808. https://doi.org/10.1007/s10973-020-09795-5.
[31] P. Promvonge, P. Promthaisong, S. Skullong, Thermal performance augmentation in round tube with louvered V-winglet vortex generator, Int. J. Heat Mass Transf. 182 (2022) 121913. https://doi.org/10.1016/j.ijheatmasstransfer.2021.121913.
[32] Bassam Amer Abdulameer Shlash, Ibrahim Koç, Turbulent Fluid Flow and Heat Transfer Enhancement Using Novel Vortex Generator, J. Adv. Res. Fluid Mech. Therm. Sci. 96 (2022) 36–52. https://doi.org/10.37934/arfmts.96.1.3652.
[33] M. Ismail, A.M. Ali, S.-C.C. Pereira, Vortex generators in heat sinks: Design, optimisation, applications and future trends, Results Eng. 25 (2025) 104216. https://doi.org/10.1016/j.rineng.2025.104216.

[34] Y.P. Leylakoohi, H.M. Deylami, Enhancing the thermal performance of a minichannel using a new design of corrugated rectangular winglet pair as vortex generator, Int. J. Heat Fluid Flow 117 (2026) 110051. https://doi.org/10.1016/j.ijheatfluidflow.2025.110051.
[35] L.H. Tang, W.X. Chu, N. Ahmed, M. Zeng, A new configuration of winglet longitudinal vortex generator to enhance heat transfer in a rectangular channel, Appl. Therm. Eng. 104 (2016) 74–84. https://doi.org/10.1016/j.applthermaleng.2016.05.056.
[36] O. Damanafshan, S.E. Habibi, Y. Amini, The role of near-wall active vortex generators on thermal-hydrodynamic efficiency of corrugated wall channels, Int. Commun. Heat Mass Transf. 167 (2025) 109339. https://doi.org/10.1016/j.icheatmasstransfer.2025.109339.
[37] R. Jiang, Z. Zhao, Y. Liu, H. Liu, Y. Ma, T. Wang, J. Feng, D. Wang, S. Li, Q. Luo, Effect of vortex generator orientation on wind turbines considering the three-dimensional rotational effect, Ocean Eng. 267 (2023) 113307. https://doi.org/10.1016/j.oceaneng.2022.113307.
[38] Z. Xu, Z. Han, J. Wang, Z. Liu, The characteristics of heat transfer and flow resistance in a rectangular channel with vortex generators, Int. J. Heat Mass Transf. 116 (2018) 61–72. https://doi.org/10.1016/j.ijheatmasstransfer.2017.08.083.
[39] D. Hu, Q. Zhang, K. Song, C. Gao, K. Zhang, M. Su, L. Wang, Performance optimization of a wavy finned-tube heat exchanger with staggered curved vortex generators, Int. J. Therm. Sci. 183 (2023) 107830. https://doi.org/10.1016/j.ijthermalsci.2022.107830.
[40] M. Khoshvaght-Aliabadi, M. Khoshvaght, P. Rahnama, Thermal-hydraulic characteristics of plate-fin heat exchangers with corrugated/vortex-generator plate-fin (CVGPF), Appl. Therm. Eng. 98 (2016) 690–701. https://doi.org/10.1016/j.applthermaleng.2015.12.135.
[41] E. Salamatbakhsh, Ö. Bayer, Hydrothermal performance of a wavy minichannel heatsink with longitudinal vortex generators, Therm. Sci. Eng. Prog. 50 (2024) 102506. https://doi.org/10.1016/j.tsep.2024.102506.
[42] A.J. Modi, M.K. Rathod, Comparative study of heat transfer enhancement and pressure drop for fin-and-circular tube compact heat exchangers with sinusoidal wavy and elliptical curved rectangular winglet vortex generator, Int. J. Heat Mass Transf. 141 (2019) 310–326. https://doi.org/10.1016/j.ijheatmasstransfer.2019.06.088.
[43] Z. Brodnianská, S. Kotšmíd, Heat transfer enhancement in the novel wavy shaped heat exchanger channel with cylindrical vortex generators, Appl. Therm. Eng. 220 (2023) 119720. https://doi.org/10.1016/j.applthermaleng.2022.119720.
[44] S. Akcay, Numerical analysis of heat transfer improvement for pulsating flow in a periodic corrugated channel with discrete V-type winglets, Int. Commun. Heat Mass Transf. 134 (2022) 105991. https://doi.org/10.1016/j.icheatmasstransfer.2022.105991.
[45] A. Tanougast, K. Hriczó, Effect of Winglet-Designed Vortex Generators on Heat Transfer Performance in Corrugated Channels, (2025).
[46] A. Tanougast, R. Bessaih, K. Hriczó, Comparative study of different vortex generator designs in corrugated channel for turbulent heat transfer enhancement, Results Phys. 77 (2025) 108450. https://doi.org/10.1016/j.rinp.2025.108450.
[47] A.A. Gholami, M.A. Wahid, H.A. Mohammed, Heat transfer enhancement and pressure drop for fin-and-tube compact heat exchangers with wavy rectangular winglet-type vortex generators, Int. Commun. Heat Mass Transf. 54 (2014) 132–140. https://doi.org/10.1016/j.icheatmasstransfer.2014.02.016.
[48] J.S. Sawhney, R. Maithani, S. Chamoli, Experimental investigation of heat transfer and friction factor characteristics of solar air heater using wavy delta winglets, Appl. Therm. Eng. 117 (2017) 740–751. https://doi.org/10.1016/j.applthermaleng.2017.01.113.
[49] B. Gong, L.-B. Wang, Z.-M. Lin, Heat transfer characteristics of a circular tube bank fin heat exchanger with fins punched curve rectangular vortex generators in the wake regions of the tubes, Appl. Therm. Eng. 75 (2015) 224–238. https://doi.org/10.1016/j.applthermaleng.2014.09.043.

[50] B. Lotfi, M. Zeng, B. Sundén, Q. Wang, Thermo-hydraulic Characterization of the Smooth Wavy Fin-and-elliptical Tube Heat Exchangers Using New Type Vortex Generators, Energy Procedia 61 (2014) 2343–2346. https://doi.org/10.1016/j.egypro.2014.11.1199.
[51] B. Lotfi, M. Zeng, B. Sundén, Q. Wang, 3D numerical investigation of flow and heat transfer characteristics in smooth wavy fin-and-elliptical tube heat exchangers using new type vortex generators, Energy 73 (2014) 233–257. https://doi.org/10.1016/j.energy.2014.06.016.
[52] B. Lotfi, B. Sundén, Q. Wang, An investigation of the thermo-hydraulic performance of the smooth wavy fin-and-elliptical tube heat exchangers utilizing new type vortex generators, Appl. Energy 162 (2016) 1282–1302. https://doi.org/10.1016/j.apenergy.2015.07.065.
[53] X. Wu, Z.-M. Lin, S. Liu, M. Su, L.-C. Wang, L.-B. Wang, Experimental study on the effects of fin pitches and tube diameters on the heat transfer and fluid flow characteristics of a fin punched with curved delta-winglet vortex generators, Appl. Therm. Eng. 119 (2017) 560–572. https://doi.org/10.1016/j.applthermaleng.2017.03.072.
[54] K. Song, Z. Xi, M. Su, L. Wang, X. Wu, L. Wang, Effect of geometric size of curved delta winglet vortex generators and tube pitch on heat transfer characteristics of fin-tube heat exchanger, Exp. Therm. Fluid Sci. 82 (2017) 8–18. https://doi.org/10.1016/j.expthermflusci.2016.11.002.
[55] G. Lu, G. Zhou, Numerical simulation on performances of plane and curved winglet – Pair vortex generators in a rectangular channel and field synergy analysis, Int. J. Therm. Sci. 109 (2016) 323–333. https://doi.org/10.1016/j.ijthermalsci.2016.06.024.
[56] Z.-M. Lin, C.-P. Liu, M. Lin, L.-B. Wang, Numerical study of flow and heat transfer enhancement of circular tube bank fin heat exchanger with curved delta-winglet vortex generators, Appl. Therm. Eng. 88 (2015) 198–210. https://doi.org/10.1016/j.applthermaleng.2014.11.079.
[57] A. Esmaeilzadeh, N. Amanifard, H.M. Deylami, Comparison of simple and curved trapezoidal longitudinal vortex generators for optimum flow characteristics and heat transfer augmentation in a heat exchanger, Appl. Therm. Eng. 125 (2017) 1414–1425. https://doi.org/10.1016/j.applthermaleng.2017.07.115.
[58] W. Li, B. Yu, Y. Wang, X.-R. Wang, Q.-Y. Wang, W.-Q. Tao, Study on General Governing Equations of Computational Heat Transfer and Fluid Flow, Commun. Comput. Phys. 12 (2012) 1482–1494. https://doi.org/10.4208/cicp.220111.281111a.
[59] A. Tanougast, K. Hriczó, Numerical modeling of unsteady heat convection in turbulent flow, in: Dushanbe, Republic of Tajikistan, 2025: p. 180006. https://doi.org/10.1063/5.0286594.
[60] K.M. Their, T. Hamad Abed, K. Azeez, M.A. Mohsin, Thermohydraulic performance study of the effect of winglet inserts and a corrugated wall in a rectangular channel, Case Stud. Therm. Eng. 52 (2023) 103707. https://doi.org/10.1016/j.csite.2023.103707.
[61] M.E. Nakhchi, J.A. Esfahani, Numerical investigation of rectangular-cut twisted tape insert on performance improvement of heat exchangers, Int. J. Therm. Sci. 138 (2019) 75–83. https://doi.org/10.1016/j.ijthermalsci.2018.12.039.
[62] A. Tanougast, K. Hriczó, Comparison of Turbulence Models in the Simulation of Fluid Flow in Corrugated Channel, Adv. Sci. Technol. 165 (2025) 53–64. https://doi.org/10.4028/p-7SAkva.
[63] J. Zhao, S. Li, X. Zhang, M. Sun, Y. Song, Enhanced heat transfer of supercritical *n*-decane in cooling channels with triangular ribs for regenerative cooling, Appl. Therm. Eng. 218 (2023) 119369. https://doi.org/10.1016/j.applthermaleng.2022.119369.
[64] A.A. Abbasian Arani, J. Amani, Experimental investigation of diameter effect on heat transfer performance and pressure drop of TiO2–water nanofluid, Exp. Therm. Fluid Sci. 44 (2013) 520–533. https://doi.org/10.1016/j.expthermflusci.2012.08.014.
[65] H. Pehlivan, Experimental investigation of convection heat transfer in converging–diverging wall channels, Int. J. Heat Mass Transf. 66 (2013) 128–138. https://doi.org/10.1016/j.ijheatmasstransfer.2013.06.033.
[66] M.M. Heyhat, F. Kowsary, A.M. Rashidi, M.H. Momenpour, A. Amrollahi, Experimental investigation of laminar convective heat transfer and pressure drop of water-based Al2O3

nanofluids in fully developed flow regime, Exp. Therm. Fluid Sci. 44 (2013) 483–489. https://doi.org/10.1016/j.expthermflusci.2012.08.009.
[67] S. Mehta, S. Pati, Numerical study of thermo-hydraulic characteristics for forced convective flow through wavy channel at different Prandtl numbers, J. Therm. Anal. Calorim. 141 (2020). https://doi.org/10.1007/s10973-020-09412-5.
[68] S.K. Mehta, S. Pati, L. Baranyi, Effect of amplitude of walls on thermal and hydrodynamic characteristics of laminar flow through an asymmetric wavy channel, Case Stud. Therm. Eng. 31 (2022) 101796. https://doi.org/10.1016/j.csite.2022.101796.
[69] M. Akbarzadeh, S. Rashidi, J.A. Esfahani, Influences of corrugation profiles on entropy generation, heat transfer, pressure drop, and performance in a wavy channel, Appl. Therm. Eng. 116 (2017) 278–291. https://doi.org/10.1016/j.applthermaleng.2017.01.076.
[70] F. Moukalled, L. Mangani, M. Darwish, The Finite Volume Method, in: F. Moukalled, L. Mangani, M. Darwish (Eds.), Finite Vol. Method Comput. Fluid Dyn. Adv. Introd. OpenFOAM® Matlab, Springer International Publishing, Cham, 2016: pp. 103–135. https://doi.org/10.1007/978-3-319-16874-6_5.
[71] A.S. Kim, Advanced Computational Fluid Dynamics for Emerging Engineering Processes: Eulerian vs. Lagrangian, BoD – Books on Demand, 2019.
[72] ANSYS FLUENT 12.0 Theory Guide - 18.3 Discretization, (n.d.). https://www.afs.enea.it/project/neptunius/docs/fluent/html/th/node365.htm (accessed October 28, 2025).
[73] P.J. Roache, Perspective: A Method for Uniform Reporting of Grid Refinement Studies, J. Fluids Eng. (1994). https://doi.org/10.1115/1.2910291.
[74] R.K. Ajeel, W.S.-I. Salim, K. Sopian, M.Z. Yusoff, K. Hasnan, A. Ibrahim, A.H.A. Al-Waeli, Turbulent convective heat transfer of silica oxide nanofluid through corrugated channels: An experimental and numerical study, Int. J. Heat Mass Transf. 145 (2019) 118806. https://doi.org/10.1016/j.ijheatmasstransfer.2019.118806.